POLITECNICO DI TORINO

**Corso di Laurea Magistrale in
Ingegneria Biomedica**

Tesi di Laurea Magistrale

Natural-based hydrogel as a 3D platform for cell co-culture towards cartilage regeneration

Supervisors

Prof. Gianluca Ciardelli
Dr. Chiara Tonda-Turo
Dr. Piergiorgio Gentile

Candidate

Annachiara Scalzone
Matricola: s232408

A.A. 2017/2018

Declaration of work

I declare that this thesis is based on my own work and has not been submitted in any form for another degree at any University or any other tertiary education. Information derived from published and unpublished work of others have been acknowledged in the text and in the list of references given in the bibliography.

Abstract

Articular cartilage (AC) is an avascularised and highly specialized tissue, populated by only one cell type, the chondrocytes. Behind its simple and homogenous appearance, this tissue hides a heterogeneous composition with a high level of organisation and biomechanical properties that makes it difficult to be repaired when there are failures. Hydrogels, 3D polymeric networks, are identified as ideal structures for their ability to recapitulate the cartilage solid/liquid ratio and to provide an appropriate niche, scaffolding and environmental bioactive signals for cells. Several natural polymers have been analysed for hydrogel manufacturing. Among them, chitosan, a biocompatible and biodegradable polysaccharide, has shown promising features for reproducing cartilage Extracellular Matrix (ECM) for its structural similarity to cartilage glycosaminoglycans (GAGs) and its mechanical properties, inducing mesenchymal stem cell (MSCs) chondrogenic differentiation. Another regenerative approach consists into autologous MSCs harvesting, expansion and injection, as a strategy to regenerate cartilage, due to their reliable potential to differentiate into soft tissue when subjected to specific environmental stimuli. The aim of this work was the combination of tissue engineering and stem-cell based therapy to obtain an innovative 3D platform for cell co-culture towards cartilage. Particularly this thesis investigated the manufacturing and characterisation (physico-chemical, mechanical and biological) of a thermosensitive chitosan (CH)-based hydrogel, ionically cross-linked with the addition of β–glycerophosphate (BGP), a chemical compound used in the body as a minerals transporter, able to cause the CH sol/gel transition at physiological conditions. Rheological and gelification analysis showed that the sol/gel transition of the CH/BGP hydrogel occurred in the range of 31-33°C within 5±1 minutes. Mechanical tests evidenced a compressive and equilibrium Young's modulus of respectively 37±4kPa and 17.0±0.8kPa. Furthermore, the Scanning Electron Microscopy analysis demonstrated that the gel possesses an excellent interconnected porosity with pores diameter of 0-30μm, suitable for cells attachment, intracellular signalling and nutrients diffusion. In fact, nutrients diffusion and release test were successful throughout the structure. Then, the Live/Dead and PrestoBlue assays confirmed that the hydrogel exhibited an ideal environment for MSCs viability. Finally, it was studied the influence of a close-contact co-culture of human articular chondrocytes (hACHs) spheroid on MSCs-laden hydrogels on the formation of new cartilage. Immunofluorescence and histological analysis assessed up to 28

days of co-culture, revealed the production of type II collagen and GAGs, compared with three controls (hACHs spheroid seeded on the gel (*i*) and MSCs spheroid seeded on a MSCs-laded hydrogel in chondrocytes proliferation medium (*ii*) or chondrogenic medium (*iii*)). Furthermore, the expression of CD44, a chondrogenic marker, showed higher ability of MSCs to differentiate when co-cultured with hACHs.

Further investigation on CH/BGP system will be planned for osteoarthritis (OA) disease treatment, the most common form of joint disease nowadays, applied as injectable thermosensitive gel for different applications, such as minimal invasive articular joints surgery as well as for the development of 3D bioprinted *in vitro* models simulating OA or healthy cartilage tissue for new therapeutic drugs screening.

"Trying and trying again"

Galileo Galilei

To my mum, my dad and Carlotta

Acknowledgements

With this master's degree thesis, the second chapter of my university journey ends and it is my duty to thank those who have been close to me in these two years.

First of all, I would like to thank Professor Gianluca Ciardelli, for giving me the opportunity to carry out this exciting research work that has far exceeded my expectations and the doctor Chiara Tonda-Turo, for the extreme availability, support and courtesy showed me.

I am really thankful to Piergiorgio, for teaching me, for trusting me and for helping me to start building the path to my future. I thank Marina inspiring me with her overwhelming work passion.

I thank Newcastle, my new home, the awesome people I met there and the doors it opened me.

I thank my parents and my sister, because the more I grow, the more difficult it is to get used to having them far away. They are my life and no more words are needed.

I thank all my relatives and in particular my maternal grandparents for the love they give me and with which they rejoice for all my goals;

I thank my grandfather Alfonso, who left me along the way, but he is always here, with me, shaking my hand and telling me that I must move to graduate.

I thank Torino and all that it taught me, my friends and their will to live, the people who helped me to overcome my limits and especially Fabi for all that we have shared in duty, pleasure, daily life and difficulty.

I thank my best friends of all time, those I share the "happy place" with, because no one will be like you and my home will always be wherever you are, despite every distance,
I thank whom I was born and grown up with and I thank whom I met during my life: Chiara, the friend I will have next to me my whole life, for always making me bang my head against the wall, but above all for always helping me to get up and face problems together without let me feeling alone; Roberto, my safe harbour and life certainty, because the estimate we feel between us is incomparable.

I thank Carol, the gift life gave me two years ago, for being my "ubiquitous" reference point in my daily life.

I thank those who have always supported me and have always believed in me, even who did never understand me and my choices, because it has allowed me to get here, stronger, but above all with the conviction that I have taken the right path.

Table of Contents

List of Figures

Chapter 1

Chapter 2

Chapter 3

List of Tables

List of Abbreviations

3D (Three-Dimensional)

AC (Articular Cartilage)

ACI (Autologous Chondrocytes Implantation)

ANOVA (Analysis of Variance)

BGP (β-glycerophosphate)

BSA (Bovine Serum Albumin)

Col II (Collagen type II)

ChS (Chondroitin Sulphates)

CH (Chitosan)

CH/BGP (Chitosan/β-glycerophosphate)

CTRL (Control)

DH_2O (distilled Water)

DAPI (4'.6-Diamidino-2-Phenylindole)

DD (Deacetylation Degree)

DMEM (Dulbecco's Modified Eagle Medium)

DMSO (DiMethyl SulfOxide)

DNA (Deoxyribonucleic acid)

DSC (Differential Scanning Calorimetry)

ECM (Extra-Cellular Matrix)

E-SEM (Environmental Scanning Electron Microscopy)

FBS (Fetal Bovine Serum)

FTIR (Fourier-Transform Infrared Spectroscopy)

FTIR-ATR (Fourier Transform Infrared Spectroscopy - Attenuated Total Reflectance)

GAGs (Glycosaminoglycans)

GFs (Growth Factors)

HA (Hyaluronic Acid)

hACHs (human Articular Chondrocytes)

ITS (Insulin-Transferrin-Selenium)

KS (Keratan Sulphates)

MSCs (Mesenchymal Stem Cells)

NSAIDs (Non-Steroidal Anti-Inflammatory Drugs)

OA (Osteoarthritis)

PBS (Phosphate-Buffered Saline)

PFA (Paraformaldehyde)

rpm (revolutions per minute)

SCM (Serum-Containing Medium)

SEM (Scanning Electron Microscopy)

SFM (Serum-Free Medium)

TC (Tissue Culture)

TE (Tissue Engineering)

TCP (Tissue Culture Plates)

TEM (Transmission Electron Microscopy)

TGA (Thermal Gravimetric Analysis)

TGF-β1 (Transforming growth factor-beta1)

WU (Water Uptake)

XPS (X-ray Photoelectron Spectroscopy)

Chapter 1: Introduction

1.1 Overview of the Human Cartilage

Cartilage is a strong, flexible and semi-rigid connective tissue distributed in different parts of the human body (figure 1.1a) (Mescher 2016). It can withstand compression forces and has different functions according to its position:

- to form the articular surfaces of bones: cartilage provides a shock-absorbing and sliding area for joints and facilitates bone movements due to its smooth-surfaced and resilient properties;

- to form the supporting framework of some soft tissues, such as the walls of airways (nose, trachea, larynx and bronchi), where it prevents airway collapse;

- to form the template for the growth and development of long bones, and most of the rest of the fetal skeleton (gradually replaced by bone).
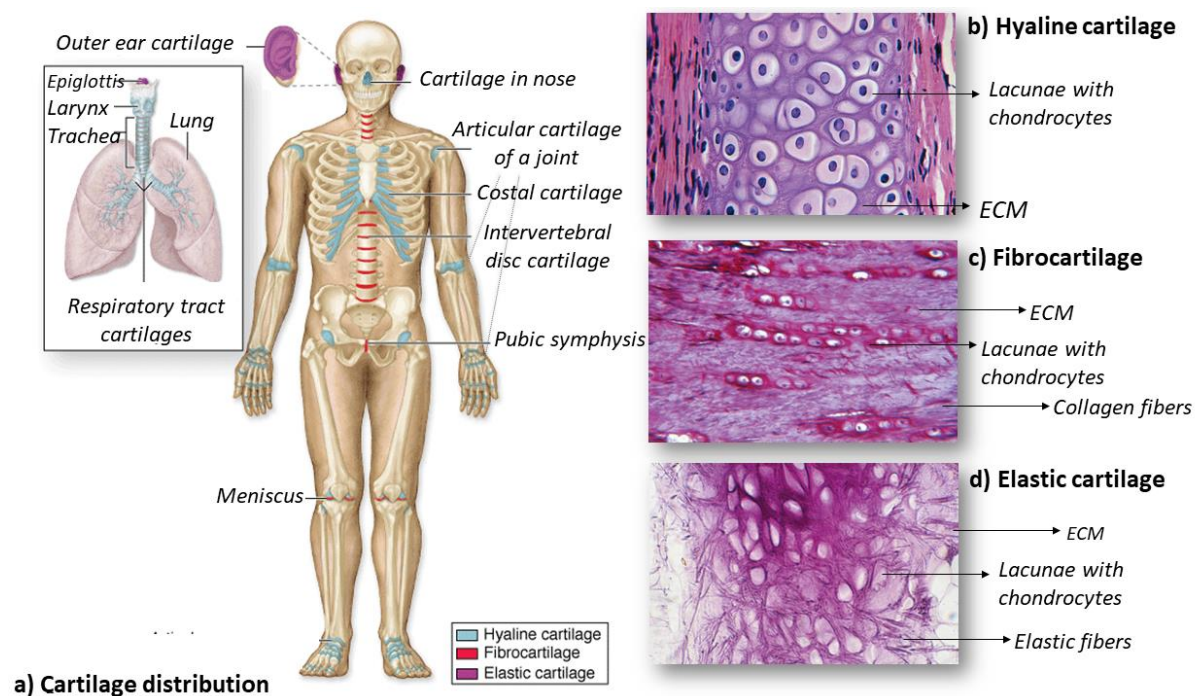
Figure 1.1: Human cartilage. There are three types of cartilage distributed in many areas of the skeleton, particularly in joints and where pliable support is useful, as in the ribs, ears, and nose. Cartilage support of other tissues throughout the respiratory system is also prominent (a). The photomicrographs show the three types of cartilage: hyaline cartilage (b), fibrocartilage (c), and elastic cartilage(d) (Mescher 2016).

Cartilage consists of one cell type, called chondrocytes (from the greek *chondros*, cartilage and *kytos*, cell) embedded in an extensive extracellular matrix (ECM) composed of fibers and

ground substance. Chondrocytes, located in matrix cavities called *lacunae*, synthesise and secrete their ECM. The principal macromolecules found in cartilage ECM are collagen, hyaluronic acid, proteoglycans (PGs), and small amounts of several glycoproteins. As a consequence of different functional requirements in the body, three forms of cartilage have evolved, whose exhibit variations in matrix composition adapted to local biomechanical needs: hyaline (figure 1.1b), fibro- (figure 1.1c) and elastic (figure 1.1d) cartilage.

The hyaline cartilage, found in the ribs, nose, larynx, trachea, is the most common one. It has a glassy appearance (from the greek *hyalos,* glass) when fresh and holds a wide number of dispersed thin type II collagen fibres (Col II), which strengthen it. Hyaline cartilage has a perichondrium, a sheath of dense connective tissue that surrounds cartilage in most places, forming an interface between the cartilage and the tissues supported by this and it is the weakest of the three types of cartilage. The fibrocartilage, found in the invertebral discs, joint capsules, in attachments of certain ligaments and in the pubic symphysis, is the strongest kind of cartilage, because it has alternating layers of hyaline cartilage matrix and thick layers of dense collagen fibres oriented in the direction of functional stresses. This type of cartilage does not have a perichondrium as it usually represents a transitional layer between hyaline cartilage and tendons or ligaments. Finally, the elastic cartilage is found in the walls of the external auditory canals, the auditory (*Eustachian*) tubes, in the epiglottis and in the larynx. Chondrocytes are found in a threadlike network of elastic fibres within the matrix. Elastic cartilage provides strength, and elasticity, and maintains the shape of certain structure. It is similar to hyaline cartilage except to the presence of an abundant network of fine elastic fibers. Like hyaline cartilage, elastic cartilage possesses a perichondrium (Bhosale & Richardson 2008).

1.1.1   Cartilage Formation and Repair

Chondrogenesis is a dynamic cellular event resulting in the formation of hyaline, fibrous, and elastic cartilage. All cartilage derives from a common precursor tissue, the embryonic mesenchyme (figure 1.2a). The first step of the chondrogenesis process is the mitotic proliferation of mesenchymal cells (MSCs), followed by their differentiation, characterised by the rounding up of the MSCs, which retract their extensions, multiply rapidly, and form cellular condensations. The cells formed by this direct differentiation of MSCs, now called chondroblasts, have a ribosome-rich basophilic cytoplasm and thereby condensations of these cells give rise to a tissue (figure 1.2b). Synthesis and deposition of their own matrix then begin

to separate the chondroblasts from one another (figure 1.2c). As the chondroblasts secrete matrix and fibres, they become trapped inside it. The matrix enclosed compartments that they sit in are called lacunae (little lakes/small pits) and mature into cells called chondrocytes. In growing cartilage, the chondrocytes can divide, and the daughter cells remain close together in groups, forming a cluster of 2-4 cells (figure 1.2d) (Lories & Luyten 2018). The superficial mesenchyme develops into the perichondrium.
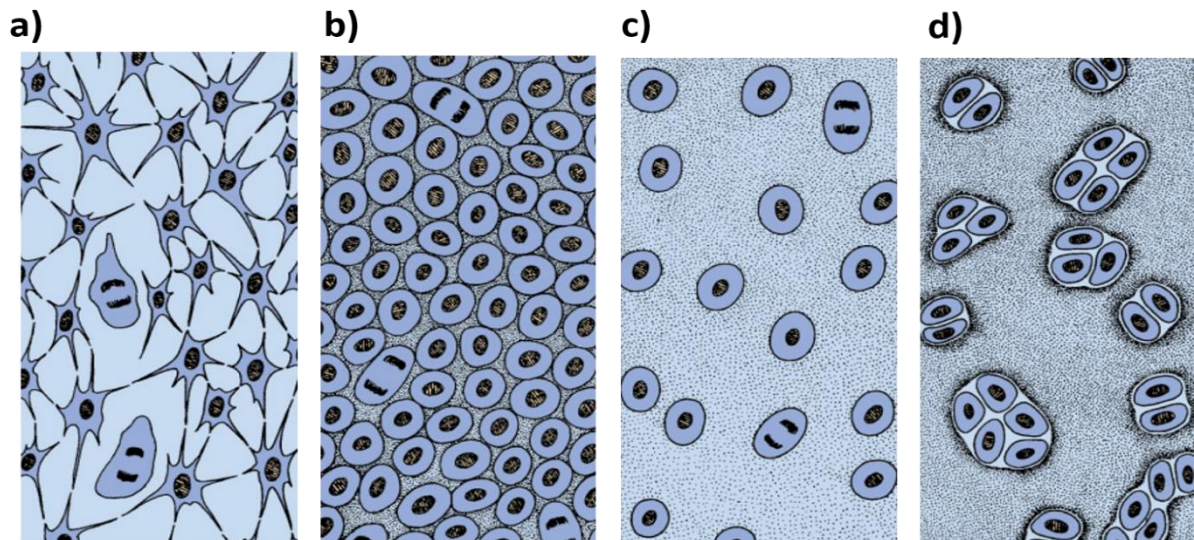
Figure 1.2: Diagrams of the major stages by which cartilage is formed (a-d). From MSCs (a) to chondrocytes (d).

Except in young children, damaged cartilage undergoes slow and often incomplete regeneration, by activity of cells in the perichondrium which invade the injured area and generate new cartilage. In extensively damaged areas—and occasionally in small areas—the perichondrium produces a scar of dense connective tissue instead of forming new cartilage. The poor regenerative capacity of cartilage is due in part to the avascularity of this tissue (Mescher 2016). Chondrocytes, which differentiate following the condensation of mesenchymal stem cells, are responsible for the secretion of extracellular matrix molecules, such as collagens and proteoglycans. Transcription factor SOX9 is critical for chondrocyte differentiation and function. Other chondrogenesis markers, present on the cell surface, inside the cell (intracellular) or secreted by the cell, are summarised in table 1.

Table 1: Chondrogenesis markers

POSITION	MARKER	FUNCTION
Cell Surface	Annexin VI	Marker or late chondrocytes differentiation
	CD44, CD151	Expressed at significantly higher levels in chondrocytes with higher chondrogenic capacity.
	ITM2A	Marker of early stage of chondrogenic differentiation
Intracellular	FAM20B	Regulates the number of glycosaminoglycan chains
	FoxC1-C2	Proteins expressed in chondroprogenitors
	SOX5, SOX6, SOX9	Play an essential role in chondrocytes differentiation and cartilage formation
Secreted	Aggrecan	Chondrocytic marker
	Cathepsin-B	Marker of de-differentiated chondrocytes phenotype
	Col II, Col IX	Markers for the differentiation state of the articular primary chondrocytes
	Matrilin-1, -3, -4	Mature chondrocytes markers
	OTOR	Initiation of periotic mesenchyme chondrogenesis
	URB	Chondrocytes marker

1.1.2 Structure and Composition of Hyaline Articular Cartilage

Articular cartilage (AC) is an avascular, aneural and alymphatic tissue and has very poor regenerative potential once reaching maturity (Buckwalter & Mankin 1997). Chondrocytes, constitute around 1-5% of the total volume of articular cartilage and vary in shape, number and size based on the anatomical zones of the AC (Alford & Cole 2005; Ng et al. 2017). These cells are responsible for the production, organisation, and maintenance of the articular cartilage ECM, and are, therefore, ultimately responsible for its integrity (Chen et al. 2006).

AC provides a low-friction gliding surface, covering the articulating surfaces of long bones in synovial joints with increased compressive strength and is known to be wear-resistant under normal circumstances. Although it is only a few millimetres thick (0.5 to 7.0 mm), AC has remarkable mechanical properties and high durability. The main function it displays is the ability to support large loads during motion, reducing stresses on subchondral bone and distributing loads across the entire joint surface. This ability is attributed to its highly organized ECM, composed of a dense network of PG, and collagen fibers (figure 1.3). The collagen content in AC is about 60% (dry weight). The predominant collagen of AC, type II, accounts 90-95% of the collagen in AC and forms the primary component of the macro-fibrillar framework. Furthermore, there are other types of collagen fibers (collagen types VI, IX, X, and XI) present,

but contribute with a minor proportion (Buckwalter & Mankin 1998). The PGs content is 10-40% (dry weight). They consist of a protein core (10% of the molecular weight) to which one or more polysaccharide units, called glycosaminoglycans (GAGs) side chains (90% of the molecular weight), are covalently attached. GAGs are linear polysaccharide chains and negatively charged, making the PGs repulse each other and also to attract cations and water (Roughley 2016). Aggrecan, is the bigger and most abundant (by weight) proteoglycan, possessing more than 100 GAG units, which are chondroitin sulphate (ChS) and keratin sulphate (KS). It is characterised by its ability to interact with hyaluronan (HA) to form large proteoglycan aggregates via link proteins. ChS, KS and HA are the three groups of GAGs in AC (Casscells 1990). The remaining component in cartilage ECM is water and small amounts of molecules, including inorganic salts (sodium, calcium, chloride, and potassium), non-collagenous proteins (including link protein, fibronectin, cartilage oligomeric matrix protein, and the smaller proteoglycans, biglycan, decorin and fibromodulin), glycoproteins and lipids (Roughley 2001; Ng et al. 2017; Chen et al. 2006)
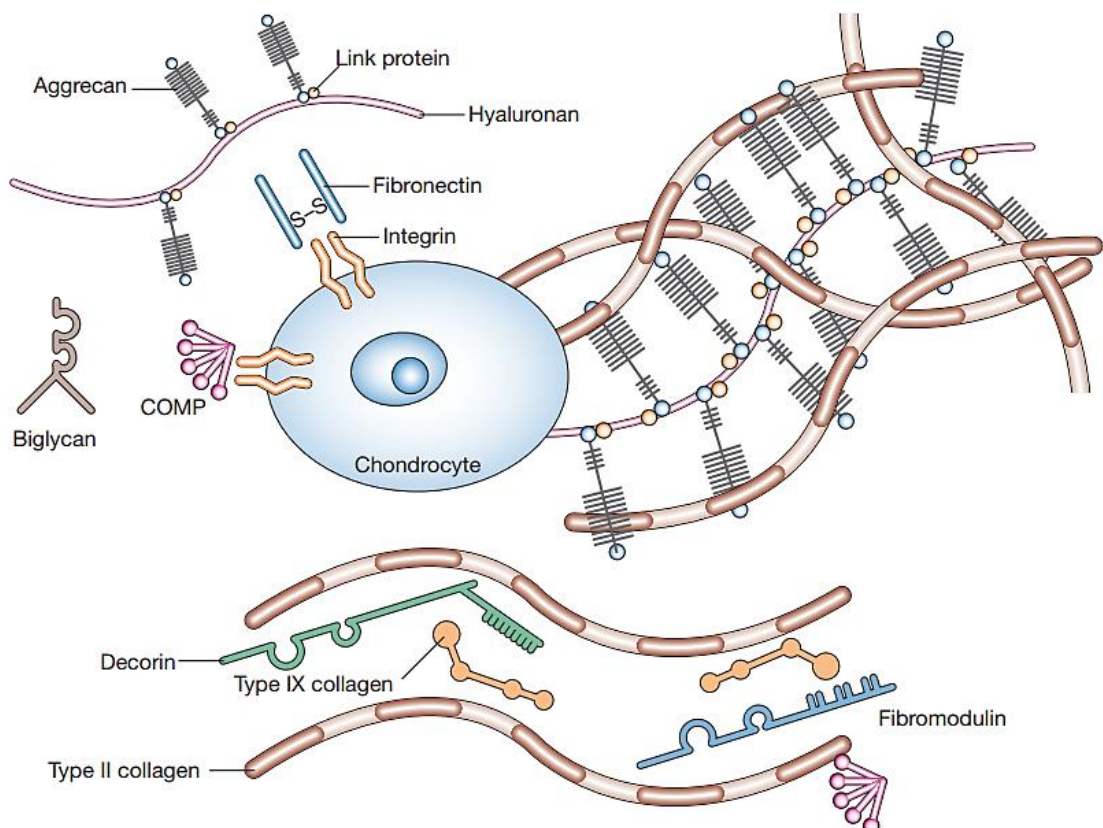
Figure 1.3: Extracellular matrix of cartilage Three classes of proteins exist in articular cartilage: collagens (mostly type II collagen); proteoglycans (primarily aggrecan); and other non- collagenous proteins (including link protein, fibronectin, cartilage oligomeric matrix protein) and the smaller proteoglycans (biglycan, decorin and fibromodulin). Abbreviation: COMP, cartilage oligomeric matrix protein. (Chen et at 2006).

1.1.3 Ultra-structure of articular cartilage

Articular cartilage has four distinct zone structures (figure 1.4 i-iv), namely superficial (transitional), middle, deep and calcified that are thought to determine its unique mechanical and biological properties. Microscopically, each zone has different structural, morphological and compositional features. The content of ECM within each zone differs with respect to the amount of collagen fibers and their organisation and orientation, PGs amount, water content and chondrocytes shape, size and metabolic activity differs as well (Buckwalter & Mankin 1997).

- The thin superficial (tangential) layer (figure 1.4i) makes up approximately 10% to 20%, with a low PGs and high-water content. In this layer chondrocytes appear elongated and collagen fibers (primarily, type II and IX) bundles are oriented parallel to the articular surface and their dense arrangement in this zone provides high tensile strength for AC, which enable it to resist the shear, tensile, and compressive forces imposed by articulation (Sophia Fox et al. 2009). This zone is in contact with synovial fluid and it also acts as a filter for large macromolecules. The integrity of this layer is imperative in the protection and maintenance of deeper layer; in fact disruptions of this zone alter the mechanical properties of the AC and thus contributes to the development of osteoarthritis (OA) (Ng et al. 2017).

- The middle zone (figure 1.4ii) constitutes about 40 to 60% of the total cartilage volume. It has higher PGs content and contains thicker collagen fibrils. Chondrocytes content is lower in this zone and they appeared to be spherical, embedded in abundant ECM. Collagen fibers have an oblique orientation and their distributions are random (Ng et al. 2017; Armiento et al. 2018) Functionally, the middle zone is the first line of resistance to compressive forces (Sophia Fox et al. 2009).

- The deep zone (figure 1.4iii) constitutes the 20% of the cartilage. It is composed by large chondrocytes surrounded by a collagen VI containing pericellular matrix, which together with the chondrocyte is known as a chondron. In this zone, the vertically oriented thick collagen fibres run parallel to stacks of chondrons, the PGs content is at its highest amount, while the water content is at its lowest amount (Armiento et al. 2018). This layer has been thought to provide the greatest resistance to compressive forces imposed by articulation (Ng et al. 2017).

- The calcified cartilage zone (figure 1.4v) is a mineralized zone that contains small volume of cells embedded in a calcified matrix and thus showing a very low metabolic activity. The chondrocytes in this zone express hypertrophic phenotype and they synthesize Type X collagen, responsible for providing important structural integrity and provide a shock absorber along with the subchondral bone (figure 1.4vi). The visible border between the third and fourth zones is termed as 'tidemark' (figure 1.4iv), which has a special affinity for basic dyes, such as toluidine blue. This zone provides an important transition to the less resilient subchondral bone (Armiento et al. 2018; Kalamegam et al. 2018).
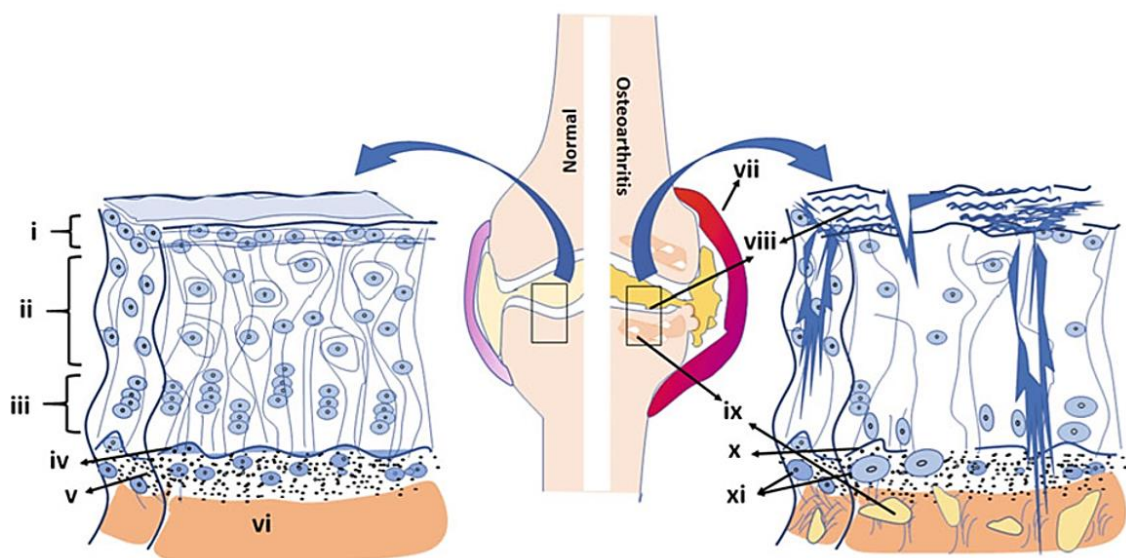
Figure 1.4: A normal and osteoarthritic (OA) joint showing the major anatomical structures and the key pathological changes is diagrammatically represented. The two enlarged boxed area from the normal and OA knee joint shows cartilage structure and the pattern of cellular arrangement or its derangement respectively (Kalamegam et al. 2018).)

1.1.4 Biomechanical properties

AC is a thin layer of specialized connective tissue with unique static and dynamic mechanical properties (Buckwalter 1998). Cellular perception of mechanical stress within cartilaginous tissues is an important modulator of chondrocyte function and their sensing of mechanical forces leads to deep changes in the health and normal function of the joint (Buckwalter & Mankin 1998; Guilak 2000). Mechanical stresses sensed by chondrocytes are often mechano-electrochemical events and these coordinate with other environmental, hormonal and genetic factors to regulate chondrocyte metabolic activity and contribution to the maintenance of the

ECM (Mow et al. 1999). The tensile resilience and strength of cartilage, is imparted primarily by the network of Col II fibers and has also been shown to be important for the dynamic functional properties of cartilage (Mow 1998; Bae et al. 2008). PGs are considered to be mainly responsible for the AC static stiffness (Rieppo et al. 2003). A link between the fluid, PGs and collagen is established through the permeability of the cartilage matrix. The total fluid content in cartilage is controlled by the swelling pressures due to the high density of fixed charges of the sulphated GAGs of PGs that draw water into cartilage resulting in high osmotic pressure, which is restrained by the collagen fibers network, thus giving rise to the compressive behaviour of cartilage. The packing and orientation of collagen fibrils modulate the fluid flow in the tissue, and PGs resist the fluid flow throughout the tissue, both being factors which influence the permeability (Federico & Herzog 2008; Freeman 1968).

A compression test is a method for determining the behavior of materials under a compressive load. These tests are conducted by loading the test specimen between two plates, and then applying a force to the specimen by moving the crossheads together. During the test, the specimen is compressed, and deformation versus the applied load is recorded. The compression test is used to determine the elastic Young's modulus (E) (stress divided by strain) at the end of the elastic-linear region in the stress-strain curve obtained from the measurements (figure 1.5a) (Mow 2009). Cartilage stiffness can be evaluated through the elastic Young's modulus.

Transient compressive mechanical behaviour of cartilage can be determined by stress-relaxation test, where a deformation is applied on a sample and the induced force is measured. The current method is to apply a known strain on the unloaded sample (figure 1.5b0). During the application of the strain slope (figure 1.5bA), it is visible a large rise of stress in the graph (Li et al. 2003), in fact the largest lateral deformation occurs, stressing the collagen fibrils in their tensile direction, exhibiting strain-dependent stiffening until the point of peak stress, where the peak Young's modulus (E_P) is calculated (figure 1.5b B). At this point, the relaxation at the fixed strain value reached, starts. This phase mainly results from the cartilage matrix permeability, which is believed to be dependent on the PG and fluid content.(Mow et al. 1992): as the fluid leaves the cartilage, load is shifted to the solid matrix and stress is reduced starting a slow relaxation process of fluid redistribution within the matrix (figure 1.5b C,D) till the equilibrium, where the equilibrium Young's modulus E_Y is recorded (Alexopoulos et al. 2005).

Equilibrium modulus is the stiffness of the cartilage as all the fluid flows out.
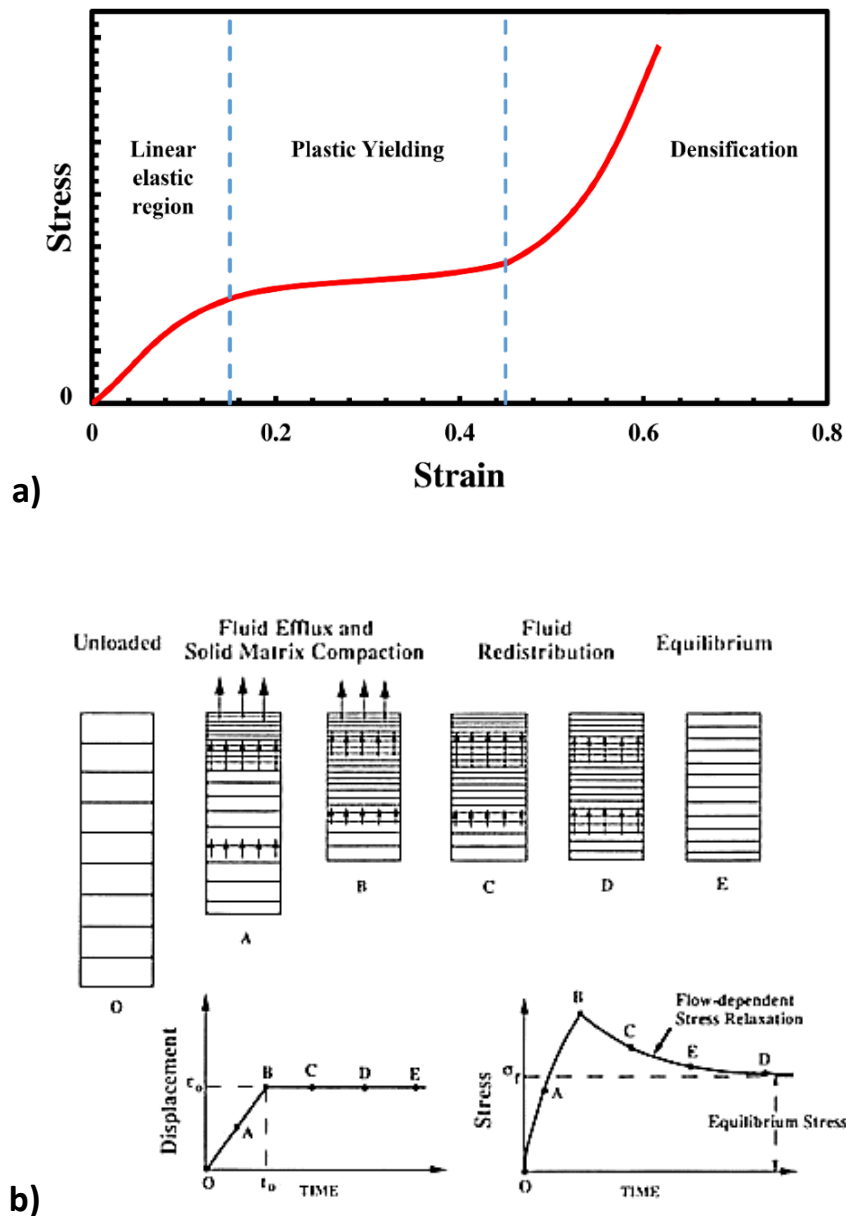
Figure 1.5: Behaviour of cartilage under compression. Static mechanical test results: stress-strain curve, which shows three different regions, related to samples behaviour; Young's modulus is evaluated at the end of the linear-elastic region (a). Dynamic mechanical test explanation and stress-relaxation curve obtained (b) (Mente & Lewis 1989).

The compressive modulus of the articular cartilage changes throughout its depth and depends on the anatomical location of the joint. For example, from the joint surface to the deep zone of bovine articular cartilage a 27 time increasing in compressive modulus has been calculated. The compressive stiffness of the articular cartilage is reinforced by the tensile strength provided by the collagen network The equilibrium tensile modulus of human knee articular cartilage was found to be higher in the superficial zone (10.1 MPa) compared to the 5.4 MPa of the middle zone, most likely due to the abundance and organisation of the collagen fibres in the superficial zone (Armiento et al. 2018). Native articular cartilage exhibits low

9

compressive Young's modulus (0.1–1 MPa) relative to its high tensile Young's modulus which regulates the mechanical response of cartilage in unconfined compression (Kelly et al. 2013).

1.2 Cartilage degeneration in Osteoarthritis

Ageing is inevitable and the relative decline in function of various system's organs, particularly connective load-bearing tissues in synovial joints of the musculoskeletal system (Kalamegam et al. 2018; Armiento et al. 2018). Arthritic diseases are a group of conditions involving inflammatory damage to synovial joints. Arthritis literally means inflammation (*itis*) of the joints (*arthr*) and it involves pain, redness, heat, swelling and other harmful effects of inflammation. Although there are over 200 different forms of arthritis, osteoarthritis is the most prevalent and chronic form of joint disease.

OA is a major cause of pain and disability affecting the ageing population with increasing prevalence as this population expands (Lutz et al. 2008). Although advancing age is a major risk factor for the development of OA, there are other significant contributing factors including gender, obesity, a history of joint trauma, increased physical activity, genetic predisposition and lifestyle (Zhang Y and Jordan M 2010) OA is one of the top five causes of disability amongst non-hospitalised adults (source: Center for Disease Control and Prevention (CDC, http://www.cdc.gov/, USA). According to estimates from the National Institute of Arthritis and Musculoskeletal and Skin Diseases (NIAMS, http://www.niams.nih.gov/) more than 20 million Americans currently suffer from OA. Conservative estimates suggest that 35–40 million Europeans have OA. In particular, more than 90% of these patients were obese confirming the strong association between obesity and OA and the incidence of OA was higher in obese female patients. It is expected that by 2030, 20% of adults will have developed OA in Western Europe and North America. Therefore, OA is expected to be a heavy economic burden on healthcare systems and community services in Europe, North America and the rest of the world as the population expands and the number of older people increase (Mobasheri et al. 2014).

Age related 'wear and tear', chondrocytes' poor response to growth factors (GFs), altered bio-mechanical properties of AC, mitochondrial dysfunction, oxidative stress and inflammation are all implicated in the pathogenesis of OA, highlighting the multifactorial and complex nature of this degenerative joint disease (Mobasheri et al. 2014; Richardson et al. 2015). In the normal knee joint, the cartilage surface is smooth, clear demarcation exists between the superficial, middle and deep zones and the tidemark, calcified cartilage and the underlying

subchondral bone are intact (figure 1.5i-iv). On the other side, in the osteoarthritic knee joint, changes include thickening of the joint capsule and inflammation (figure 1.5vii), cartilage destruction and fragmentation (fibrillation) (figure 1.5viii).Moreover, in the subchondral bone OA impact include degradation, cystic degeneration (figure 1.5 ix), damaged or absent tide mark (figure 1.5x), osteophyte formation, degradation and loss of chondrocytes (hypocellularity), and their hypertrophy (figure 1.5xi) (Kalamegam et al. 2018).

Furthermore, meniscal degeneration is commonly seen in OA, where menisci appear torn, fissured, fragmented, macerated or destroyed. Along within damaged meniscus, AC can wear away over time causing a narrowing in the joint space (figure 1.6f). Degeneration of menisci initiates within the substance of the tissue and spreads out to the surface (figure 1.6c), with a lot of intra-meniscal changes that contribute to meniscal degeneration and reduced meniscal tensile strength. The meniscus is less able to withstand loading and force transmission during normal movements of the joint, further leading to degenerative tears (figure 1.6d-e), whose are often accompanied by varying degrees of meniscal extrusion. The tear might be a preceding feature of incipient OA and meniscus damage and extrusion often have a key role in the structural progression of the disease (Man & Mologhianu 2014).
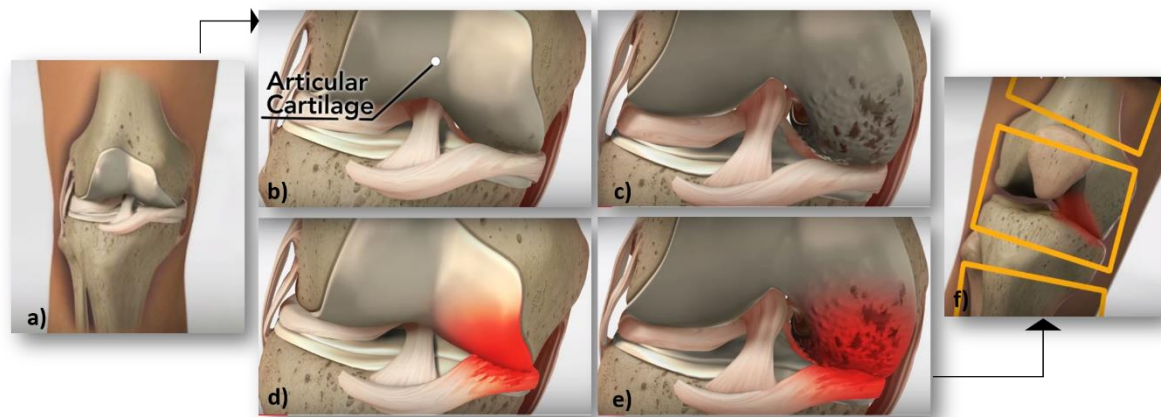
Figure 1.6: Schematic meniscal degeneration from healthy (a) to injured knee (f). OA meniscus is less able to withstand loading and force transmission during normal movements (b-c) of the joint, further leading to degenerative tears (d-e)

1.3 Scientific Background

1.3.1 OA current treatments strategies

For the past three centuries, physicians and scientists have sought several different ways to repair or regenerate articular surface of synovial joint following traumatic damage or degeneration of the cartilage (Bhosale & Richardson 2008). The lack of vasculature, nerve system and limited migration ability of chondrocytes in articular cartilage severely restrict its self-regeneration ability (Jayasuriya et al. 2016). A spectrum of treatment is and will be needed because the type of cartilage injury and degeneration vary in size, depth, shape, location and age. Moreover, the environment of the joints should be considered in the treatment approach to correct malalignments, instabilities of ligamentous and meniscus and an appropriate rehabilitation program instituted to get successful outcomes (Simon & Jackson 2018; Bhosale & Richardson 2008) The main methods of OA treatment involve (*i*) non-pharmacological and pharmacological measures for mild to moderate degenerative joint diseases with the aim of reducing pain, and (*ii*) surgical measures for moderate to severe degenerative joint diseases for improving tolerance for functional activity (Kalamegam et al. 2018; Ng et al. 2017). A primary role as a primary prevention strategy is a lifestyle modification, based on a weight loss for obese patients and exercise to improve strength and aerobic capacity (Gudbergsen et al. 2012; Nelson et al. 2014). This usually results in symptoms improvement and reduced risk of symptomatic OA (Glyn-Jones et al. 2015).

Non pharmacological treatments include heat and cold modalities, selective use of unloaded bracing , orthotics physical therapy, non-irritating aerobic conditioning, activity modification and patients educations (Simon & Jackson 2018; Mine et al. 2017). Oral non-steroidal anti-inflammatory drugs (NSAIDs), which give pain relief, do not modify the progression of degenerative joint diseases and have associated increased risk of gastrointestinal, renal, cardiac and vascular side effects (Ng et al. 2017). On the other side, topical NSAIDs have a minimal systemic absorption and related sides effects, but an increase in skin irritation (Derry et al. 2011). Viscosupplementation of hyaluronate or hyaluronate-derived agents have slight protective effects for joints, but the effect might not be significant.

A number of surgical options exist for the treatment of OA and the success rates for these options vary depending on the above mentioned different factors in different type of cartilage injuries (Simon & Jackson 2018; Kalamegam et al. 2018).

The treatment of articular cartilage defects started in 1959 with Pridie's resurfacing technique inspired by observing that full thickness defects showed an ability to repair thanks to the involvement of the subchondral bone that allows the resident progenitor cells to infiltrate the site of the defect and promote the repair process (figure 1.7) (Pridie 1959). From this discovery, a series of bone marrow stimulation techniques were developed such as subchondral drilling, arthroscopy abrasion, and micro fracture (Rodrigo 1994). Joint debridement, originally described by Magnusson in 1941 was a broad term, is considered as a Part I of any marrow stimulation techniques which included articular trimming, meniscectomy, removal of osteophytes and loose bodies, articular abrasions and even synovectomy (Magnusson 1941). These repair strategies led to tissue with inferior mechanical properties and deteriorated clinical results. Osteochondral plugs as autograft and allograft for the treatment of cartilage defects were first introduced during the 1970s (Bentley & Greer III 1971). Although successful cases of tissue integration have been reported, major drawbacks still exist such as the lack of available tissue, the donor site morbidity, and the mechanical inferiority of an osteochondral plug taken from a non-load bearing area for autologous grafting and the mismatch between the graft and the implant and the host immune reactions for the allograft (Revell & Athanasiou 2009). As an alternative approach, mosaicplasty, firstly described in 1993 has been adopted in the treatment of small to medium size defects up to 4 cm^2 to improve integration of the two tissues (Matsusue et al. 1993). In 1994, the first cell transplantation technique for articular cartilage repair was introduced by Brittberg and colleagues: the autologous chondrocyte implantation (ACI) (Brittberg et al. 1994). The original technique is based on the transplantation, under a periosteal flap, of *in vitro* culture-expanded chondrocytes from a biopsy taken from a non-load-bearing area. Chondrocyte transplantation is regarded as the gold standard in AC repair, for patients with large size defects (up to 12 cm^2) or when micro fracture fails, and long-term follow-ups have demonstrated improvement of clinical symptoms and activity levels (Minas 2001). However, despite these positive outcomes, shortcomings still exist, including the invasiveness of the surgery and the potential for dedifferentiation of chondrocytes during *in vitro* expansion with consequent reduced capacity to deposit ECM upon transplantation (Gooding et al. 2006). Various modifications of ACI are currently being tried out, focusing especially on the minimally invasive surgery. Since 2017, ACI is approved by NICE and available in UK, but not routinely provided by the NHS for treating symptomatic articular cartilage knee defects and is only carried out in few hospitals (NICE 2017). Combination of ACI with 3D scaffolds and growth factors (MACI or third generation

ACI) (Kalamegam et al. 2018; Bhosale & Richardson 2008). This was the first tissue engineering approach to cure OA.

MACI is the first FDA-approved cellularised scaffold product that applies tissue engineering processes to grow cells on scaffolds using healthy cartilage tissue; it was already authorised in certain EU countries but EU licence was suspended due to commercial reasons (Agency 2009). MACI implants are commercially available and clinical studies were conducted in over 6000 patients worldwide by using i.e. Chondro-gide®/MACI, Hyalograft®, Bioseed® scaffolds (Zhang et al. 2016). While the majority of patients treated with these clinical strategies improved, there were still issues on functional outcomes and quality of repair tissue that were not fully addressed (Wylie et al. 2016) .

Stem cell-based therapy is emerging as viable alternative for OA treatments, for the ability of the mesenchymal stem cells (MSCs) to proliferate and multilineage differentiation potential, for example into chondrocytes and osteoblasts, the key cells from the two tissues that constitute the osteochondral unit(Hunziker 2009). Harvest of multinucleated cells from within the bone-marrow and direct injection to the cartilage defect area using the bone-marrow aspirate concentrate (BMAC) system, which is gaining prominence amongst the clinicians as it helps to circumvent the labour-intensive protocols with cell culture and the associated high costs. However, the interaction of the transplanted cells with the host tissue, their differentiation into articular cartilage, fulfilment of the biomechanical properties and long-term benefits remains to be understood (Kalamegam et al. 2018)
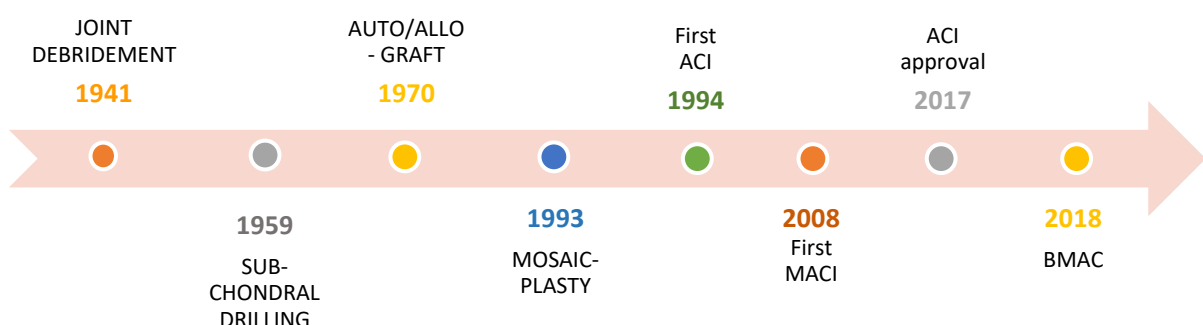
Figure 1.7: Schematic process of major milestones surgical cartilage repairs in human.

This kind of techniques reported, are existing treatment methods fail to cure OA, leading to active research initiatives and integration of multiple disciplines to find a permanent cure and regenerative medicine is a translational research solution which integrates both cells/stem cells and tissue engineering principles to regenerate tissues/organs and help functional

restoration. It is expected that regenerative medicine will provide strategies for effective regeneration of articular cartilage.

1.3.2 Using Tissue Engineering Strategies to Address AC disease

Over the past 25 years numerous tissue-engineering approaches have been developed to address AC disease but with controversial results. Many of these tissue engineering constructs are based on the concept that the primary goal is to recapitulate functional and structural features of the AC and that engineered cartilage should be indistinguishable from mature cartilage with respect to zonal organisation, biochemical composition and mechanical properties(Schon et al. 2017). The key to successful repair and regeneration of cartilage is to provide the repair site with stimulating factors and sufficient cells in a suitable delivery vehicle to ensure maximal differentiation and deposition of an appropriate ECM. This requires selection of three major components: (1) a source of cells (MSCs, chondrocytes, induced pluripotent stem cells (iPSC)), which are harvested and expanded; (2) biomaterial scaffolds, where the cells are seeded after expansion and, (3) stimulatory factors to mimic the natural AC environment (figure 1.8). These three components critically influence the outcome of a tissue-engineered construct. There are two basic approaches: firstly, *in vitro* tissue engineering, in which the tissue is generated entirely, with full functionality, before transplantation; and secondly, *in vivo* tissue engineering, in which the construct is implanted with or without prior partial *in vitro* cultivation and allowed to mature *in vivo* for tissue repair and regeneration (Chen et al. 2006). Both approaches require appropriate scaffolds, responsive cells, and a chondroinductive and chondroconductive environment.
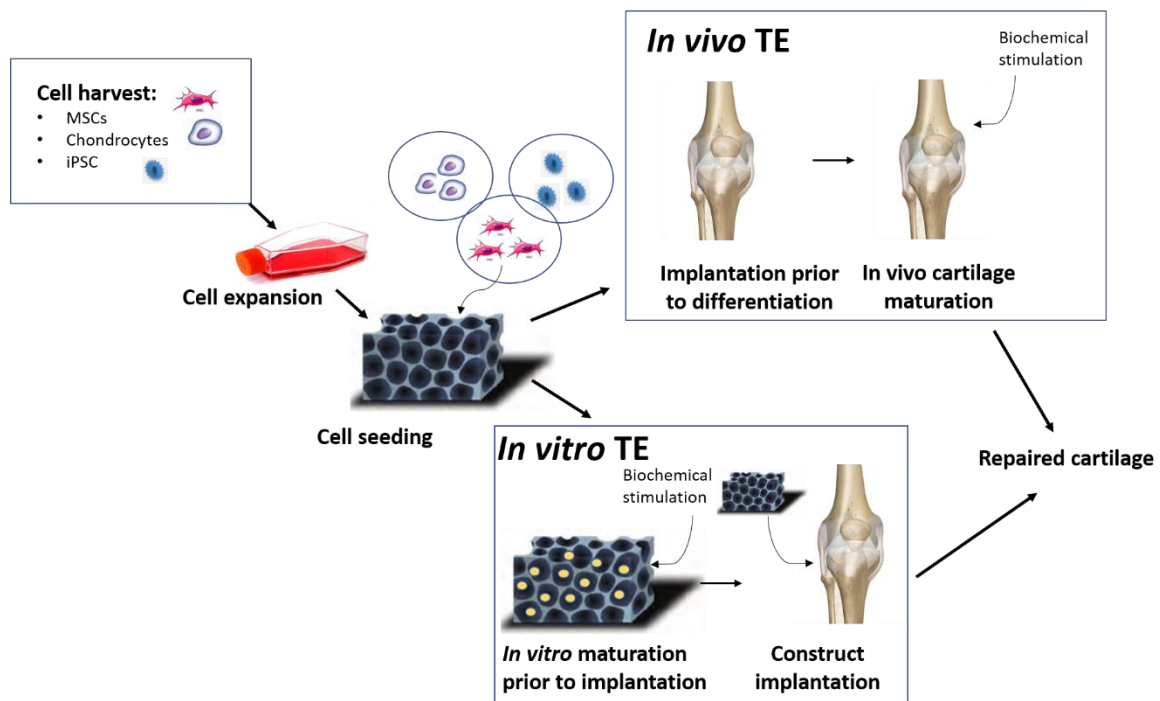
Figure 1.8: Schematic of the cartilage tissue engineering process. Firstly, cells are harvested and expanded, secondly the scaffold is seeded with cells and there are two basic approaches to obtain cartilage tissue engineering: *in vitro* and *in vivo* tissue engineering.

1.3.3 Design and materials requirements

The first challenge in cartilage regeneration is creating an environment suitable for stem cell homing and growth. The scaffold provides the form and shape, guides the stem cells differentiation and replacement tissue development. Recent research into biomimetic designs and fabrication for engineering of cartilage tissue have focused on the domain of 3D platforms as scaffold for both *in vitro* and *in vivo* regeneration and replacement of biological tissues. A 3D environment is considered as a crucial factor for encouraging cells to restore the chondrogenic phenotype (Mitchell & King 2014). However, cells behaviour is affected by both the structural characteristic and the chemical composition of scaffolds. Regardless of the biological tissue, critical requirements of any biomaterial scaffold for its suitability in TE applications are summarized in table 2.

Table 2: Scaffold requirements

MATRIX PROPERTIES	BIOLOGICAL BASIS
Porosity	Cell migration
Carrier	Lodgement and release of signalling substances
Adhesion	Cell attachment
Biodegradability	Physiological remodelling
Volume stability	Smooth surface contour of repair tissue flush with that of native articular cartilage
Biocompatibility	Good contact with the native tissue compartment
Bonding	Enhances interfacial integration between collagen fibrils in repair and native tissue compartments
Internal cohesiveness	Prevention of matrix outflow
Elasticity	Resiliency during and following dynamic or static deformation
Structural anisotropy	Promotion of native anisotropic tissue organization
Sol/ gel transition *in situ*	Fluid state during application with subsequent solidification *in situ* for Arthroscopic implantation.

Ideally, a matrix should be porous so as to permit either the migration of loaded cells through its interstices or the infiltration of native ones from the implant surrounds. Its surface properties should promote cell adhesion, a feature that can be enhanced by coupling the basic matrix material with specific cell adhesion-promoting peptides. The material must also be biocompatible, i.e., induce only minimal adverse immunological reactions within its destined tissue compartment. In some instances, the matrix may be required to facilitate or even promote the proliferation of one cell population whilst inhibiting this activity in another. The material must also be biodegradable and be capable of replacement by physiological extracellular components. In this context, it must be taken in mind that the degradation products yielded by many matrices have cytotoxic, or other undesirable effects. Certain physical characteristics, such as deformability, elasticity and volume stability must also be satisfied by the matrix. The scaffold material should also withstand the *in vivo* loading environment and protect the embedded cells from mechanical stresses. Clearly, it is not realistic to expect that any one material will fulfil the entire formidable list of requirements.

However, by combining different types of material and by effecting certain chemical modifications, we can go some way towards achieving the ideal (Hunziker 2002).

In addition, the ideal material for cartilage TE should allow the recreation of the composition of cartilage in terms of the liquid/solid phases of the connective tissue, reproduce its zonal and regional organisation, and facilitate the integration of the new formed tissue with the adjacent native one. Moreover, a scaffold material should maintain its structural integrity and stability during fabrication, clinical handling, and fixation at site of implantation (Stoop 2008). Decellularized ECMs (dECMs) are used for cartilage repair because they have negligible cytotoxicity effects and contain many of the natural structural components that modulate cell attachment, growth, and differentiation (Cheng et al. 2014; Jayasuriya et al. 2016; Yang et al. 2011). The dECM can be used as a scaffold that closely mimics the natural tissue matrix in which cells can reside and function, preserving the local tissue microenvironment for improving cellular function, as demonstrated by a recent study using the dECM in combination with adipose-derived stem cells to achieve a superior cartilage healing response, resulting in the production of a tissue that closely resembles AC in molecular and biomechanical properties (Kang et al. 2014) The use of dECM is a relatively new concept in cartilage TE and the exact potential chondroinductive effects of GFs and GAGs retained within the ECM, and the immunogenicity of the matrix remains to be elucidated. Also, the decellularisation process compromises the mechanical function of these ECM-derived scaffolds.

Alternatively to using whole dECMs, individual ECM proteins or synthetic biomaterials have been tested *in vitro* as well as in experimental animals and in human patients, for their efficacy in facilitating or promoting AC repair (Hunziker 2002) (table 3).

Between protein-based polymers, collagen has been largely used in the field as the active component of sponges to promote adhesion and chondrogenesis of MSCs cells thanks to its biocompatibility (Qi et al. 2012; Kuo et al. 2015; Antoine et al. 2014). Silk fibroin, even, due to its excellent biological compatibility and mechanical strength has been used as a biomaterial for some biomedical applications, such as for reinforcing hydrogel structures for cartilage tissue engineering with great results (Mirahmadi et al. 2013). Gelatin matrix, which is the denatured form of collagen, have not been used purely as scaffolding structures to enhance spontaneous repair in articular cartilage defects (J. Li et al. 2012), but they have attracted some attention as a substrate for the support of chondrocyte growth, both *in vitro* and *in vivo*. Fibrin clot have been used for incorporating chondrocytes clot and its healing response can also be enhanced by including GFs, as shown in equine and canine models for the repair of AC

(Marquass et al. 2011). Moreover, in form of glues, fibrin was used as matrix to enhance AC repair, but owing to the exceedingly high (unphysiological) concentrations and protein densities involved they didn't allow an easy cells penetration and healing response (van Susante et al. 1999). Hyaluronan is a physiological component of the AC matrix, biocompatible and biodegradable, usually cross-linked by esterification or other means to obtain enhanced physico-chemical and mechanical properties and as a result, its biocompatibility is compromised (Goa & Benfield 1994; Spoliti et al. 2012; Bornes et al. 2015). Agarose is a polysaccharide, isolated and purified from certain Asian seaweeds, which gained importance as a matrix for the culturing of chondrocytes and it has been largely used in many basic *in vitro* studies relating, for example, to chondrocyte differentiation from MSCs (Thompson et al. 1985)(Soltz 2000; Buschmann et al. 1992)(Soltz 2000; Buschmann et al. 1992). Its poor biodegradability, unfortunately, makes it an unattractive matrix candidate for cartilage repair studies *in vivo*. Alginate is a gelatinous carbohydrate, isolated and purified from brown algae, used as a matrix favouring chondrogenesis and the maintenance of chondrocytic phenotype in 3D culture (Fragonas et al. 2000). When implanted alone, it has been shown to inhibit spontaneous repair responses and alginate-based cartilage tissue engineered *in vitro* induces severe foreign body giant cell reactions and immunological responses (Diduch et al. 2000).

Synthetic polymers are more controllable and predictable, where chemical and physical properties of a polymer can be modified to alter mechanical and degradation characteristics. The most currently explored for cartilage repair include: PGA, PEG, PLLA, PLGA (Hsu et al. 2013; Lee et al. 2009). However, unless specifically incorporated, synthetic polymers do not benefit from direct cell-scaffold interactions, which can play a role in adhesion, cell signalling, directed degradation, and matrix remodelling. In addition, degradation products may be toxic or leading to an inflammatory response. Meshworks composed of carbon fibers have been used for more than two decades in orthopaedic tissue engineering (Hunziker 2002). Most importantly, considerable attention has been given to chitosan-based scaffolds, which will be following discussed.

Table 3: Chemical classes of materials mostly used for cartilage TE

PROTEIN-BASED POLYMERS	
• Silk	(F. Li et al. 2012)
• Fibrin	(van Susante et al. 1999; Marquass et al. 2011)
• Collagen	(Qi et al. 2012; Ben-Yishay et al. 1995; Antoine et al. 2014; Kuo et al. 2015)
CARBOHYDRATE-BASED POLYMERS	
• Hyaluronic acid	(Goa & Benfield 1994; Spoliti et al. 2012; Bornes et al. 2015; Brix et al. 2014)
• Agarose	(Benya & Shaffer 1982; Thompson et al. 1985; Soltz 2000; Buschmann et al. 1992; Coleman 2013)
• Alginate	(Fragonas et al. 2000; Diduch et al. 2000)
• Gelatin	(J. Li et al. 2012; Ponticiello et al. 2000)
SYNTETHIC POLYMERS	
• Poly(lactic acid) (PLA), Poly(glycolic acid) (PGA), Poly(lactic-co-glycolic acid) (PLGA), Poly(ethylene glycol) (PEG).	(Hsu et al. 2013; Lee et al. 2009)
• Carbon fibers	(Hunziker 2002)

1.3.4 Hydrogels in Articular Cartilage tissue engineering

Above mentioned biomaterials have been manufactured into macroporous structures or nanostructures (nanofibers, nanoparticles, nanotubes) to allow seeding of cells into their porous regions, or into hydrated polymeric networks, hydrogels, for embedding cells. The "network" indicates, crosslinks hinder dissolution of the hydrophilic polymer chains into the aqueous phase (Hennink & van Nostrum 2012). To engineer a tissue with high water content like articular cartilage, hydrogels, being water-based and concurrently water insoluble, were identified as ideal scaffold for their ability to recapitulate the cartilage solid/liquid ratio and efficiently replace damaged tissue (Armiento et al. 2018). Hydrogels are water-swollen networks, supporting the transportation of cells, bioactive agents, nutrients and waste, and can homogenously suspend cells in a 3D environment, where seeded cells retain a rounded morphology that may induce a chondrocytic phenotype. Importantly, hydrogel can be cross-linked either physically or chemically and this enables the material to hold together by molecular entanglements and secondary forces such as ionic, hydrogen bonding, and hydrophobic interactions and covalently bonded. They are smart materials that respond to environmental stimuli (temperature pH, ionic strength, electric field, the presence of enzyme, etc.) and swell or shrink accordingly. Hydrogels have also been combined with various materials for applications in cartilage tissue engineering, and as an injectable. hydrogel to

support mesenchymal precursor cell delivery for intervertebral disc repair (Zhu & Marchant 2011).

However, hydrogels have limited mechanical property, which is considered the major drawback for their use in tissue engineering, as found in the load-bearing bone and cartilage tissues. In order to solve this problem, one approach is increasing polymer concentration and crosslinking density (Boere et al. 2014). But this impacts the diffusion rates of nutrients, bioactive factors and cell metabolites through the hydrogel. Porosity have an important role on the diffusion of nutrients and oxygen, particularly in the lack of a functional vascular system (Annabi et al. 2010). Hydrogels can be used as injectable scaffolds because they simply fill defects with any shape and size, implanted in a minimally invasive way, their tissue-like properties and controllability of release behaviour (Toh & Loh 2015). Injectable hydrogels have two forms: *in situ*-forming and preformed hydrogels. *In situ*-forming hydrogels formation is occurred in physiological conditions after injection. Before administration they have the form of clear polymer solutions that change into a gel in response to alterations in external stimuli. Among injectable systems, stimuli-sensitive polymeric hydrogels, including temperature-sensitive and pH sensitive, have been widely investigated with potential application as drug, protein, cell delivery carriers and scaffolds for tissue engineering (Ruel-Gariépy & Leroux 2004). Temperature sensitive hydrogels have advantages in comparison to injectable materials with chemical gelation mechanism. For example, sol–gel transition of them does not need any of toxic chemical reagents (such as crosslinkers, organic solvents, catalysts)(Boffito et al. 2015). Furthermore, there are pH sensitive injectable hydrogels that show significant potential in regenerative medicine. To obtain pH-sensitive injectable hydrogels, it is necessary to incorporate the hydrogel with a pH-sensitive moiety. For example, Shim et al have synthesized a pH-sensitive injectable hydrogel by adding pH-sensitive sulfamethazine oligomers (SMOs) to both ends of a temperature-sensitive poly (ε-caprolactone - co-lactide) – PEG – poly (ε-caprolactone-co-lactide) (PCLA–PEG–PCLA) block copolymer. This pH-sensitive SMO–PCLA–PEG–PCLA– SMO injectable hydrogel exists in solution at high pH (pH 8.0), but rapidly changes into a stable gel under physiological conditions (pH 7.4) (figure 1.9)(Shim et al. 2006).
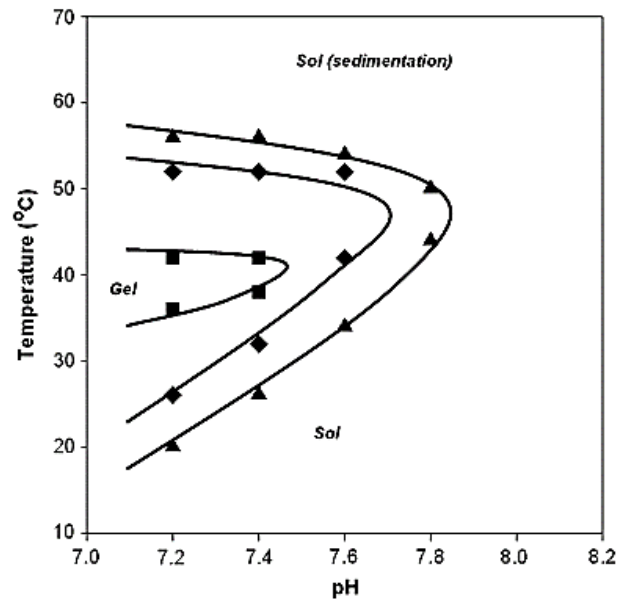
Figure 1.9: The sol–gel phase diagram of the pH- and thermosensitive SMO–PCLA–PEG–PCLA–SMO (10 wt. % (square), 15 wt. % (rhombus), and 20 wt. % (triangle)) block copolymer. Based on the sol–gel transition studies, we conclude that increasing the pH value above 7.9 could be an effective measure to control the in situ gelation of the SMO–PCLA–PEG–PCLA–SMO block copolymer at body temperature (Shim et al. 2006).

Other physical injectable hydrogels, such as ion-sensitive and stress-sensitive hydrogels, for cartilage tissue-engineering applications have also been studied. For instance, Park et al have prepared an ionically cross-linkable hyaluronate-grafted-alginate hydrogel that easily forms gels in the presence of calcium ions (figure 1.10) and has been demonstrated to be useful in cartilage regeneration by the subcutaneous injection of primary chondrocyte encapsulated hyaluronate-grafted-alginate into the dorsal region in a mouse model (Park et al. 2014)

Hyaluronate-*g*-alginate (HGA) Calcium ion Ionically cross-linked HGA gel
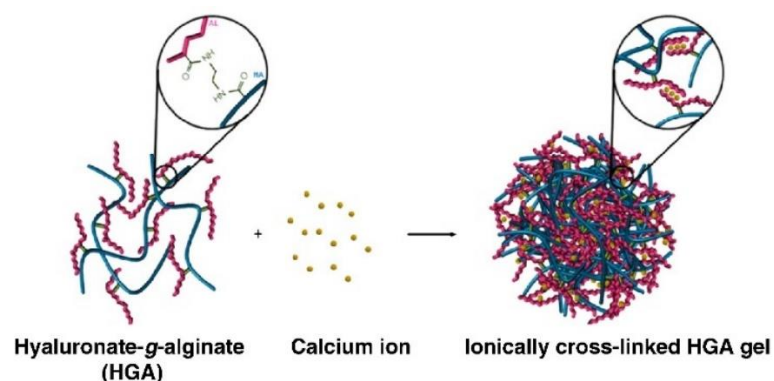
Figure 1.10: Schematic description for hyaluronate-g-alginate (HGA) and its hydrogel formation in the presence of calcium ions. Hyaluronate (HA) was initially modified with ethylene diamine (NH_2-HA). Then, NH_2-HA was reacted with alginate (AL) via carbodiimide chemistry (Park et al. 2014)

On the other side, hydrogel chemically cross-linked, are produced through a variety of chemical processes: enzymatic cross-linking, Schiff base cross-linking Michael additions, click chemistry, and photo-crosslinking. For example, in the enzymatic crosslinking, one of the most

common used enzyme in synthesizing injectable hydrogels is the HRP, a single-chain β-type haemoprotein that catalyses the conjugation of phenol and aniline derivatives in the presence of H_2O_2 (figure 1.11a). Jin et al have also enzymatically cross-linked Dex–TA conjugates in the presence of HRP and H_2O_2 to prepare an injectable hydrogel for cartilage tissue repair (Jin et al. 2010). Chondrocytes encapsulated in the Dex–TA hydrogels have been found to retain their viability and normal morphology after 2 weeks, and to secrete GAGs and Col-II after culturing for 14 and 21 days, thus indicating that their enzymatically- cross-linked hydrogel is promising for cartilage tissue-engineering applications. Furthermore Schiff base reaction, between the amino functionalities of chitosan and the aldehyde groups of dextran aldehyde in aqueous solutions, has been proposed by Cheng et al for the manufacturing of an injectable chitosan-based polysaccharide hydrogel for cell and protein delivery(figure 1.11b) (Cao et al. 2013). Hyaluronic acid, chitosan, and PEG are frequently used biomaterials for injectable hydrogel preparation via the nucleophile Michael addition reaction for cartilage tissue engineering under physiological conditions (figure 1.11c) (Chen et al. 2013; Pritchard et al. 2011) Click chemistry is a really promising crosslinking technique, based on rapid polymerization kinetics and low reactivity with cellular components (figure 1.11d). For example, Kaga et al have fabricated a dendron–polymer–dendron conjugate-based injectable hydrogel through radical thiolate "click" reactions (Kaga et al. 2016). In this fabrication process, the dendron– polymer conjugates were prepared through an azidealkyne "click" reaction of alkene-containing polyester dendrons, bearing an alkyne group at their focal point, with linear PEG-bisazides. The sequential thiolene "click" reaction uses a tetrathiol-based cross-linker to cross-link these alkene-functionalized dendron–polymer conjugates, thus resulting in clear and transparent hydrogels. In recent years, photo-cross-linking methods have been widely applied to prepare injectable hydrogels for cartilage tissue engineering because of the ability to control the timing and location of cross-linking under physiological conditions (figure 1.11e) (Cho et al. 2016). For example, Papadopoulos et al have developed a poly(ethylene glycol)dimethacrylate copolymer-based injectable hydrogel by photo-crosslinking for cartilage tissue-engineering applications (Papadopoulos et al. 2011).
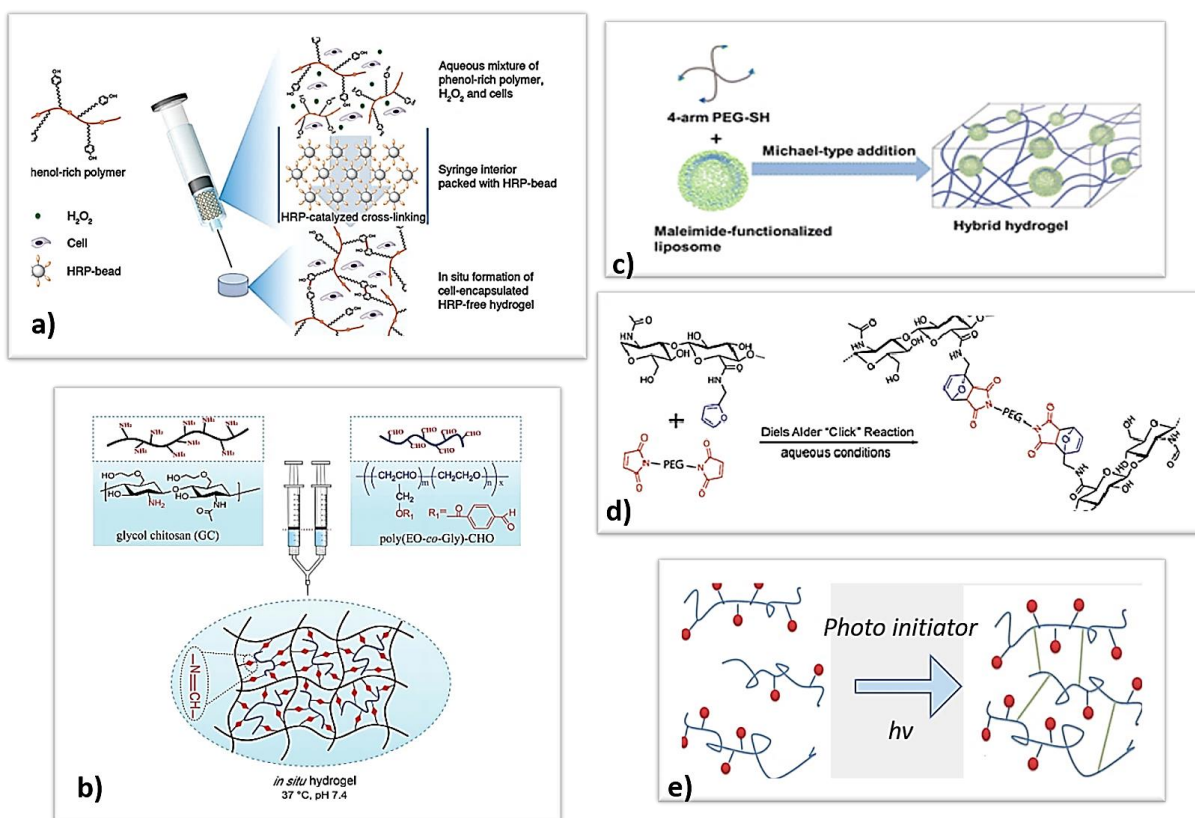
Figure 1.11: Schematic illustrations of injectable hydrogels chemical crosslinking methods. Enzymatic cross-linking method with horseradish peroxidase (HRP) and H_2O_2 (Cao et al. 2015)(a) , Schiff base cross-linking between aqueous solutions of GC and poly(EO-co-Gly)-CHO (Bae et al. 2014)(b), Michael addition cross-linking method (Liang & Kiick 2016) (c), Click chemistry method (Uliniuc et al. 2012)(d), Photo-cross-linking method.

1.3.5 Thermosensitive chitosan-based hydrogel

In this work, we proposed a thermosensitive chitosan-based hydrogel and analysed, in collaboration with "Politecnico of Turin", its physico-chemical and biological properties in order assess if it to satisfied all the requests that a material needs for being suitable in cartilage tissue engineering.

As described above, thermally responsive hydrogels are interesting due to their gelation and swelling behaviour that can be triggered by temperature change (Klouda 2015). These thermosensitive polymers at temperatures below their lower critical solution temperature (LCHT) are completely soluble in aqueous and they form a gel at temperatures above their LCHT.

The chitosan-based thermogelling systems with the combinations of chitosan and polyol-phosphates represent interesting materials developed by Chenite et al. in 2000 using β-glycerophosphate (BGP) as gelling agent (Chenite et al. 2000). Some more details on the two components are described below:

Chitosan, discovered and named in 1859 by Roget (Patrulea et al. 2015), is a biocompatible, biodegradable, antibacterial, non-antigenical and high adsorptive polysaccharide composed of glucosamine (figure 1.12). It is derived by deacetylation of marine chitin, a poly (β-(1→4)-N-acetyl-D-glucosamine), first identified in 1811 by French chemist Henri Braconnot, synthesized by an enormous number of living organisms (insects cuticles and crustaceans skeletons), under alkaline conditions (Hamedi et al. 2018). Chitosan is an excellent materials for tissue engineering and various GAGs that exist in AC and chitosan are similar in structure, which makes it a suitable matrix for cartilage repair (Francis Suh & Matthew 2000). Chitosan is soluble in dilute aqueous acidic media at a degree of deacetylation (DD) of 50% and higher (depending on the origin of the polymer) due to its primary amino groups that have a pKa value of 6.3. Solubilization occurs by protonation of the $-NH_2$ group of the D-glucosamine repeating unit, whereby the polysaccharide is converted to a polyelectrolyte in acidic media. Mw and DD have important effect on chitosan solubility (Hamedi et al. 2018).The solubility differences between chitosans with different DD may have profound influence on accessibility of chitosans to enzymes and the biological effects of chitosans (Vårum et al. 1994). Furthermore, solubility of chitosan will be enhanced by decreasing its Mw that changes the content of N-acetylglucosamines units in chitosan, which will have intramolecular as well as an intermolecular influence, resulting in different chitosan conformations.
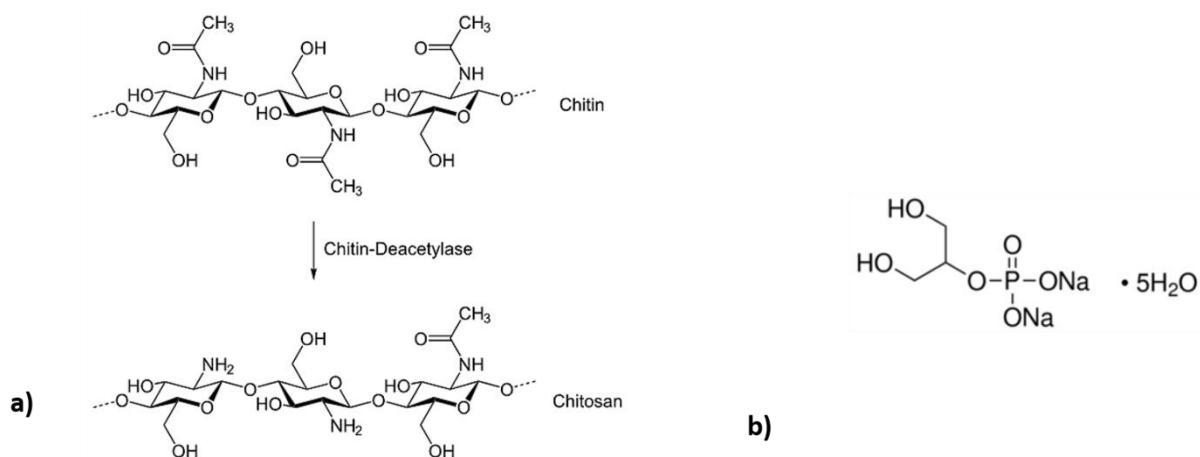
Figure 1.12: Chitosan (a) and β-glycerophosphate (b) chemical structures.

On the other hand, BGP is an organic compound naturally found in the body which is usually used as a source of phosphate in the treatment of unbalance of phosphate metabolism and

its venal administration has been approved by Food and Drug Administration (FDA) (figure 1.12). It used in the body as a minerals transporter.

Chitosan is not a thermosensitive polymer, but the addition of BGP allows CH solution to be thermoresponsive at physiological pH. This polyol plays three essential roles in the system as described recently by Zhou (Zhou et al. 2015):

- to increase the chitosan solution pH into the physiological range of 7.0–7.4, due to the neutralizing effect of the phosphate group;
- to prevent immediate precipitation or gelation;
- to control the sol/gel transition with temperature.

Thermogelling behaviour and hydrogel characteristics can be fine-tuned by varying the formulations parameters such as the molecular weight (Mw) and the deacetylation degree (DD) of the chitosan, ratio of CH and gelling agent, pH of the final solution (Supper et al. 2014). Particularly, the sol/gel transition temperature is pH-sensitive, decreasing when the pH increases and it is dependent on CH and BGP concentrations), decreasing with both concentration increase (figure 1.13). Moreover gelation time is known to be temperature-dependent (Chenite et al. 2001). This is a crucial point in this research activity, because the gelation time of the hydrogels should be quick to achieve cell retention without compromising their use in practical application (Li et al. 2018). Practical application expects a gelification time in a range of 5-15 minutes.

a)   b)
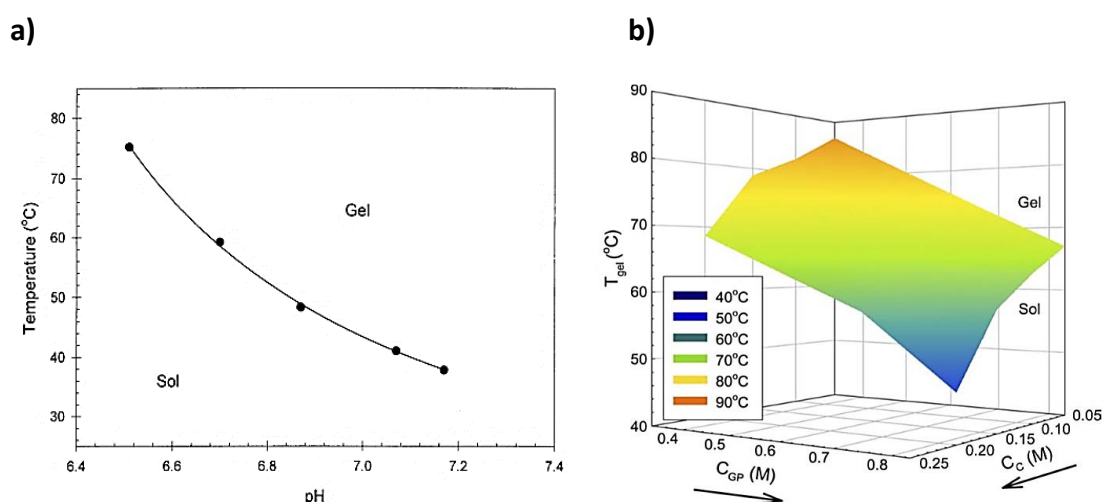
Figure 1.13: Gelation temperature dependence on pH and concentrations. a) Gelation temperature as function of the pH of the chitosan solution (chitosan, 2%; BGP, 0.262 M) (Chenite et al. 2001) and b) under various BGP (C_{GP}) and CH (C_C) concentrations (Cho et al. 2006). Tgel is gradually decreased with increasing of both concentrations. However, a synergetic effect at high concentrations results in a sudden drop of the gelation temperature and a phase transition which is on the edge between concentration-induced and heat-induced gelation.

The molecular mechanism of gelation may involve multiple interactions between chitosan, β-glycerophosphate and water (figure 1.14) (Nisbet et al. 2006). The effective interactions responsible for the sol/gel transition may include:

(1) increase of chitosan interchain hydrogen bonds because of the reduction of electrostatic repulsion due to the basic action of the salt, which works as a neutralising buffer;

(2) electrostatic interactions between chitosan and β-glycerophosphate via the amino groups of CH and the phosphate groups of BGP respectively;

(3) chitosan–chitosan hydrophobic interactions that may be enhanced by the structuring action of glycerol on water.

Moreover, it is postulated that the polyol part of BGP slowed down the gelation process at low temperature by promoting the protective hydration of the CH chain (Supper et al. 2014).
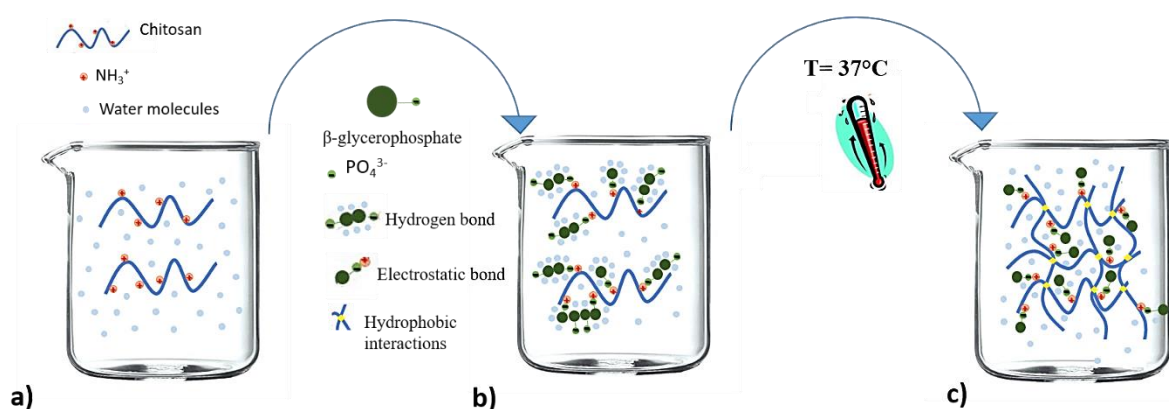
Figure 1.14 Illustration of interactions involved in the CH/BGP gelation process. Hydrogen bonds, electrostatic interactions and hydrophobic interaction are the gelation driving forces.

Several literature reports focus on the complex thermogelling process, with controversial concerns, as reported below:

- Cho et al. (Cho et al. 2005) sustained that the hydrophobic interactions between CH chains and hydrogen bonds are the gelation driving forces at high temperature, based on studies that showed a significant decrease of the degree of ionization of CH after heating. This suggests its solubility reduction and possible ionic interactions between the CH positively charged glucosamine units and the negatively charged BGP. This may happen due to a reduction of electrostatic repulsion force between positive charged amine thanks to an increase of BGP divalent anions with the temperature increase

- Lavertu et al. (Lavertu et al. 2008) reported that the CH/BGP system ionic strength decreases with the heating. As a consequence, electrostatic repulsion, rather than ionic strength, has been identified as drastically influenced by the CH/BGP system temperature: the thermosensitive behaviour of the system was explained by CH--CH interchain attractive forces (i.e. hydrogen bonding and hydrophobic interactions) responsible to avoid or slow the gelation mechanism

- Another study showed that glycerol-moieties of BGP plays a significant role on the gelation mechanism, protecting at low temperature the CH molecules with a hydration layer. Then, heating the solution results in breaking this protective "water shield", increasing the CH-CH attractive interactions and finally allowing the sol/gel transition (Supper et al. 2013).

1.3.6 Biomedical applications of CH/BGP hydrogels

The CH/BGP gelation kinetic as well as the hydrogel morphology can be controlled by selecting the most suitable polymer (Mw and DD) and by varying the formulation parameters (e.g. CH and BGP percentage, pH solution) (Supper et al. 2014). Moreover, by selecting the appropriate formulation parameters, the hydrogel exhibits good biocompatibility and biodegradability results (Zhu et al. 2014). Indeed, the biochemical properties and the 3D networks of this hydrogel system makes it widely used in biomedical field including local drug delivery (e.g. hydrophilic and hydrophobic small molecules, proteins and peptides, as well as vaccine drug) and tissue engineering (figure 1.15) (G.Tahrir et al. 2015; Assaad et al. 2015).
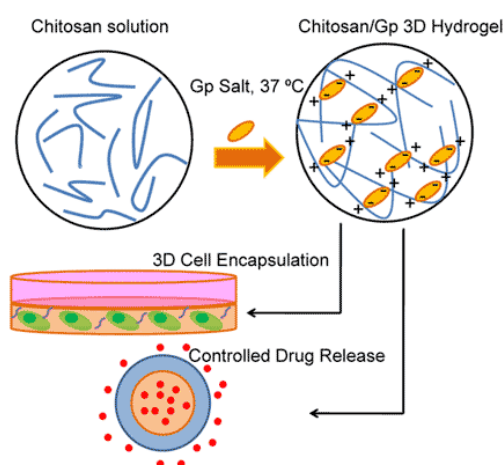
Figure 1.15 Injectable Thermosensitive CH/BGP Based Hydrogels Biomedical applications: Tissue Engineering and Drug Delivery (G.Tahrir et al. 2015).

1.3.6.1 Local drug delivery

Due to the advantages of pH sensitivity and mucoadhesive properties, CH/BGP hydrogels are effectively used in localised and controlled drug delivery (Zhou et al. 2015) (Table 3).

Ruel-Gariepy et al. described the *in vitro* release of model compounds loaded into the CH/GP system and demonstrated its ability to significantly reduce the initial burst of chlorpheniramine maleate, one of the most commonly used antihistamines in small-animal veterinary practice) compared with a CH solution without gelling agent (Ruel-Gariépy et al. 2000). The release of this positively charged low-Mw compound was reduced from 53% to 15% after 4 h by addition of GP to the CH solution and its release was sustained by the hydrogel over 2 days, whereas a complete release was achieved in less than 1 day from the pure CH hydrogel. Another investigation on the release mechanism of this hydrogel has been done with venlafaxine, a water-soluble compound used as antidepressant, belonging to a group of drugs called selective serotonin and norepinephrine reuptake inhibitors (SSNRIs) through mathematical models (Y. Peng et al. 2013). It has been found that an increase in drug load and BGP content led to higher initial release and rate constants, while CH concentration didn't affect the release. *In vivo* additional studies in rabbits, demonstrated that there was a reduction of the maximum plasma drug concentration and a prolongation of the mean residence time of the drug after subcutaneous administration of the optimized CH-loaded hydrogel compared to a CH hydrogel. Therefore, the delivery of low-Mw drugs may be prolonged for few hours to few days when the compounds are entrapped in CH/BGP hydrogel. Other works are present in literature for the release of antitumoural drugs. The use of CH/BGP hydrogel has been proposed for the local delivery of paclitaxel anticancer drugs after intratumoral injection also for over 1 month *in vitro* (Ruel-Gariépy et al. 2004). The drug release rate was inversely correlated to the initial drug loading, since hydrogels loaded with 6.4 and 64 mg/mL paclitaxel resulted in release rates of 4.2%/day and 2%/day, respectively. Paclitaxel is a hydrophobic molecule, which is therefore dispersed in the hydrogel and consequently the concentration-dependent release rate is attributed to the necessity of a first dissolution step prior to diffusion from the matrix. In 2008, Zhou et al. reported a study on Adriamycin (Doxorubicin) and the 6-mercaptopurine release, where the hydrophilic Adriamycin showed slower *in vitro* release kinetic from CH/GP than the hydrophobic 6-mercaptopurine (Zhou et al. 2008). However, almost complete release was achieved in less than 1 day for both compounds, but slower releases were observed when increasing the CH Mw from 1.13 to 1.36 MDa, due to the compaction of the hydrogel structure induced by higher

Mw. Another study tested the intratumoral injection of a doxorubicin (DOX)-loaded CH/BGP hydrogel in combination with a vaccinia virus-based vaccine as chemo immunotherapy and showed improved anti-tumoral effect compared with monotherapy in mice (Han et al. 2008). Kim et al. have reported a thermosensitive chitosan hydrogel for the delivery of ellagic acid for the treatment of brain cancer. The chitosan gels containing 1% (w/v) of ellagic acid significantly reduced viability of U87 (glioblastoma cells)and C6 (from the brain tissue of a rat (Rattus norvegicus) glial tumour) compared with the CH gels at 3 days incubation (Kim et al. 2010). In order to enhance the tumour targeting of the hydrogel, Zhang et al. have developed a magnetic thermosensitive hydrogel as intravescical Bacillus Calmettee-Guérin delivery system which is formulated with CH/BGP and Fe_3O_4magnetic nanoparticles. The gel allowed an intravescical continuous release of Bacillus Calmettee-Guérin over the period of 48 h in the presence of magnetic field and its sustained delivery markedly increased the antitumor efficacy and induced a high local immunity in bladder (Zhang et al. 2013).

Different studies have been carried out for the release of insulin from CH/BGP hydrogels (Table 3), such as in form of phospholipid complex encapsulated into biodegradable poly(3-hydroxybutyrate-co-3-hydroxyhexanoate) nanoparticles (Q. Peng et al. 2013). The *in vitro* release studies evidenced that only 19% of total insulin was released from the nanoparticle-loaded hydrogel within 31 days and, the hypoglycaemic effect of nanoparticle-loaded hydrogel following subcutaneous injection in diabetic rats persisted for more than 5 days. Finally, a minimally invasive thermogelling system for prolonged local delivery of alendronate (osteoporosis treatment drug, ALN) has been developed and tested. CH/BGP hydrogel ensured controlled ALN release over 45–65 days depending on initial ALN loading and showed less inflammatory response, faster proliferation and maturation of granulation tissue relative to plain thermogel (Nafee et al. 2017a).

Another application of CH/BGP hydrogel as a delivery systems for clotrimazole, anti-Candida activity drug, showed enhanced activity and favourable drug release profile compared to commercially available product (Szymańska et al. 2014).

Table 4: Various formulations of CH/GP in drug delivery

AIM OF THE STUDY	DRUG INVOLVED	YEAR	REFERENCES
Controlled *in vitro* release of chlorpheniramine maleate	*Chlorpheniramine maleate*	2000	(Ruel-Gariépy et al. 2000)
Release mechanism investigation	*Venlafaxine hydrochloride*	2012	(Y. Peng et al. 2013)
Intratumoral administration of paclitaxel	*Paclitaxel*	2004	(Ruel-Gariépy et al. 2004)
Controlled *in vitro* release of hydrophilic and hydrophobic drug substances	*Adriamycin or 6-mercaptopurine*	2008	(Zhou et al. 2008)
Intratumoral injection of CH/GP hydrogel containing doxorubicin in combination with a vaccinia virus-based vaccine	*Doxorubicin*	2008	(Han et al. 2008)
Ellagic acid delivery system for cancer treatment	*Ellagic acid*	2010	(Kim et al. 2010)
Magnetic thermosensitive hydrogel as intravesical Bacillus Calmette–Guérin delivery system	*Bacillus Calmette–Guérin*	2013	(Zhang et al. 2013)
Controlled *in vitro* release of insulin	*Insulin*	2012	(Khodaverdi et al. 2012)
Sustained *in vitro* release of insulin (free or in nanoparticles) from CH/BGP hydrogel	*Insulin*	2013	(Q. Peng et al. 2013)
Slowly nasal drug delivery system decreasing nasal mucociliary clearance rate	*Insulin*	2007	(Wu et al. 2007)
Prolonged local delivery of Alendronate for osteoporosis	*Alendronate*	2017	(Nafee et al. 2017b)
Model drug of anti-Candida activity of clotrimazole	*Clotrimazole*	2014	(Szymańska et al. 2014)

1.3.6.2 TE applications

CH/BGP hydrogels can be applied as injectable scaffolds mimicking ECM for the regeneration of different tissues, such as nerve, bone and cartilage. Different studies proposed the use of CH/BGP gels alone or in combination with other biomaterials, with or without cell encapsulation. Some examples are reported below.

- **Nerve tissue engineering**

A polylysine-functionalised thermoresponsive CH/BGP hydrogel has been constructed for cell adhesion and neurite outgrowth, resulting in good cell adhesion, good neuron compatibility (cells doubled) at low concentrations and no change in neurite outgrowth (Crompton et al. 2007). Kwon et al. used this hydrogel as a 3D substrate for the attachment, proliferation, and

differentiation of rat muscle-derived stem cells (Kwon et al. 2012). In the presence of valproic acid, rat muscle-derived stem cells exhibited higher expression of the neural markers, neuron-specific enolase and β-tubulin III, the oligodendrocyte marker, oligodendrocyte transcription factor 2,and the astrocyte marker, glial fibrillary acidic protein, than those in the absence of valproic acid.

- **Bone tissue engineering**

The injectable CH/BGP hydrogel has been prepared with dexamethasone/recombinant human bone morphogenetic protein (HBMP) loaded hydroxyapatite nanoparticles (Gao et al. 2013). The results showed that hydroxyapatite nanoparticles could be dispersed homogeneously in the matrix of CH/BGP hydrogels and the combination of dexamethasone and recombinant HBMP could promote the proliferation and osteoblastic differentiation of MSCs. Wang and Stegemann have encapsulated adult human bone marrow-derived stem cells in hydrogels composed of CH/BGP/collagen (Wang & Stegemann 2010). Cells exhibited high viability at 1 day after encapsulation, but DNA content dropped by about half over 12 days in pure chitosan materials while it increased twofold in materials containing collagen. The presence of chitosan in materials resulted in higher expression of osterix and bone sialo protein genes (with or without osteogenic supplements) and also increased alkaline phosphatase (ALP) activity and calcium deposition in osteogenic medium.

- **Cartilage tissue engineering**

Richardson et al. have cultured human mesenchymal stem cells in CH/BGP hydrogel for the regeneration of the degenerate human intervertebral disc. Gene expression analysis for chondrocytes-cell marker genes demonstrated differentiation of human mesenchymal stem cells to a phenotype which showed similarities to both articular chondrocytes and nucleus pulpous cells (Richardson et al. 2008). Cheng et al. added gelatin to improve the mechanical properties of CH/BGP hydrogel for the nucleus pulpous (NP) regeneration application (Cheng et al. 2010). Compared to CH/BGP, CH/gelatin/BGP hydrogel indicated an enhanced strength as well as a diminished gelation time at body temperature. NP cells cultured in either gels showed significantly high GAGs production. Mirahmadi et al. have fabricated CH/BGP hydrogel containing two forms of silk fiber used as scaffold for hyaline cartilage regeneration (Mirahmadi et al. 2013). The results of GAGs and Col II in cell-seeded scaffolds indicated support of the chondrogenic phenotype for chondrocytes with a significant increase in

degummed silk fiber-hydrogel composite for GAGs content and in two-layer electrospun fiber-hydrogel composite for Col II.

1.3.8 Cell source for AC tissue engineering: MSCs or chondrocytes?

Seeded cells are essential for cartilage TE, determining the degree of regeneration of the damaged tissue that it is possible to obtain. In AC tissue engineering, seeded cells are derived from autologous cartilage cells (chondrocytes) or multiple differentiation potential MSCs (Filardo et al. 2016; Nazempour & Van Wie 2016)

Mesenchymal stem cells (MSCs) are adult stem cells that can be isolated from both human and animal sources. Human MSCs are the non-haematopoietic, multipotent stem cells having the ability to differentiate into different lineages: mesodermal (*i.e.* chondrocyte), ectodermal (*i.e.* neurocytes) and endodermal (*i.e.* hepatocytes) (Ullah et al. 2015). These cells can be quite easily harvested from different human tissues such as bone marrow, adipose tissue, amniotic fluid, dental tissue, endometrium and umbilical cord (Nagamura-Inoue 2014; Mutlu et al. 2015; Estrela et al. 2011; Wouters et al. 2007; Mahmoudifar & Doran 2010; Pontikoglou et al. 2011).

MSCs are self-renewable, easy to culture *in vitro* and they also have immunomodulatory features since they secrete a cocktail of neurotrophic and growth factors, cytokines as well as anti-inflammatory anti-angiogenic molecules, making them perfect candidates for cell-based therapies and regenerative medicine (Kim & Park 2017; Kariminekoo et al. 2016). The possibility to have an almost unlimited cell source allowing the differentiation towards chondrocytes greatly encouraged the idea of a stem-like cell-based approach for the treatment of articular cartilage defects.

Being the cell unit of articular cartilage, chondrocytes are a logical choice for use in cell-based reparative approaches but there are still a number of drawbacks to their successful use: 1) the relatively limited availability of donor sites with the comparatively low yield of cells isolated from autologous tissue (1–5% of the total tissue volume), and 2) the lack of suitable *in vitro* culture expansion protocols that reduce the risk for chondrocytes to undergo a dedifferentiation-like state, resulting in a more fibroblast-like cell phenotype (Benya & Shaffer 1982).

1.3.9 Co-culture impact in cartilage regeneration

The possibility to have an almost unlimited cell source allowing the differentiation towards chondrocytes encouraged strongly the idea of a MSCs-based approach for the treatment of articular cartilage defects. (Dahlin et al. 2014). In recent years, MSCs and chondrocytes co-culture has been used in cartilage tissue engineering, and has several advantages compared to monoculture (Zhang et al. 2018). Mono-culture provides only the necessary physical and chemical conditions for cell growth (temperature, pH, GFs and other nutrients), while co-culture provides to obtain intercellular signals that have been reported to be important for the biological behaviour of cells. Moreover in co-culture, MSCs secrete trophic or cell–cell communication factors to promote proliferation and delay dedifferentiation of chondrocytes (Hendriks et al. 2007; Wu et al. 2011). On the other hand, chondrocytes can induce differentiation of multiple differential potential MSCs to chondrocytes without an inducer (Acharya et al. 2012). Furthermore, co-culture reduces the amount of harvested cartilage tissue, decreases the *in vitro* culture time, and lowers the degree of chondrocyte degeneration. (Florian et al 2009).

Co-culture systems are complex and have various mechanisms of action. As example there is a strong influence of the MSC-to articular chondrocyte (hACHs) ratio on the chondrogenesis and hypertrophy of co-cultured cells due to variations in the local concentration of morphogenetic signals secreted by the cells. Moreover there is a difference in the co-culture structure (figure 1.15). Cells can be seeded on 2D substrates, which may cause their de-differentiation, or within 3D co-culture systems, such as pellet or embedded into porous scaffolds which can better mimic the *in vivo* environment.

Novel co-culture systems are frequently carried out in a 3D environment, often with active perfusion or other mechanical stimulation, a further complexity to the model. Direct and indirect co-culture systems differ in the modalities of intercellular interactions, including cell–cell and cell–matrix interactions and release of soluble factors. These cell–cell communication modalities might be responsible for chondro-induction and maintenance of chondrocyte phenotype.

Indirect contact co-culture technology separates cell types physically (for example in in a Transwell chamber, or through use of membranes or micro patterned co-culture systems) and these systems have been used to evaluate the effect of cytokines secreted by one cell type on another cell type via autocrine or paracrine signalling (Huang et al. 2009; Kaji et al. 2011; Kubosch et al. 2016). Direct physical contact facilitates cell–cell interactions though surface

receipts, which mimics the *in vivo* situation and may enhances transduction of the molecular

signals that coordinate chondrogenic differentiation (Heng et al. 2004)
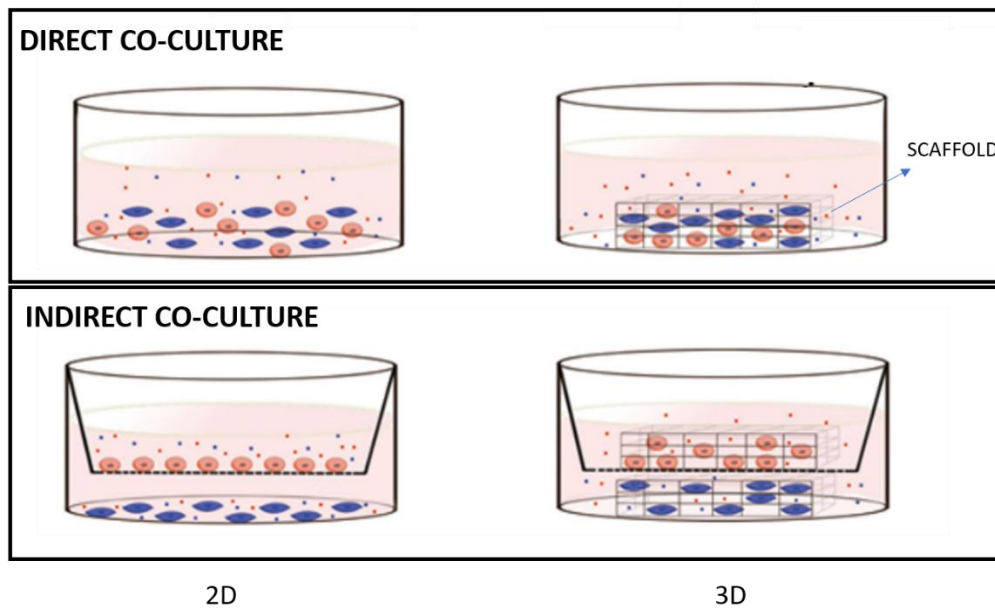
Figure 1.15: Overview on co-culture models, such as direct or indirect co-culture, 2D or 3D of self-assemble, and scaffold co-culture (Zhang et al. 2018).

In table 5 there are summarised different co-culture methods and structures that have been

reported in literature for AC regeneration.

Table 5: Co-culture models for AC regeneration in literature

Co-culture Type and cells	Results obtained	Ref.
Indirect **hACHs & BMSCs (63:1)** 	• In the absence of serum or GFs, this co-culture model closely resembled *in vivo* conditions and the derived MSC-differentiated cell population mimicked ACHs in morphology, phenotype and behaviour, thanks to paracrine signaling. • The level of differentiation was proportional to the number of chondrocytes present in co-culture	(Yang et al. 2012)
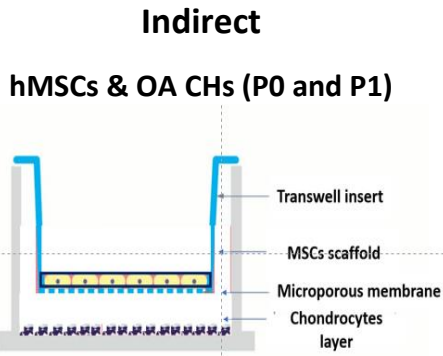
Indirect **hMSCs & OA CHs (P0 and P1)** 	• hMSCs Co-cultured with P0 OA CHs exhibited higher levels of cartilage-specific markers and produced more ECM even without GFs and suppression of type X collagen expression in differentiating MSCs ,compared to the same Co-culture with conditioned medium and to Co-culture with P1 OA CHs	(Aung et al. 2011)
Direct and Indirect **ACHs/Human MSc (1:19,4:16,10:10)** 	Comparing the direct and indirect Co-culture it was found • a higher GAGs and Col II content in the direct Co-culture and less collagen X expression marker of hypertrophy of CHs or MSCs during chondrogenesis. • the constructs seeded with more chondrocytes developed lower mechanical stiffness, GAGs, and Col II content than those seeded with fewer chondrocytes, indicating (in contrast with other studies) that the increased biosynthesis of GAG and Col II was likely due to enhanced chondrogenesis of MSCs rather than enhanced biosynthesis by the chondrocytes.	(Bian et al. 2011)
Direct **FPSCH & CHs or BMSCs & CHs** 	The aim is to recapitulate the joint development where a population of superficial progenitor cells (FPSCH or BMSCs) drives the development of the tissue (with CHs), compared to mixed co-culture. • The DNA, sGAG and Col II content of a mixed co-culture of FPSCH and CCH was found to be lower than the combined content of two control hydrogels. The opposite was found for BMSCs. • Structured co-culture, at the appropriate cell density, led to greater sGAG accumulation than a mixed co-culture for both MSC sources enhancing the development of the engineered tissue.	(Mesallati et al. 2017)
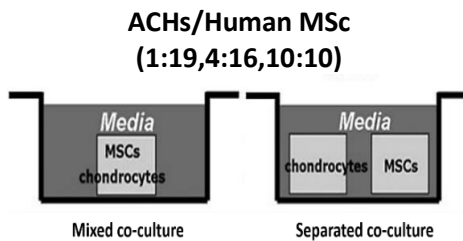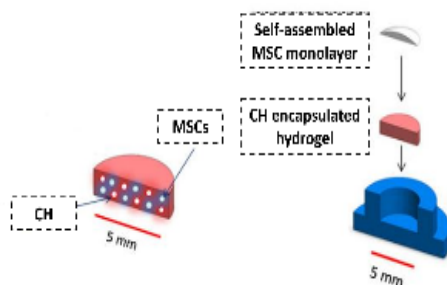
1.4 Aims and objectives of the work

This thesis work aimed at exploring the use of the thermosensitive CH/BGP hydrogel as a platform for investigating articular cartilage tissue regeneration. The corresponding objectives (OBJ), as shown in figure 1.16, were:

OBJ 1: the investigation of the morphological (ESEM), thermal (DSC, TGA), physico-chemical (FTIR, XPS, gelation time, thermal-reversibility, swelling, permeability, drug release, conductivity ad ζ-potential) and mechanical (static, dynamic and rheology) properties of the chitosan-based gels. The characteristics can be affected by temperature, Mw, DD and concentration of chitosan as well as BGP amount. The work is part of a collaboration with Politecnico di Torino with Newcastle University and the research activity was based on a previous optimisation of the formulation, done in Torino, where the BGP amount was selected at higher concentration (compared with the works reported in literature) in order to get a faster gelation (5-8 min), fundamental for _in vivo_ clinical applications..

OBJ 2: the biological characterisation of the above mentioned gels embedded with Y201 stromal MSCs, in terms of cells viability and metabolic activity.

OBJ 3: the investigation of a co-culture technology in order to mimic the _in vivo_ AC environment, where stromal MSCs were in close contact with chondrocytes. In particular, the co-culture assessed was made by a human articular chondrocytes spheroid, cultured on a MSCs-laden construct hydrogel. Histological study on GAGs and Col II production, immunofluorescence analysis on collagen production and CD44 expression and mechanical analysis were carried on after _in vitro_ culture. The co-culture behaviour was compared with three different controls (CTRL): MSCs spheroid on MSCs-laden hydrogel in chondrogenic medium (CTRL1), and MSCs spheroid on MSCs-laden hydrogel in chondrocytes growth medium (CTRL2) and chondrocytes spheroid on empty hydrogel (CTRL3) both in chondrocytes growth medium.
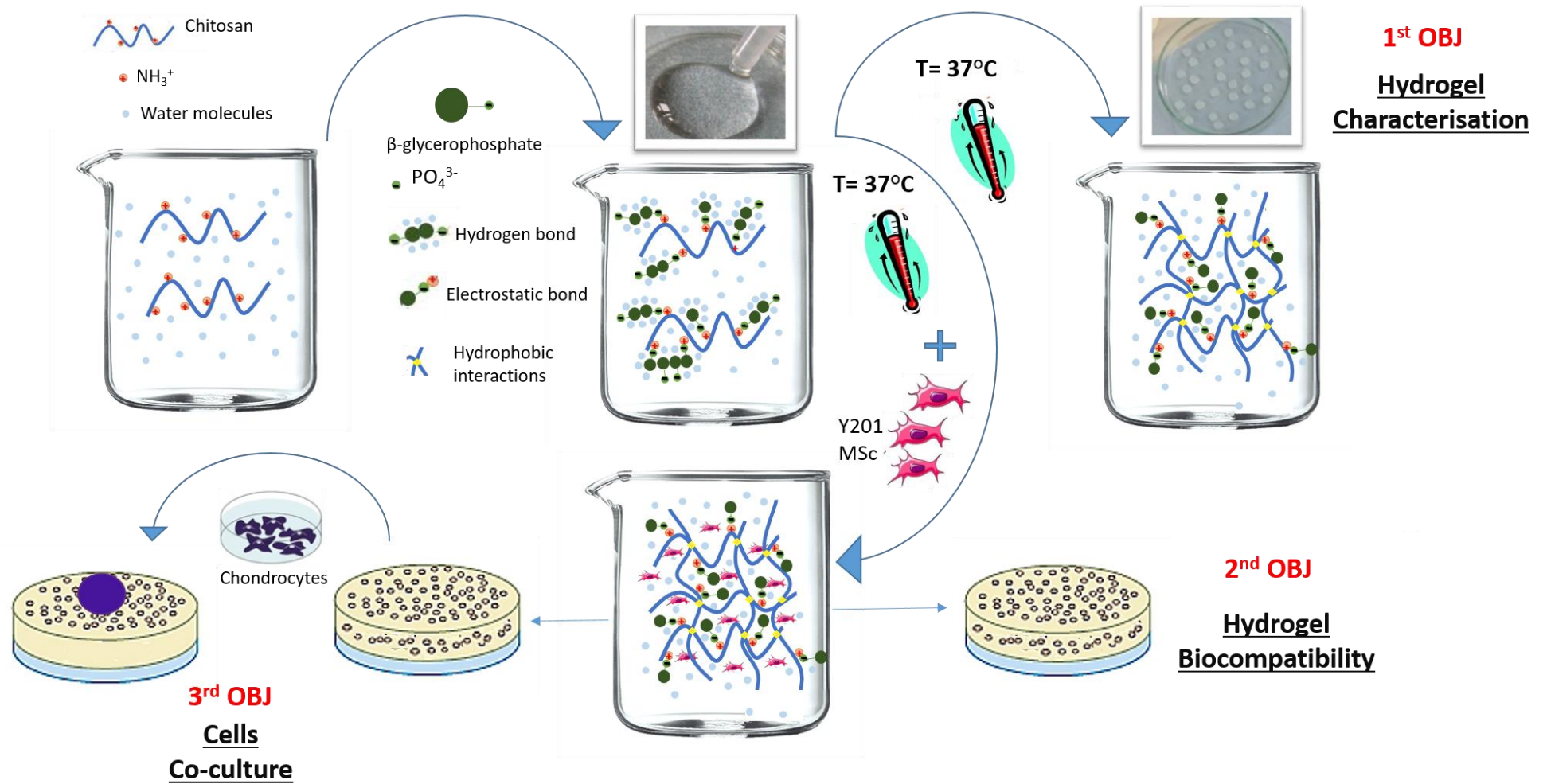
Figure 1.16: Illustration of the main objectives of the work.

Chapter 2: Hydrogel Manufacturing and Physico-Chemical Characterisation

2.1 Materials

Materials used were: chitosan (Mw 100kDA, DD 95%) (HMC+, Germany), β-glycerophosphate disodium salt pentahydrate (Santa Cruz Biotec, CA), Hydrochloric acid (HCl) (reagent grade 37%), (Sigma-Aldrich, UK), Dulbecco's Modified Eagle's Medium (DMEM) obtained from Life Science supplemented with 10% fetal bovine serum (FBS) and 5000 U/mL penicillin/streptomycin from Sigma Life Science and Dulbecco's phosphate-buffered saline (PBS; Sigma Life Science).

2.2 Methods

2.2.1 Hydrogel preparation procedure

Firstly a sterile CH solution (3.6% w/v) was obtained adding slowly autoclaved CH (at 121°C for 20 minutes) to 0.2M HCl solution, left under stirring for at least two nights in order to achieve an homogenous solution at room temperature and, then stored in the fridge at 5°C. For the preparation of the thermosensitive hydrogel, 1104.5 mg of BGP were dissolved in 1 ml of sterile PBS under stirring using a vortex (IKA, Germany) for few minutes; Dulbecco's Modified Eagle's Medium (Life Science, DMEM), supplemented with 10% fetal bovine serum (FBS) and 5000 U/mL penicillin/streptomycin (Life Science), was added to the salt solution in order to reach a final volume of 2.2 ml and then kept at 5°C in the fridge for 15 minutes. Finally, the prepared BGP solution was added drop by drop to the CH solution (5 ml) in cold conditions (using an ice bath) under stirring to obtain a final concentration of 2.5% w/v. The pH was measured by using a laboratory pH meter (Five Easy pH/mV Bench Meter, Mettler Toledo, US). The CH/BGP solution was poured in a multiwell in order to obtain disks of 3-4 mm height and 6 mm diameter and allow them to gellify at 37°Cin an incubator (SANYO MCO-18M Multigas Incubator). After the obtainment of the gels, the multiwell was stored in the fridge s or cut in disks for the characterisation (figure 2.1).
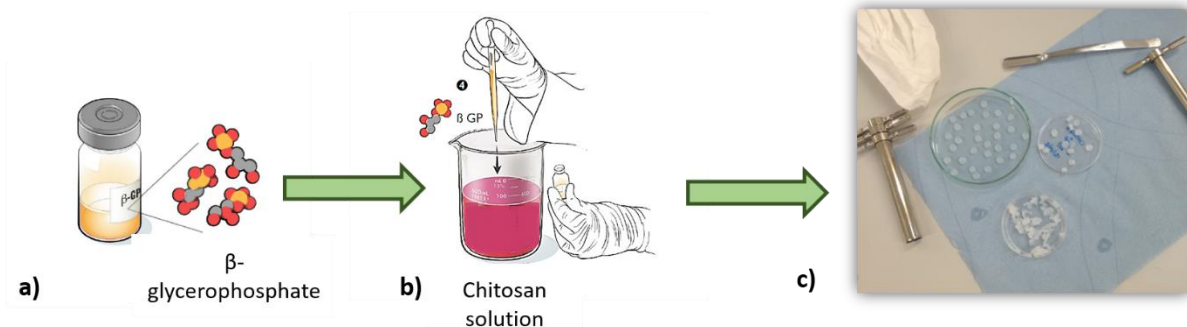
Figure 2.1: Schematic representation of the CH/BGP samples preparation procedure. BGP solution preparation (a), followed by the addition of BGP to CH solution dropwise (b) and the samples cut after letting them gellify, with a puncher (c).

2.2.2 Physical characterisation

2.2.2.1 Measurement of gelation time

Hydrogel gelation time was measured at fixed temperature of 25, 37 and 50°C using the test tube inverting method (Nafee et al. 2017b). CH/BGP solution (1 ml per bijou vial) were placed in a water bath to measure the gelation time at 37 and 50°C or maintained at room temperature to measure it at 25°C. The flowability of the samples were observed every 30 seconds by tilting the vials. The gelation time was considered as the time at which the flow of samples stopped.

2.2.2.2 Thermal reversibility

Test tubes used for testing the gelation time 37°C, were utilised in order to study the thermal reversibility of the gelation according the protocol proposed by Ganji et al (Ganji et al. 2007). The obtained chitosan hydrogels were then cooled at a temperature about 4°C. If the gels returned to a liquid solution, they were called as thermo-reversible hydrogels; while those remained gel at 4°C, were called as thermo-irreversible hydrogels.

2.2.2.3 Conductivity and ζ-potential

Conductivity of CH solution and two different solution of CH/BGP with different amount of BGP was measured at 5, 25 and 37°C using the Zetasizer Nano ZS Instrument (Malvern Panalytical Ltd). This analysis was conducted in order to a better understanding of the CH/BGP solution behaviour with increasing temperature and the effect of BGP in terms of solution conductivity. The two CH/BGP solution analysed and compared with CH were:

- CH/BGP 2.5% w/v with a molar ratio of BGP and amino groups (R) equivalent to 4. This represents the formulation used along all the research work as described at *par. 2.2.1*;

- CH/BGP 2.5% w/v and R=2.5, where a lower amount of BGP has been used (690.3 mg) respect to the previous solution;

Furthermore, by using the same equipment, the ζ-potential of the above mentioned solution was evaluated at physiological conditions (at 37°C) in order to evaluate the effect of the charge on the gelification time.

2.2.2.4 Water uptake test

For the water uptake analysis, samples were freeze-dried in order to eliminate all the water content. Hydrogels were frozen at -20°C overnight and then lyophilized under a pressure of 0.37 mBa and -55 ± 3 °C for 48 h in a freeze-dryer (Alpha 1-2 LDplus, CHRIST, Germany). Lyophilized hydrogel samples were weighted and placed separately in a 5 ml bijou vial containing 5 ml of PBS and stored at 37°C. The weight of all the samples was measured before immersion and after 30 min, 1, 2, 4, 6, 24 and 48 hours of incubation in PBS. At each time, the samples were weighted after gently drying the extra PBS on the surface using tissue papers. The water uptake percentage was calculated using the following equation:

$$WU\ (\%) = \frac{W_t - W_i}{W_i} \times 100 \quad (Eq\ 1)$$

where WU is the water uptake ratio, W_i is the initial weight of the hydrogel, W_t is the weight of the hydrogel after the particular time point.

2.2.2.5 Nutrients diffusion and release

The hydrogel was tested to assess its permeability and nutrient release. A glucose solution was prepared with the light sensitive 2-NBDG (2-(N-(7-Bitrobenz-2-oxa-1,3-diazol-4-yl) Amino)-2-Deoxyglucose) (Sigma Aldrich, UK), dissolved in PBS (0.06845 mg/mL). To test the permeability a qualitative analysis was performed: 2 ml of CH/BGP solution was let gellify in a 5 ml vial and then, 500 µl of 2-NBDG solution was added to the vial and observed over time. The time to obtain a gels of a yellow colour, corresponds to the nutrients absorption time [REF].

For the nutrient release, a quantitative analysis was carried out. Freeze dried hydrogels were weighted, washed with PBS and allocated in a 48-well plate where the glucose solution was added (1 mL for each hydrogels (6mm diameter and 4mm height), in order to completely cover

the gels and let it being in contact with the gel. At each time point (30 minutes, 1, 3, 6, 24 and 48 hours) the gels (three samples for each time point) were transferred to a new 48-well plate with 1 ml PBS to test the 2-NBDG release. All the samples were incubated overnight at 4°C, protected from the light. Finally 200µl of each well solution was transferred to a 96-well plate and read with a LS-50B Luminescence Spectrometer (465 nm excitation/540 nm emission) (Perkin Elmer, Waltham, USA)).

2.2.3 Morphological characterisation

Freeze-dried hydrogels were investigated before and after the water uptake analysis by environmental scanning electron microscope (E-SEM) in order to evaluate the morphology. The samples were cut into small squares (2 mm of diameter and 1 mm of height), fixed on the aluminium stub using carbon tape (Etxabide et al. 2018) and gold-coated using a BIO-RAD Sputter Coater machine. The following step was to obtain SEM micrographs at different magnification, using a PHILIPS scanning electron microscope XL30 FEG which operated at an accelerating voltage of 10 kV. For pore size evaluation SEM images were analysed using an image software (ImageJ). Two images for sample type were analysed and for each one approximately 50 pores were measured. The pore size is averaged to give a mean pore size assuming all pores are circular.

2.2.4 Chemical characterisation

2.2.4.1 Fourier Transformed Infrared Test (FTIR-ATR)

Infrared spectroscopy was carried out in order to characterize the sample surface and to confirm the composition and gelation chemical effects. Measurements were obtained with a Spectrum Two PE instrument equipped with a horizontal attenuated total reflectance (ATR) crystal (ZnSe) (PerkinElmer Inc., USA).

Samples analysed were CH and BGP raw powders, and CH/BGP freeze-dried hydrogels before and after water uptake. The samples were placed directly onto the ATR crystal and spectra were collected in absorbance mode. Each spectrum was the result of the average of 16 scans with 2 cm^{-1} resolution. Measurements were recorded in the wavelength range of 4000–550 cm^{-1}.

2.2.4.2 X-ray Photoelectron Spectroscopy (XPS)

X-ray Photoelectron Spectroscopy is an exceptionally sensitive tool to investigate the chemical elements constituting the outermost layer of a surface approximately up to 200Å. Thus, dried hydrogels were examined by a scanning microprobe Kratos Axis Ultra-DLD XPS spectrometer (EPSRC service Cardiff, UK), equipped with a monochromatised AlKα X-ray radiation source. The base pressure in analysis chamber was 10^{-9} mbar. Samples were analysed in High Power mode with an X-ray take-off angle of 45° (scanned size~1400 × 200 μm). For each specimen, survey scans (Fixed Analyser Transmission mode, binding energy (BE) range 0–1200 eV, pass energy 117.4 eV) and high-resolution spectra (FAT mode, pass energy 29.35 eV) were acquired of C_{1s}, N_{1s}, O_{1s}, P_{2p}. Atomic concentration (At.%) on the survey scan was performed using the built-in CasaXPS software package and in order to detect the BE representing the chemical binding states of the each elements within the films, the XPS spectra for the chemical elements detected from the films were subjected to peak deconvolution using the same software.

2.2.5 Thermal characterisation

2.2.5.1 Heat flux: Differential scanning calorimetry (DSC)

CH and BGP salt in raw powders and the freeze-dried CH/BGP hydrogels before and after water uptake were investigated by thermal analysis in order to evaluate the heat flux with the temperature increase at a heating rate of 5°C/min from 20 to 350 °C under nitrogen (DSC214 Polyma, NETZSCH). In the specific, 6–8 mg of dried sample were hermetically sealed in aluminium pans (to prevent any loss of liquid during measurements).

2.2.5.2 Mass Loss: Thermo Gravimetric Analysis (TGA)

The thermal degradation characteristics of CH, BGP and CH/BGP solution were obtained using thermogravimetric analysis (TA instruments TGA Q500) in a nitrogen atmosphere.

2.2.6 Mechanical characterisation

2.2.6.1 Unconfined Compression test

Hydrogel mechanical properties under compression (CH/BGP cylinder-shaped samples 0.6 cm diameter and 0.3 cm height) were evaluated using a mechanical testing machine (EZ-SX, Shimadzu, Japan). Three specimens for each composition were tested at room temperature (25 °C) whereas a 20N load cell was used. The crosshead speed was set at 1 mm·min^{-1} and the

load was applied while the specimen was compressed until break (~60% of original height). Stress vs Strain curves were obtained: the stress was calculated by dividing the applied force with the initial scaffold surface area, whereas strain was calculated from the displacement of the scaffolds in relation to the original thickness. The compressive Young's compressive moduli (E) were calculated as the slope of the initial elastic/linear region of the curve (0-10% strain).

2.2.6.2 Stress-relaxation test

Then, to evaluate stress-relaxation properties, it was followed the protocol used by Bian et al. (Bian et al. 2011). Stress relaxation tests were performed with a single compression ramp at a speed of 10%/ min until reaching 10% strain. Subsequently, the strain was held constant for 1000 s, while the load was recorded as a function of time. Within 10% compression, the stresses versus strain relations of the gels were almost linear. The peak stress was obtained at the moment of reaching 10% strain. The equilibrium Young's modulus (E_Y) was determined by the equilibrium load obtained after 1000 s of relaxation under unconfined. The peak stress and the E_Y are the two parameters that have been calculated for this test.

The data obtained were analysed using MATLAB R2017 software (Bonifacio et al. 2018). In particular, fitting a third order exponential decay (Eq. 2) to the relaxation curves, obeying the generalized Maxwell model, three relaxation times were acquired. The first part of the curve, corresponding to the linear region of the stress increasing with the strain, was not included when fitting the relaxation curves.

$$\sigma(t) = A(e)^{-t/\tau_1} + B(e)^{-t/\tau_2} + C(e)^{-t/\tau_3} + D \quad (Eq\ 2)$$

where σ_t is the total stress, while A1, A2 and A3 are the amplitudes corresponding to the three different relaxation times τ_1, τ_2 and τ_3.

Furthermore, the hydrogel viscosity has been evaluated fitting a first order exponential decay, in the form of:

$$\sigma(t) = A(e)^{-t/\tau} \quad (Eq\ 3)$$

which is a simple version of Maxwell's model, where, this time A is the amplitude corresponding to the relaxation time τ. A similar matlab code was also created in order to determine the relaxation time (τ) which will help in calculating the viscosity of the hydrogels using the following formula (Eq 4):

$$\tau = \frac{\eta}{E_y} \quad (Eq\ 4)$$

Moreover, the viscosity (η) was obtained multiplying the relaxation time τ by the linear equilibrium modulus E_Y, the equilibrium modulus calculated from the stress-time curves of each sample tested (Verhaar 2009).

2.2.6.3. Rheological measurements

Rheological measurements were performed on an oscillatory and rotational Anton Paar's Modular Compact Rheometer (MCR 302) using diameter disks. The CH/BGP solution was prepared at 4°C and poured between the two plates for the analysis and different rheological tests were carried out:

- The Ramp Sweep Test was done in order to know how the hydrogel viscosity changed with the temperature increasing at a certain rate. The viscosity (η), defined as the flow resistance of molecules in solutions when an internal friction is applied, is represented as shear stress τ (force per area unit; N/mm^2) divided per shear rate Ẏ (velocity of the moving plates divided by their shear gap; 1/s). The continuous rotation was set at 1 s^{-1} shear rate (Ẏ), while the temperature range between 0-50°C.

- The Strain Sweep Test was done to verify the values of the strain amplitude in order to ensure that all the measurements were performed within the linear viscoelastic region. This is defined as the region were the storage modulus (G') and the Loss modulus (G'') were independent of the strain amplitude, being linear and parallel between each other's. This test was performed at 37°C, after ensuring the solution gelification at 37°C for 30 minutes, with a rotational oscillation frequency of 1Hz.

- In the Frequency Sweep Test, frequency dependent G' and G'' were measured over angular frequencies (ω) range of 0.1 and 100 rad/s, increasing through logarithmic steps. Even this test was performed at 37°C, after ensuring the temperature stabilisation for 30 minutes at 1% strain amplitude. This test was useful to know the behaviour of the sol/gel transition at different temperatures while increasing rotational oscillation was applied.

- The Temperature Sweep Test was done in order to determine the exact sol/gel transition temperature of the CH/BGP solution. This value is determined by G' and G''

curves crossing. The oscillatory measurement was set at a frequency of 1 Hz, according to the frequency sweep test and 1% strain amplitude. The temperature was increased at the rate of 5°C in the range of 0-50°C.

- The <u>Time Sweep Test</u> was performed to know exact sol/gel transition time. This value is known when G' and G'' cross. To determine the gelation time, oscillatory measurements at 1 Hz and 1% strain, were started just after introducing cold solutions (at 4°C) into the rheometer chamber pre-heated at 37°C. The temperature was constant during the test at the same value.

2.2.7 Statistical analysis

Tests were performed at least in triplicate for each sample. The results were represented as mean ± standard deviation. Differences between groups were determined using One-way analysis of variance (ANOVA) with Turkey's multiple comparison multiple comparison test using levels of statistical significance of $p < 0.05$ (*), $p < 0.01$ (**), $p < 0.001$ (***), and $p < 0.0001$ (****).

2.3 Results

2.3.1 Physical characterisation

Figure 2.2 shows the tube inverted method, used to test the gelation time of CH/BGP solutions at different temperature. In particular, the CH/BGP system resulted to be liquid at room temperature (RT) up to 2h 45min ± 10 min, while it was able to become a gel within 5 min ± 1 min at 37°C. Moreover, a further decrease in gelation time was measured with increasing the temperature: the CH/BGP solution become into gel state within 2 min± 30 s at 50°C.

The hydrogel thermo-irreversibility was demonstrated maintaining the gel state after keeping the CH/BGP at 4 °C where it maintained the structural stability without becoming liquid.
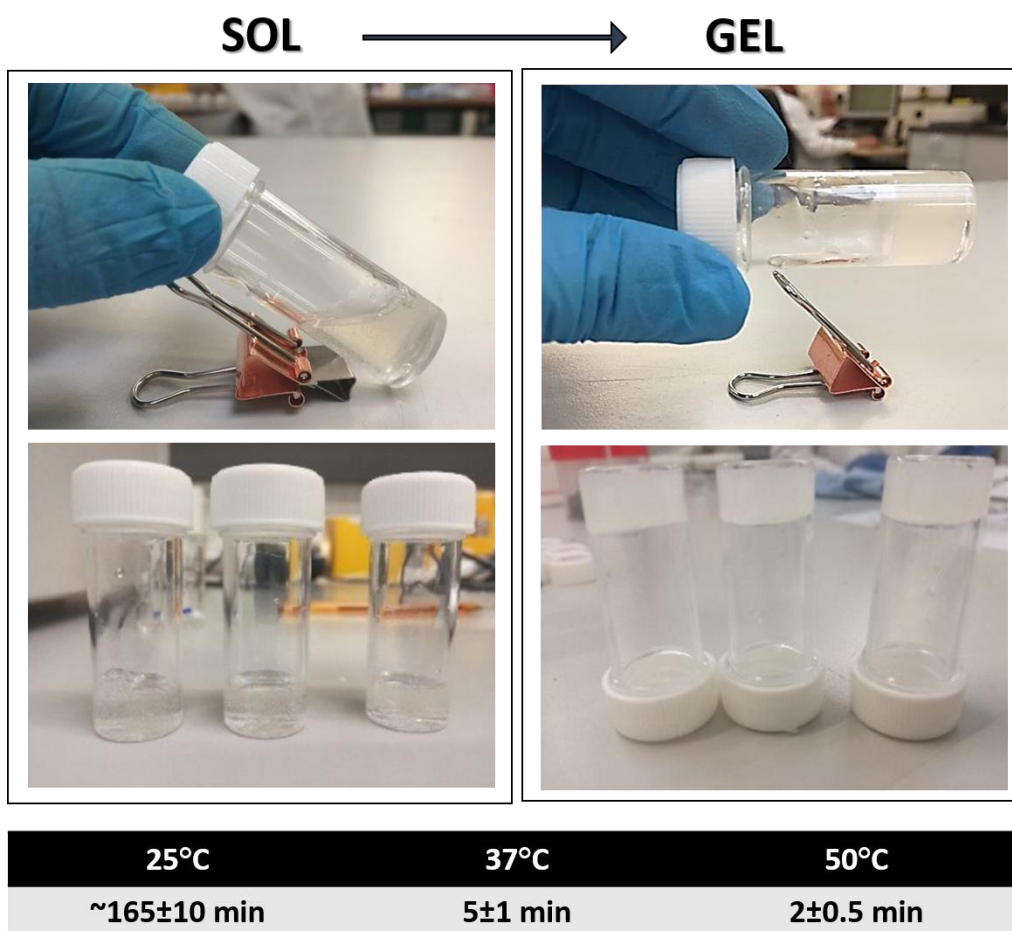
Figure 2.2: This image is representing the sol/gel transition of CH/BGP with temperature. It is shown the tube inverted method on the top images (a triplicate for each temperature) and it is reported the gelation time at the respective temperature tested (5, 25 and 37°C) on the bottom.

The water uptake ability of the chitosan-based hydrogel at 37°C is reported in figure 2.3.The samples displayed an initial rapid water uptake within 30 minutes up to the 183.6±43.7% (figure 2.3, insert). Then, it was found a water uptake decrease within time achieving a value of about the 107.9±14.0 % within around 8 hours. After stabilisation, a water uptake plateau is observed within 48h of analysis.
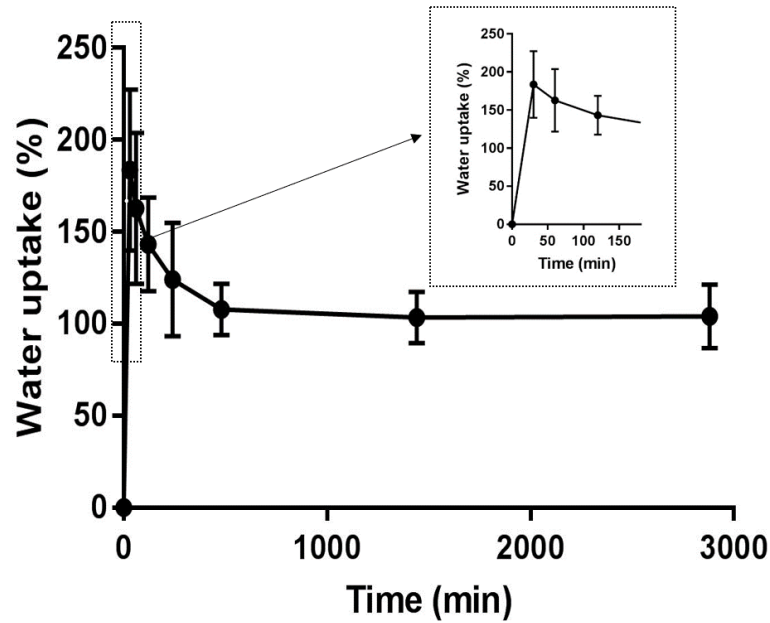
Figure 2.3: Water uptake (%) study of CH/BGP at different time points (n= 3). The insert shows a zoom on the first part of the curve (the first two hours of analysis).

The nutrients diffusion through the hydrogel was tested qualitatively, observing the change in colour of the gels over time when the glucose dye solution was poured in the vial with the gel inside (figure 2.4).

0 min   **30 min**   **3 hour**
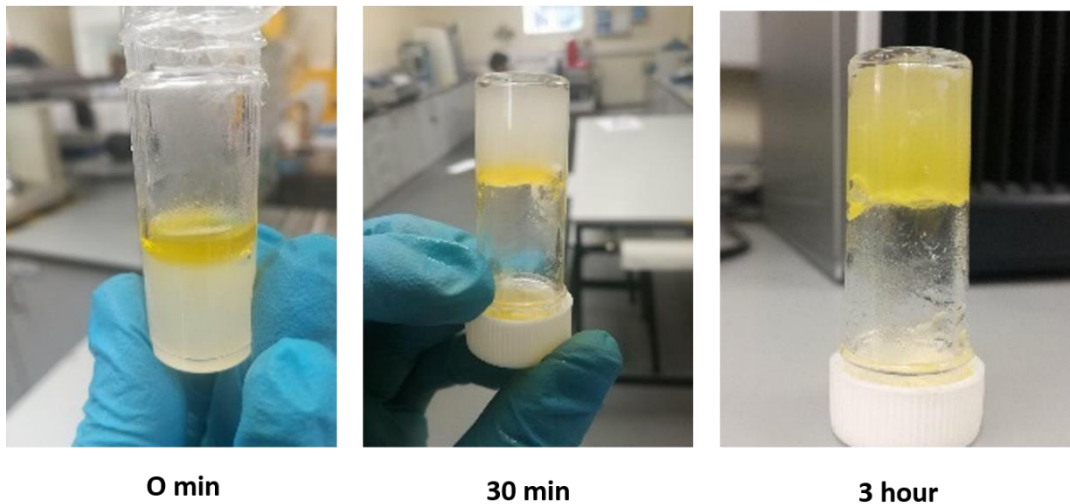
Figure 2.4: Representation of gels nutrients uptake: At the start of the experiment there is an evident separation between the gel and the glucose solution, after 30 minutes it is shown a superficial absorption and after 1 hour the solution has been totally absorbed from the gel.

At the start of the analysis, a clear separation between the white gel and the solution was visible. After 30 minutes, it was noticed a superficial uptake of the dye from the gel, while

after 3 hours it was a total yellow colour of the gel was observed due to a complete uptake of the dye into the hydrogel: this was defined as the time to get a total nutrient uptake. No extra dye was evidenced into the vial, due to the complete absorption into the gel.

The hydrogel absorbance and nutrient permeation capability was evaluated in fluorescence over the course of 48 h. The results are displayed in figure 2.5. The 2-NBDG (glucose analogue) dye uptake was very quick in the first 3 hours of observation, reaching a close-to-maximum uptake plateau between 180 and 200 min. The dye in the solution was able to diffuse across the membrane within 6 hours and after the glucose uptake value stabilised within 12 hours.
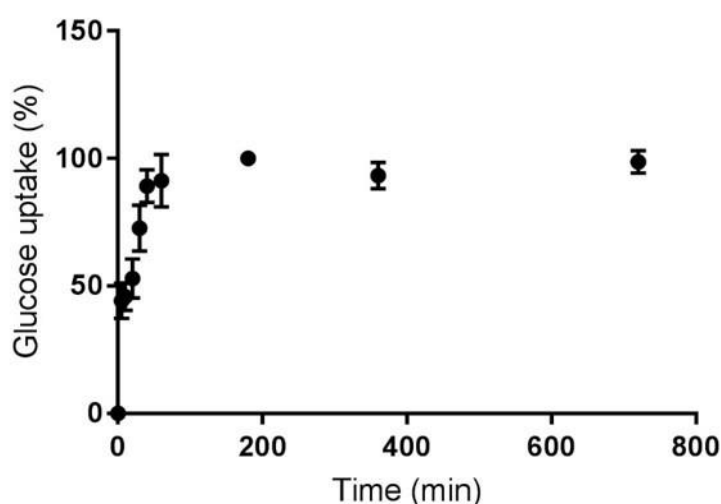
Figure 2.5: CH/BGP gel glucose uptake. A plateau on the uptake of 2-NBDG was reached after about 6 hours (corresponding to 85-90% of maximum uptake) after keeping the gel in contact with the dye solution.

Conductivity analysis demonstrated a BGP concentration-dependent behaviour (figure 2.6). In fact, the chitosan showed the lowest conductivity at each temperature compared to CH/BGP solutions. CH solution conductivity, resulted statistically different from CH/BGP(a), which is the solution with the lowest amount of BGP at 5°C and 25°C ($p < 0.05$) respectively and from CH/BGP(b), that was the composition used in this work with higher BGP concentration, at 5°C ($p < 0.05$), 25°C ($p < 0.001$) and 37°C ($p < 0.0001$). The CH/BGP(a) and CH/BGP(b), with different BGP concentrations resulted as well as statistically different at 5°C ($p < 0.05$) and 25°C ($p < 0.01$) respectively.
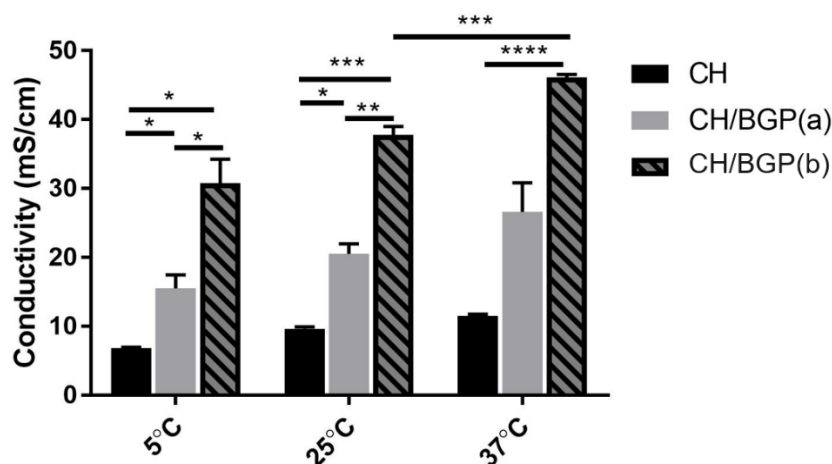
Figure 2.6: Bar Chart representing the conductivity of different solutions at increasing temperatures: 5°C, 25°C, and 37°C. The three different solutions are: CH, CH/BGP 2.5% w/v and R= 2.5 (a), CH/BGP 2.5% w/v and R= 4 (b) (p< 0.05 (*), p < 0.01 (**), p < 0.001 (***), and p < 0.0001 (****).

The temperature-dependence of conductivity is even demonstrated in figure 2.6. In particular, CH/BGP (b) showed a significant increase in conductivity moving from 25°C to 37°C (p < 0.001).

The ζ-potential values obtained from the analysis showed the net charge of the solutions at 37°C due to the amount of negatively charged group present into the CH/BGP solution. Table 7 shows that the CH/BGP(b) solution was characterised by a negative charges.

Table 6: ζ-potential results at 37°C

CH	CH/BGP(a)	CH/BGP(b)
30.2 ± 3 mV	0.06 ± 0.33 mV	-0.47 ± 1mV

2.3.2 Morphological characterisation

Environmental Scanning electron microscopy analysis was performed to evaluate the influence of BGP on the internal chitosan hydrogel morphology, analysing the structure before and after the water uptake (Pre-WU and Post-WU respectively). It was noticed that both samples possess a porous structure with a high degree of interconnectivity and irregular pores shape (figure 2.7). The interior morphology of this hydrogel demonstrated highly porous structure, and the pores formed an interconnecting "open-cell" structure. Differences were found in the hydrogel appearance in the two analysis.

The post-WU sample appeared having smoother pores wall and surface than the pre-WU and this can be clearly observed at the highest magnification (2000x).
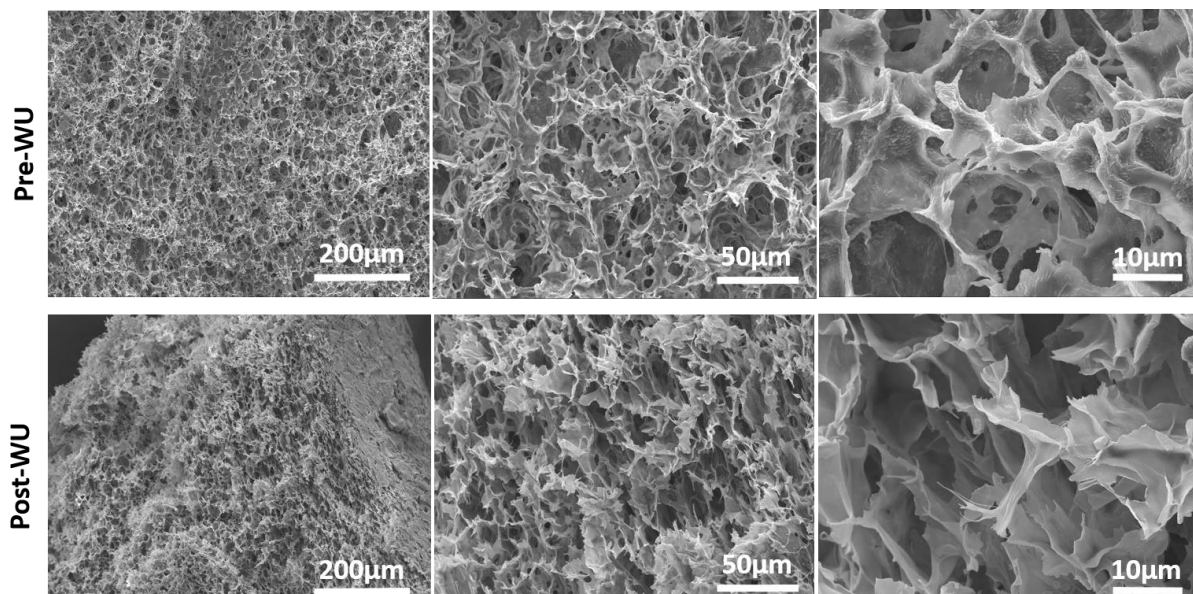
Figure 2.7: Scanning electron microscopy images, representing cross-section microstructure of CH/BGP hydrogel. Two different samples are analysed: pre water-uptake (Pre-WU) and post water-uptake (Post-WU) freeze dried hydrogels, at three different magnifications: 150x, 500x, 2000x.

Differences in pores size were found in the pre and post swelling samples (figure 2.8). In both cases the pores were in the range 5-10 µm. Particularly, in the pre-WU it was found the most of the pores with a diameter below 10µm (64% of pores). The average pore size measured was 5.6±2.6µm. On the other hand, the pores diameter in the post swelling seemed to be bigger and most of them are in the range 5-20µm (86% of pores). The average pore size measured was 11.5±4.1µm.
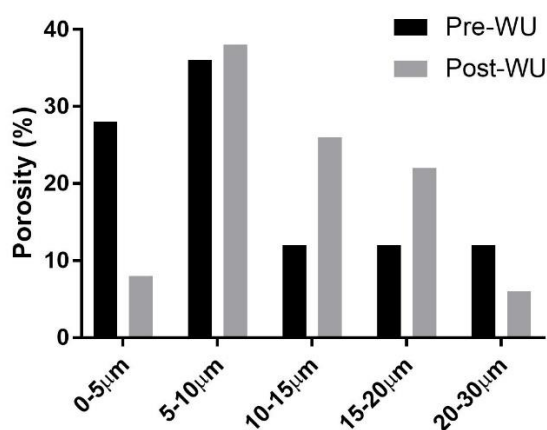
Figure 2.8: Bar Chart representing the percentages of pores, before and after the water uptake analysis. Pores diameter range are: 0-5 μm, 5-10 μm, 10-15 μm, 15-20 μm and 20-30 μm.

2.3.3 Chemical characterisation

ATR-FTIR spectra were measured for individual components (BGP and CH) as well as freeze-dried CH/BGP hydrogels before and after the WU, for analysing the chemical compositions of the four different samples. Figure shows the infrared spectra in a region ranging from 4000 to 550 cm^{-1}. The samples characteristic peaks were highlighted below:

- In the BGP spectrum, the small peak at 1078 cm^{-1} was characteristic for the C-O bond, while the sharpen peak at 963 cm^{-1} was characteristic of the P-O bonds.

- In the CH spectrum, the broad spectrum corresponding to the O-H oscillation was observed in the range of wave number of 3600-3100 cm^{-1} and the asymmetric peak in the range of lower wavenumbers indicated the overlapping with the N-H stretching band masking the broad O-H absorption; the stretching vibration of aliphatic groups (-CH_2) and (-CH_3) was observed at 2970-2880. Primary and secondary amide bands C=O and N-H of CH appear at 1656 and 1601 cm^{-1}, respectively, and in the range of 1500 and 1200 cm^{-1} there were peaks associated with OH oscillations and C-O stretching and finally in the range 1200-800 cm^{-1} the bridge (-O-) stretch of the glucosamine residues and a broad band at 660 cm^{-1} which was connected with vibrations of the O=C-N group

- CH/BGP spectrum indicated shift of the C=O bond from 1656 to 1661 cm^{-1} and the N-H amide band from 1601 to 1567 cm^{-1} (figure 2.9, insert), Moreover, it presented a weaker peak of C=O, O–H and N–H stretching band after gel formation, whereas, two new bands characteristic of BGP appeared in this region which were characteristic for BGP (figure 2.9, insert). The band at 1000 cm^{-1} and 800 cm^{-1} were characteristic of BGP

and indicated aliphatic P-O-C stretching while the band at 1050 cm^{-1} was characteristic of the -PO$_4^{2}$; a shoulder at 920 cm^{-1} was characteristic of the -HPO$_4^{-}$. Finally the CH band at 669 cm^{-1} was divided in two bands in the range 600-700 cm^{-1}.

- CH/BGP spectrum after swelling showed more similarities with the CH spectrum. In fact the BGP characteristic band between 1000 and 800 cm^{-1} were not very evident as well as the intensity of the peak at 920 cm^{-1} decreased compared with the pre-WU hydrogel (figure 2.9, insert). Primary and secondary amide bands C=O and N-H of CH re-appeared at 1656 and 1601 cm^{-1}.
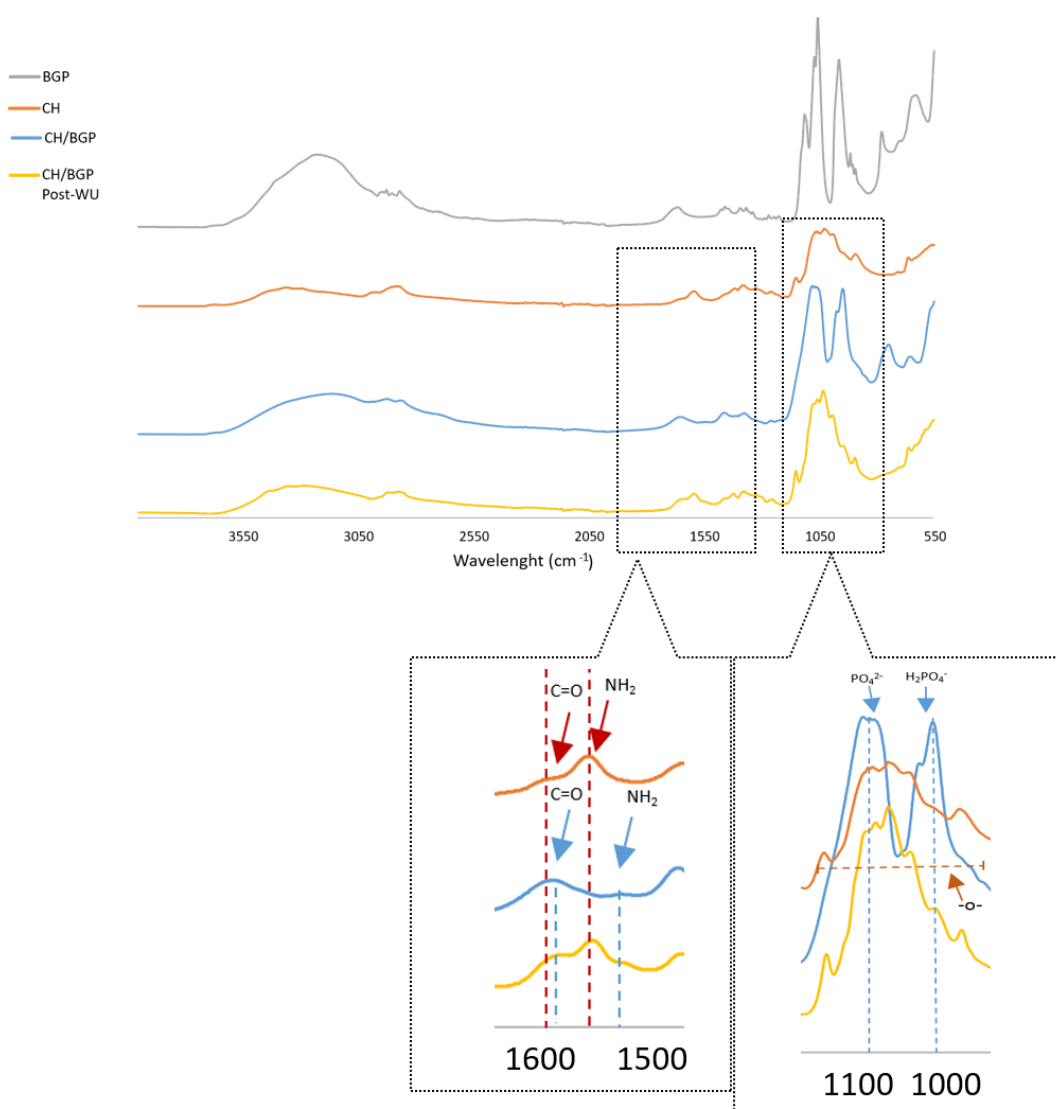
Figure 2.9: ATR-FTIR spectra of β-glycerophosphate salt (BGP), chitosan powder (CH), CH/BHP freeze dried hydrogel and CH/BGP freeze dries hydrogel post water-uptake (CH/BGP Post-WU). Insert: magnification of the wavelength range where the main shifts or changes in peaks were observed.

CH/BGP hydrogel surface chemical composition before and after the WU was also studied by XPS analysis and compared with the CH sample. Figure 2.10(a) reports the three spectra survey while the table (figure 2.10(b)) summarises the element detected in each sample and their corresponding percentage. The results show the presence of oxygen (O_{1s}), nitrogen (N_{1s}) and carbon (C_{1s}), chitosan main elements, in all the samples. Furthermore the sodium (Na_{1s}) and the phosphate (P_{2p}), BGP salt basic elements appeared only after the hydrogel formation in the CH/BGP samples before (18.6% and 7.6%) and after WU (3.70% and 3.1%), with an evident decrease of nitrogen content from 6.7% to 0.9%, as well as che carbon decrease from 63.0% to 32.5% from CH to CH/BGP. The re-increase of those percentage (from 0.9% to 4.6% in nitrogen and from 32.5% to 55.9% in carbon) are evident in the post WU samples . The small presence Magnesium (Mg1s) in the CH and CH/BGP samples can be due to the presence of contamination in the PBS (0.2% in CH and 1.5% in CH/BGP).

a)

b)

SAMPLE	Mg_{1s} (%)	Na_{1s} (%)	O_{1s} (%)	N_{1s} (%)	C_{1s} (%)	P_{2p} (%)
CH	0.2	–	29.8	6.7	63.0	–
CH/BGP	1.5	18.6	38.8	0.9	32.5	7.6
CH/BGP Post-Wu	–	3.70	32.7	4.6	55.9	3.1
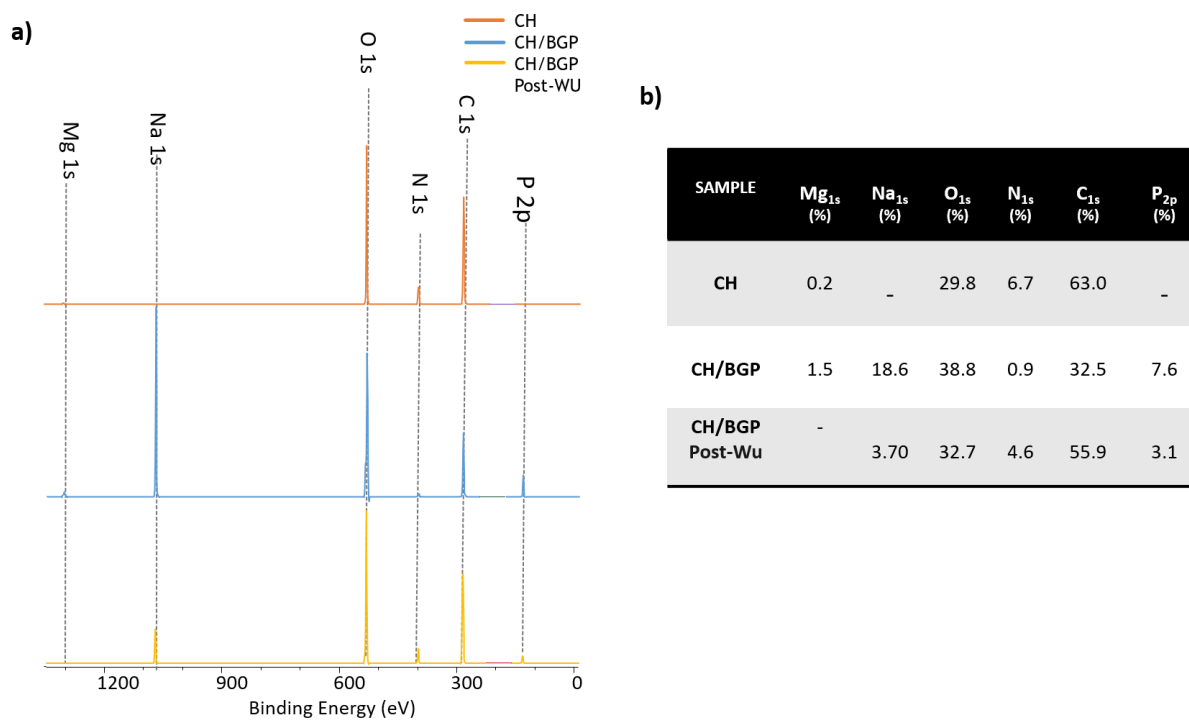
Figure 2.10: XPS spectra survey of CH, CH/BGP freeze dried hydrogel and CH/BGP freeze dries hydrogel post water-uptake (CH/BGP Post-WU). Main elements peaks: Mg1s, Na1s, O1s, N1s, C1s, P2P (a) and the relative atomic percentage of each element in the three spectra are reported in table (b).

High resolution XPS was performed for the C_{1s}, N_{1s}, O_{1s} and P_{2p} and deconvoluted spectra were obtained as shown in figure 2.11 (a), while the table in figure 2.11(b) reports for each element the binding energy of the main bonds and their contribution (%) for each sample. The most evident changes in bonds percentage were:

- C=O (Binding energy 288.5 eV), appeared at 15.8% in CH and decreased to 10% in CH/BGP and 4.7% in CH/BGP Post-WU.

- C-OH (Binding energy 532eV), from 100% in the CH to 40.8% in CH/BGP; an increase to 74.4% was found in the Post-WU samples.

- C=0 (Binding energy 530.9 eV) wasn't present in the CH samples, but appeared in the CH/BGP at a percentage of 40.4% abd in the CH/BGP Post-WU at 22.1%.

- O(H2O) (Binding energy 536 eV), as the previous bond, was not present in the CH samples, but it was present in CH/BGP (18.75%) and CH/BGP Post-WU (3.48%).

- $(PO_4)^{3-}$ (Binding energy 133.2 eV), was absent in the CH samples, but appeared at 100% in CH/BGP and decreased to 17.7% in CH/BGP Post-WU.

- PO_3^- (Binding energy 134 eV) was only present in the CH/BGP Post-WU samples.

	C=0 (-288.5 eV)	C-0H/-NH$_2$ (-286 eV)	C-C (-284.8 eV)	C-NH$_3$ (401.5 eV)	Ar.N (400 eV)	C-N (399.0 eV)	C-0H (532 eV)	C=0 (530.9eV)	O(H$_2$0) (536 eV)	(PO$_4$)$^{3-}$ (133.2 eV)	PO$_3^-$
CH	15.8%	60.6%	23.6%	44.7%	18.2%	37.1%	100%	-	-	-	-
CH/BGP	10.0%	63.6%	26.4%	22.8%	21.3%	56.0%	40.8%	40.4%	18.75	100%	-
CH/BGP Post-WU	4.7%	69.6%	25.6%	14.0%	35.0%	14.5%	74.4%	22.1%	3.48%	17.7%	81.3%
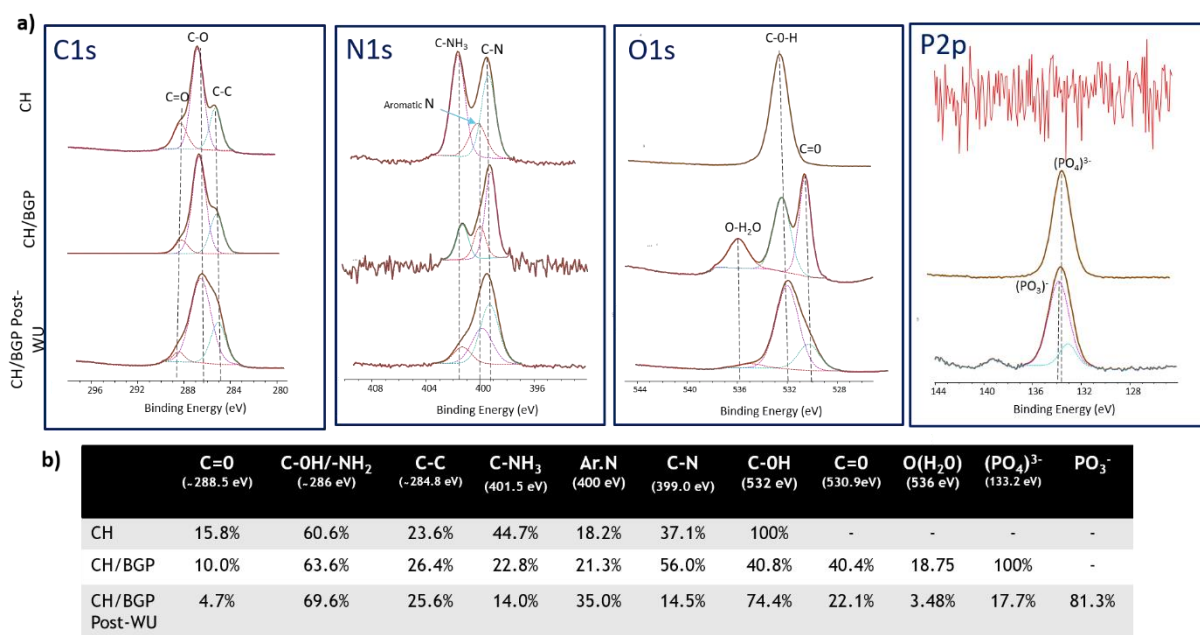
Figure 2.11: XPS high resolution spectra, showing the main elements band and the peaks deconvolution for CH, CH/BGP and CH/BGP Post-WU (a). In the table (b) it has been calculated the percentage of each bond at a determined binding energy,

2.3.4 Thermal characterisation

CH/BGP hydrogels were lyophilized, and the thermal stability and the degradation behaviour of CH, BGP and CH/BGP were investigated through TGA and DSC, as shown in figure 2.12. (Deng et al. 2017).

In the DSC, the first endothermic peak presents in all the sample is at about 70°C. Chitosan presents another, wider, endothermic peak at around 150°C and a big exothermic peak at 300°C. The CH/BGP samples, on the other side, presented a sharper and bigger second endothermic peak at 140°C and a small exothermic peak at 310°C. The first peak was linked to the BGP behaviour with temperature, in fact a similar peak was found in the DSC curve of BGP at lower temperature, which was the only BGP significant peak.

In the TGA, the first weight loss of all three samples took place from about 40 to 100 °C with a weight loss of ~15%. Chitosan showed a second sharp weight loss of about 35% at 160–280 °C and the third stage of its degradation displayed a gently weight loss over 300 °C.

Compared to protonated chitosan, CH/BGP, after the first weight loss in common with the chitosan, presented other two weight loss at 130°C and 250–325 °C, and after those the weight started to decrease slowly, as water began to run off.
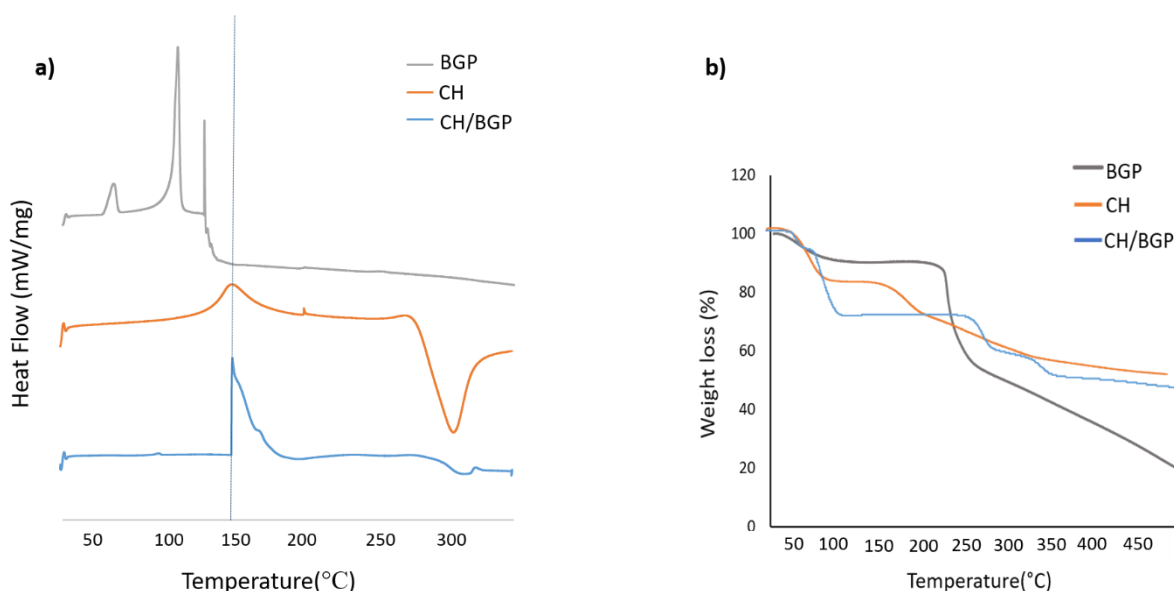
Figure 2.12: DSC and TGA spectra of BGP, CH and CH/BGP. DSC (a) for calculating the Heat flow between 20-350 ° and the TGA (b) for obtaining the weight loss of the BGP, CH and CH/BGP in a range between 25-450°.

2.3.5 Mechanical behaviour

The stress vs. strain curve obtained by the static compression test (figure 2.13), showed an elastic region up to 20% strain for each sample analysed, followed by a densification region up to 50-60% strain that represented the limit where the samples broke (as shown in figure 2.13). All the samples had the trend in terms of transition from the elastic to the densification

region and a representative curve was showed in the figure. The determination of compressive elastic Young's modulus was performed by calculating the slope of the region between 0% and 20% strain. From the obtained curves it was calculated an E of approximately 36 ± 4 kPa.
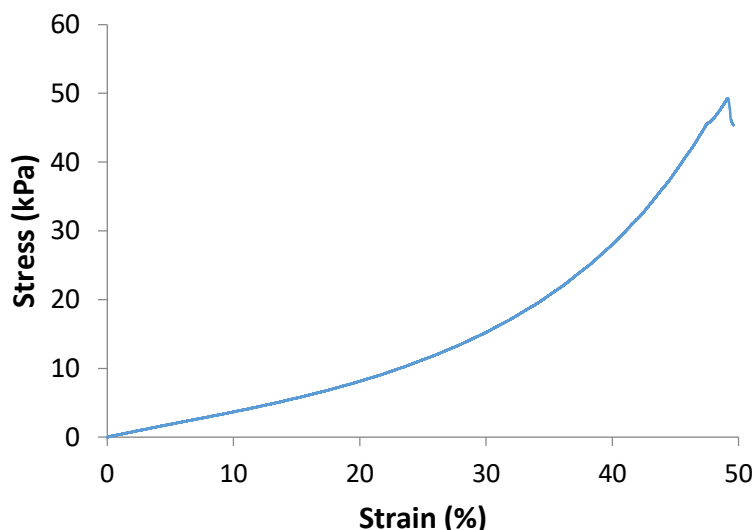
Figure 2.13: Stress-strain curve obtained with one of the three samples analysed.

Following the static mechanical test, the dynamic stress relaxation test was performed (as explained in *par. 1.1.4*).

Figure 2.14a shows the stress-relaxation curve obtained. In the first 60 seconds the stress increased up to 2.8 ± 0.3kPa, which represented the peak stress due to the strain increase from 1% to 10%. The peak elastic modulus was calculated, following the protocol of Liming Bian et al. (Bian et al. 2011) obtaining a value of 29.1 ± 1.0 kPa Then, the strain was maintained constant at 10% and the stress values decreased rapidly from the Peak value to the equilibrium value, obtained after 1000s, that was due to the relaxation "behaviour" of the hydrogel. The equilibrium modulus, obtained from the equilibrium stress value divided by the 10% strain was 17.4 ± 0.8 kPa.

Furthermore, figure 2.14b reports the stress-relaxation curve obtained in Matlab fitting the experimental values with a third order exponential equation, calculated as described in *par.2.2.6.1*. The calculated relaxation times (τ_1 =9.2±0.5 s, τ_2 =65±4.8 s and τ_3 =450+35.7 s) were related with the calculated equilibrium modulus.

Finally, for the viscosity values, the first order exponential equation was used and the relative graph is shown in figure 2.14c). The viscosity value calculated was 88 ± 2.5 MPas.
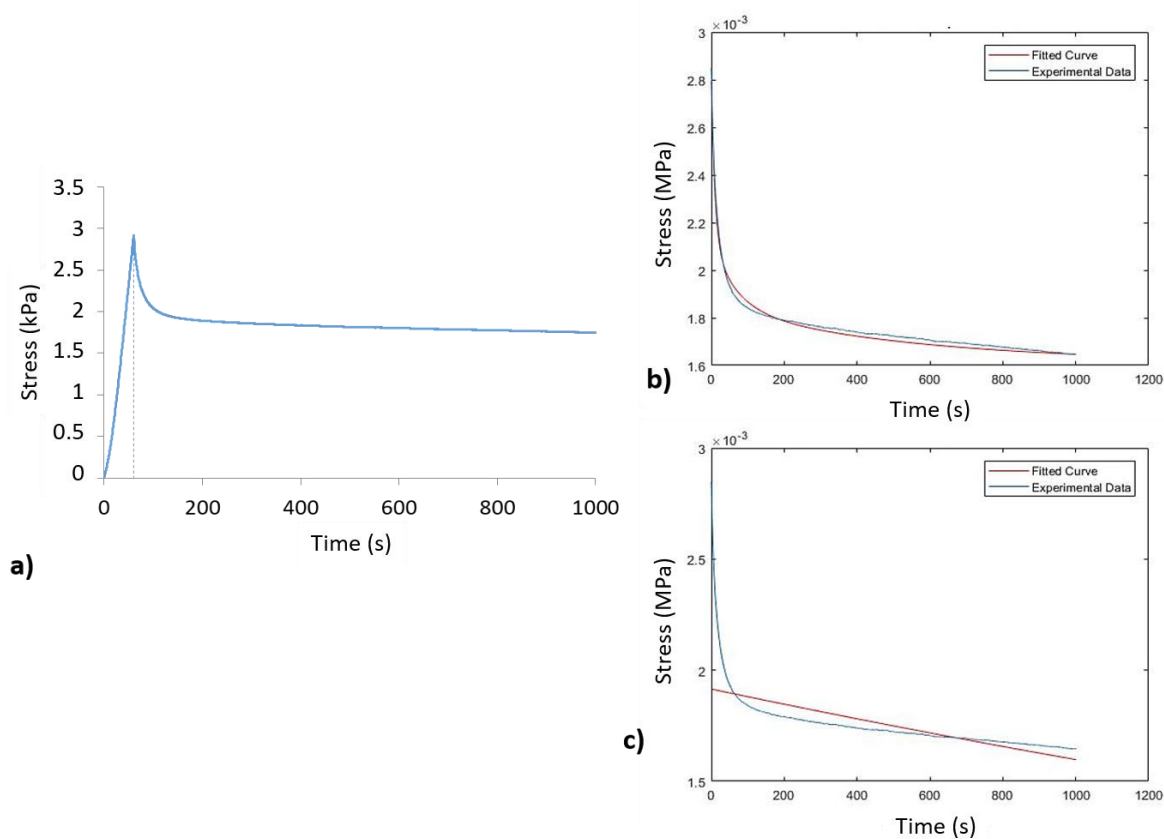
Figure 2.14: Stress relaxation graphs: a) Stress-relaxation curve from experimental data; b) The typical stress relaxation curve obtained after 1000 s, fitting the experimental data with a third order exponential

A further analysis on the mechanical properties has been performed by rheology. Particularly, from the Ramp Sweep Test, different values of viscosity were observed in response to an increase on temperature at constant continuous rotation of 1.5°C/min. Two values are indicated by red arrows in figure 2.15 :(1) is referred to the temperature at which the sol/gel transition started, while (2) belongs to the maximum viscosity temperature. Moreover, the graph shows that the starting transition temperature appeared to be ~35°C and the maximum viscosity of CH/BGP solution was ~340 Pa·s.
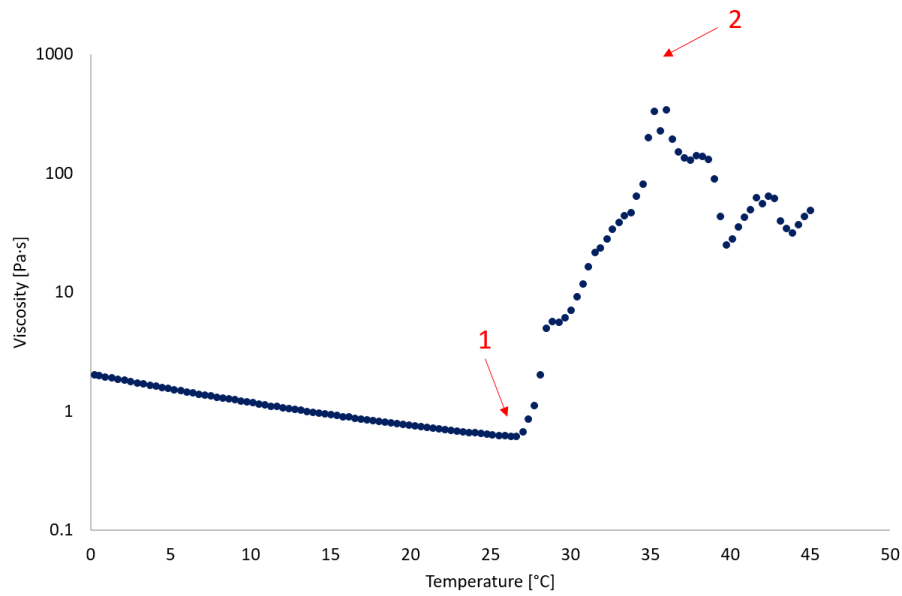
Figure 2.15: Viscosity of CH/BGP solution with the temperature increase. The red arrows are indicating the sol/gel transition temperature (1) and the maximum viscosity value (2).

By monitoring the moduli vs. strain one it was possible to determine the linear viscoelastic region where G' and G'' were independent from shear strain. G' and G'' values analysed for different strain are shown in figure 2.16. The strain range in which those two moduli were linear was from 0.1 to 10 %. Consequently, 1% amplitude of strain was selected to assess the following rheological measurements.
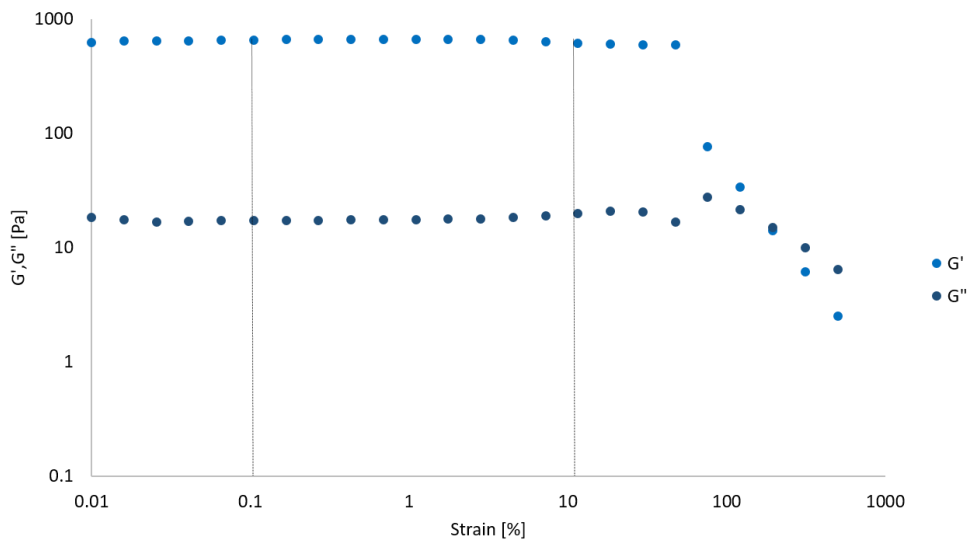
Figure 2.16: Storage (G') and Loss (G'') moduli as a function of strain. The vertical lines delimit the G'-G'' linearity region.

Frequency sweep tests results of CH/BGP solutions at different temperatures with increasing angular frequency from 0.1 to 100 rad/s displayed that G' and G'' exhibited parallel lines and G' values higher than G'' ones along all the frequency range.
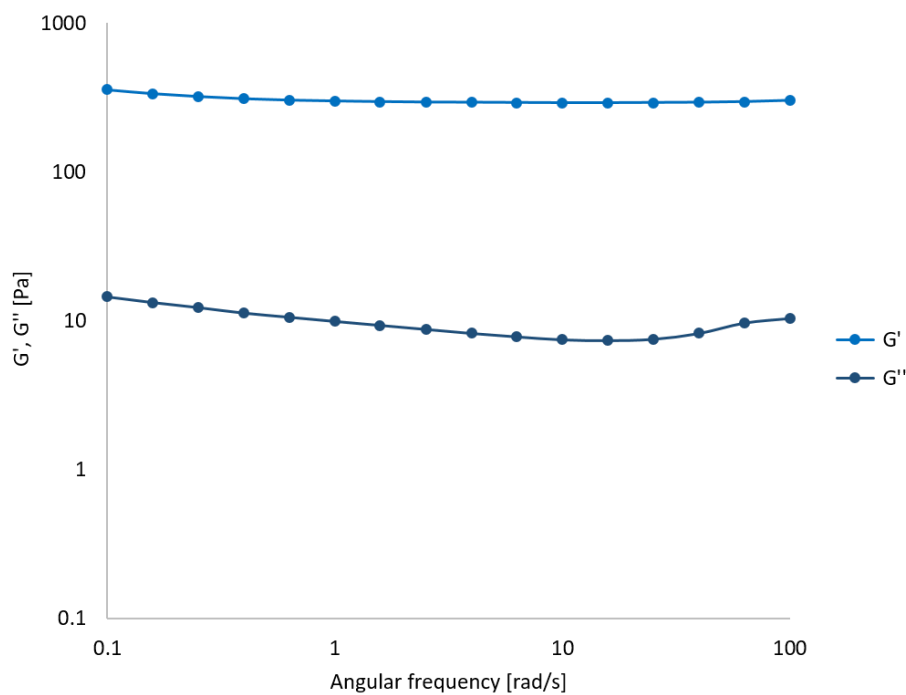
Figure 2.17: G' and G'' as a function of angular frequency between 0.1 and 100 rad/s.

The evolution of G' and G" with the temperature increase was shown in figure 2.18, at constant rotational oscillation. Before the curves crossing, the two moduli decreased as the temperature increased with G'<G" (at 20°C G'= 0.8 Pa while G"= 4.6 Pa). After the crossing point, where the sol/gel transition temperature occurred (in the range 31-33°C), G' became higher than G" (at 50°C G'= 1.6 kPa while G"= 40 kPa).
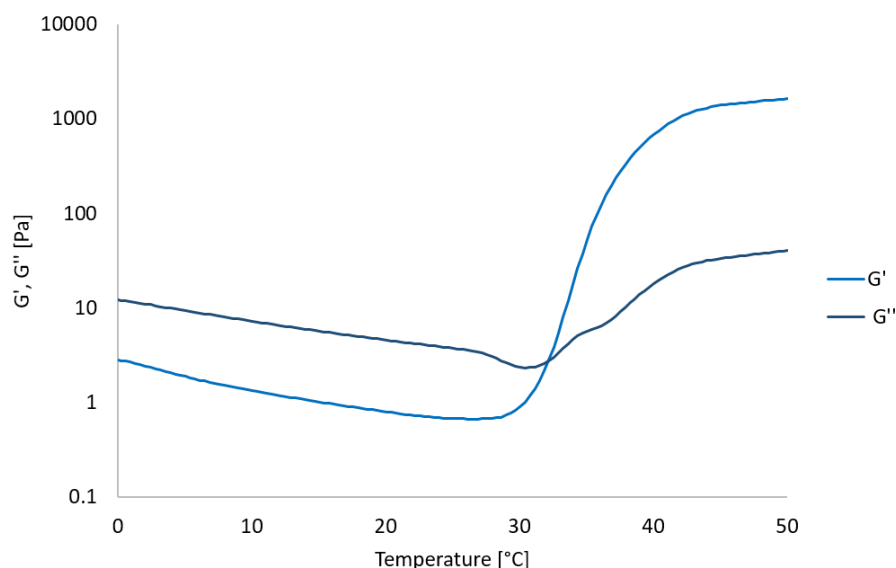
Figure 2.18: G' and G'' as a function of temperature between 0 and 50°C. The curves crossing point is defined as the gelation temperature.

Values of Storage Modulus and Loss Modulus depending on time at constant rotational oscillation and temperature were shown in figure 2.19. When G' and G'' crossed, it meant that G' became higher than G'', and this value of time is the exact time at which the solution became a gel. Increasing the time at 37°C the strength of the hydrogel increased to reach a maximum value after ~20 minutes. Two samples of CH/BGP solution were studied and the gelation times were $t_{S/G}$=156 s and $t_{S/G}$=132 s. Thus, a gelation time of $t_{S/G}$=144 s was considered as the correct value.
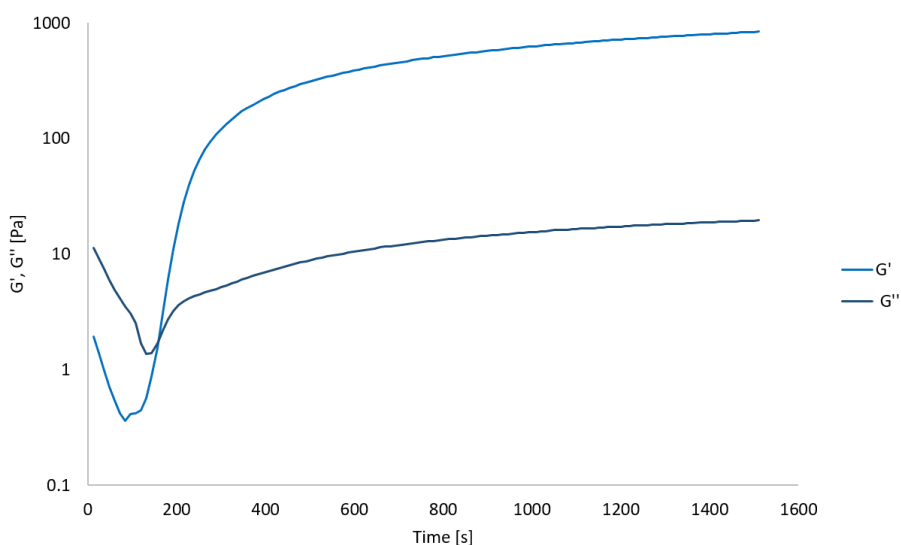
Figure 2.19: G' and G'' as a function of time.

62

2.4 Discussion

A biopolymer-based solution capable to gellify at physiological conditions (37 °C and pH range of 7.0-7.4), in a controlled time, would be ideal for cartilage repair, in a surgical context. The CH/BGP solution has been designed to remain liquid below room temperature and to become gel at physiological conditions (Chenite et al. 2000). In this research work it has been found a gelation time of around 5 ± 1 min at 37°C, suitable for *in vivo* applications with a neutral pH (around 7.0) able to avoid possibility of irritation at the injection site. Considering surgical applications, the gelation time is a challenging factor which can be one of the main determinants for the evaluation of the *in vivo* suitability of the hydrogel. Particularly, with a long gelation time the material can become unstable in terms of handling and implant into the injection site, with possibility to react with surrounding tissues. On the other hand, a rapid gelation time can create issues for the surgeons that cannot have sufficient time for injecting the biomaterials in the area order to secure a successful tissue engineering application (Chalovich & Eisenberg 2013). The studied system was thermally sensitive, liquid (SOL) at the start of analysis at room temperature, flowing into the tube when tilted and gel (GEL) as temperature increased to body temperature, being unable to flow when inverting the tube.

The gelation mechanism of this CH/BGP hydrogel with temperature has been deeply investigated and different theories are proposed in literature. At low temperatures, strong chitosan-water interactions protect the chitosan chains against aggregation and the presence of BGP with mild basic character (pKa 6.63) allows chitosan being in solution, at neutral pH: the glycerol moiety in BGP is presumed to coat CH and prevent chain aggregation. By increasing the temperature, sheaths of water molecules around chitosan chains are removed and chitosan-chitosan hydrophobic interactions are strengthened (Jarry et al. 2002). These hydrophobic interactions and hydrogen binding between chitosan chains play a major role in the gelation of CH/BGP hydrogels. As a result, the gelation of this thermally sensitive hydrogel will be enhanced, and its gelation time will be decreased if the temperature of solution increases.

In general, with a higher salt concentration, the gelation temperature required decreases with a shorter gelation time. In fact, the BGP plays important roles in the system (Zhou et al. 2015): to increase the pH, approaching the precipitation point of chitosan (pH > 6.5), into the physiological range of 7.0–7.4 and to prevent immediate precipitation or gelation, controlling gel formation when an increase in temperature is imposed. At low concentration of BGP salt, the electrostatic repulsion between positively charged chitosan chains does not allow

coagulation of chitosan chains. To neutralize the positive charge density on chitosan chains, a minimum amount of BGP salt is needed. Over this threshold, electrostatic attraction between the phosphate groups of BGP molecules and the ammonium groups of chitosan allows extensive hydrogen bonding via OH–NH and O–HN of chitosan chains. In particular, the time required for gelification at 37°C is reduced with the increase of orthophosphate moles (Nafee et al. 2017a). Nafee et al found a gelation time of 3 min at 37 ^{o}C with a composition of CH (2% w/v)/BGP (8% w/v), which is in contradiction with our results. In this work we evaluated a gelation time of approx. 5 minutes for a system CH (2.5% w/v)/BGP (16% w/v). Thus. other parameters may affect the gelation time, such as the DD or Mw of chitosan and the volume of the solution under analysis (as confirmed from the rheological analysis where a thinner layer is tested and shorter gelation time is observed with all the same parameter than the tube inverted method) (Szymańska et al. 2015). The chitosan DD, has an important role on the gelation time, where high DD increases the cross-link density between the phosphate groups of BGP and the ammonium groups of chitosan chains. In this work the chitosan was characterised by high DD (95%), able to affect dramatically the gelation time (Ganji et al. 2007).

Finally, rheological measurements have been carried out, to have a better comprehension of the CH/BGP system gelation mechanism. The evolution of the storage (G') and loss modulus (G'') were investigated during the heat induced gelation of the CH/BGP solutions in the temperature sweep test (figure 2.18). Three regions were defined according to the temperature range during the heating process, each of them linked to different mechanical properties. In the first phase, at low temperatures, CH/BGP samples showed a viscoelastic fluid-like behaviour where G'<G'' both with a descending trend, common polymeric behaviour (Cho et al. 2005); the minima in both moduli values were preceded by very sharp decreases, reported by Sarkar (Higham et al. 2014; Sarkar & Walker 1995), who interpreted it as the precipitation of a small polymer fraction. In the second phase, after the cross, a fast gelation process occurred, where storage and loss moduli abruptly increased upon heating because of the fast formation of 3D networks between 20 and 30 °C; the growth rate of G' was higher than of G'', indicating that the evolution of the gel structure mainly contributed to the increases of the elasticity in the system. The last phase, the slower gelation process, was characterised by a lower diffusivity due to the increase in viscosity with temperature, as demonstrated by the ramp sweep test (Tao et al. 2000). For 10 < G' < 1000 Pa and G' > G'', the system can be considered as "soft gel" (Hvidt, Joergensen, Brown, & Schillen, 1994).

The ramp analysis demonstrated the viscosity dependence on the temperature (figure 2.15). In fact, the viscosity decreased linearly and slowly from 0°C to 28°C, then the sol/gel transition occurred, leading to an increased viscosity, reaching a maximum value of 340 Pas at 37°C. Similar consideration for the gelation time can be done by monitoring the temporal evolution of G' and G'' in the time sweep test at 37°C (figure 2.19). At time less than 200 s, the magnitude of G' was less than G'', with G' dramatically rising after the crossing point. At 280 s, both modulus started to rapidly increase up to 320 s. Then, a slower increase was observed, and a plateau region was reached at 460 s. These observations could be interpreted in accordance with the gelation mechanism as follows: considering the distance from the crossover point at 37°C, the hydrophobic interactions already formed before starting the test; in the first 280 s, gelation went through a nucleation and growth mechanism, and percolation of hydrophobic aggregates started at 280 s and continues up to 320 s; then, the lower rate of increase of G' and G'' could be ascribed to the gel stiffening through an Ostwald ripening process (Nisbet et al. 2006; Zhou et al. 2015). All these results were in accordance with literature (Chen et al. 2012).

A further key feature for injectable thermogels is the thermal stability of the formulation and the CH/BGP hydrogel demonstrated a good stability. Particularly the thermoirreversibility has been confirmed keeping the gels at RT or 4°C without changes in their physical state. The thermoirreversibility is related to BGP amount and the relative crosslinking strength. For example, as demonstrated by Ganji et al. (Ganji et al. 2007), if the BGP salt concentration increases from 0.33 M to 0.40 M in a solution composed of 2% w/v chitosan (DD=98%) a thermoreversible hydrogel becomes an irreversible hydrogel.

The thermoreversibility of gelation of chitosan hydrogels may be also related to the competition between the different molecular forces involved in gel formation: at low concentration of GP salt, gelation may mainly occur by hydrophobic interactions, which are known to be temperature dependent and cooling the hydrogel causes this weak hydrogel to invert its phase (from gel to sol); at high concentration of GP salt, the hydrogen bonds between chitosan chains and chitosan-water molecules is predominate due to the neutralization effects of GP salt. Since hydrogen bonds are not temperature dependent, cooling the hydrogel did not affect the gel structure (Supper et al. 2014).

The temperature increase and BGP concentration have effects on the CH/BGP hydrogel conductivity. At each temperature (5°C, 25°C and 37°C), the CH/BGP solution with the highest amount of BGP, showed highest conductivity. Moreover a significant increase in CH/BGP

solutions conductivity at high temperature was found that can be correlated with the ionic strength of the solution (Aliaghaei et al. 2012) (figure 2.6). Although the divalent ionization of BGP strongly increased as a function of temperature, ionic interactions such as ionic bridging were reduced at high temperature between BGP and chitosan, because the protonation of chitosan decreased and consequently, the ratio of NH_3^+ in chitosan and $OPO(O^-)^2$ in BGP. As before mentioned, the contribution of ionic cross-linking is not the main driving force for gelation. At room temperature or below, water molecules are presumed to form enclosed structures that surround the polymer chains and, therefore, ionic bridging are likely to be the main force within the solution. The temperature increase enhances the vibration and rotation energy of water, exceeding the ability of weak hydrogen bonds to orient the dipolar water molecules around the polymer chains. As a consequence, the energized water molecules surrounding the polymer are removed, and the dewatered hydrophobic polymer segments (CH_3) begin to associate with each other resulting in an increasing ionic strength as a function of temperature: higher content of not-bonded amine charge are present in solution and the conductivity of the solution, defined as the amount of free charges, is enhanced (Cho et al. 2005). On the other side, this solution has a negative ζ-potential, different from the chitosan solution, which showed a positive value of ζ-potential. This result is related to the amount of negative charge group present in the CH/BGP solution; the CH/BGP solution a lower amount of BGP in fact has a neutral ζ-potential value.

Another important feature that can be considered in the manufacturing of the hydrogels is the water uptake, to assure a good nutrient transport and drug release profile. However an extensive water uptake, linked to a big swelling, could cause discomfort in *in vivo* applications. The water uptake of the hydrogel is a complex process which can be subdivided into several stages (figure 2.3):

- diffusion of PBS into the polymer network through pores in the first 30 minutes, achieving a WU percentage of about 200% (this water uptake ability might be attributed to their high porosity as indicated by the SEM picture in figure 2.7;
- relaxation of hydrated chains and the expansion of the polymer network in the aqueous media up to 8 hours, even if it results to be limited by the presence of BGP;
- stabilisation of the structure over time to 100% of WU, evaluated up to 48 hours (Szymańska et al. 2015).

These WU results showed that the scaffolds were hydrophilic in nature with capacity to hold a large amount of water molecules. However, the ability of the scaffold to hold water molecules within its network is dependent on the architecture of the scaffold (Yan et al. 2010). The sudden decrease in water uptake percentage could be correlated to the salt released from the hydrogel due to the high amount used for obtaining a fast gelification. To better evaluate the salt behaviour during the gel immersion in aqueous solution, chemical, thermal and morphological analysis were carried out before and after the WU analysis.

ATR- FTIR spectrum of the system after gelation indicated changes in terms of chemical bonds such as a reduced peak strength of C=O that revealed the hydrogen bonding presence between the C=O of the chitosan and O-H of BGP, and the N-H chitosan bond with the O-H in BGP group, could explain the strength reduction with the hydrogel formation such as the N-H in the chitosan (figure 2.9) (Skwarczynska et al. 2018). Moreover, the salt loss was demonstrated by the reduction in BGP characteristic peaks in the post WU spectra of the hydrogel, where the amide characteristic peaks of CH were shifted (C=O bond from 1656 to 1661 cm^{-1} and the N-H amide band from 1601 to 1567 cm^{-1})and the BGP peaks at 1050 and 920 cm^{-1} were less Intense.

Furthermore XPS analysis shows significant changes in the structure of the hydrogel before and after the water uptake tests. The survey spectra analysis revealed the BGP addition with the presence of new elements, phosphate and sodium not present in chitosan survey (figure 2.10). A focus on the C_{1s}, N_{1s}, O_{1s} peaks deconvolution showed a strong participation of amino groups and OH in the formation of hydrogels: it was observed a decrease in the contribution of $C-NH_2$ (similar tendency can be observed for C-OH groups), that can be related to the hydrogen bonding and hydrophobic interaction, main reasons for gel formation (Shariatinia & Jalali 2018) (figure 2.11). The decrease of $C-NH_3$ bond can confirm also the ionic interaction between NH_3^+ groups in chitosan and -O- in BGP. In the analysis of oxygen high resolution spectrum, an increasing numbers of C=O bonds due to the presence of BGP sodium and -O- decrease probably after CH chain breaking (Skwarczynska et al. 2018) was observed. Finally, after water uptake test, the samples showed a different shape of P_{2p} peak, characterised by two deconvoluted areas: PO_4^{3-} and PO_3^- as confirmed by the binding energies, compared with the as-prepared samples where P_{2p} only presented the PO_4^{3-} group.

The hydrogel morphology has been analysed before and after the WU, to find differences in the structures (figure 2.7). The lyophilised hydrogel section appeared more rough and heterogeneous before the water uptake that was due to the salt presence on the pores walls.

A different behaviour was found after the water uptake: the pores walls were smoother and the presence of the salt seemed completely disappeared. This demonstrated that after the water uptake stabilisation (about 8 hours), most of the salt was released, while the already formed hydrogel was structurally stable. This quick release of BGP salt is suitable for tissue engineering application and particularly in cell-laden hydrogels, because the salt can influence negatively the biocompatibility and cell viability, against previous studies demonstrated (Assaad et al. 2015).

Furthermore, tissue engineering scaffolds should ideally exhibit similar structural complexity as the native tissue to satisfy the intended biological function. The CH/BGP hydrogel was found to possess an open porous and interconnected network in both cases, essential for cell nutrition, proliferation and migration. Natural tissue, such as articular cartilage have a gradient porous structure and this gradient also enables specific cell migration during tissue regeneration, and is also required for the treatment of articular cartilage defects in osteochondral tissue engineering (Gerhardt & Boccaccini 2010; Harley et al. 2006). This porous structure is also important for the mechanical integration with the surrounding tissue, to obtain a mechanical stability, essential for the articular cartilage.

The porosity and pore size of 3D scaffolds have direct implications on their functionality during biomedical applications (Loh & Choong 2013). Moreover, the high water content of scaffolds, analysed in the water uptake test, allows for the transport of nutrients and waste through the matrix. Indeed, nutrients absorption was enabled by this structure, as demonstrated by the 2-NDBG uptake in around 3 hours: this analysis was used primarily to directly monitor glucose uptake by hydrogel encapsulated or migrating living cells and neoformed tissues (figure 2.5). Protein adsorption is regarded as the initial event which occurs when biomaterial construct is placed in biological surroundings. Biomaterial constructs requires protein adsorption as prerequisite for cellular adhesion and interaction. Proteins are key intermediates for cellular interaction and further signalling cascades governing cell migration, attachment and differentiation (Dang et al. 2012). The diffusion and release of nutrients test, on the other side, demonstrated the structure ability to uptake and release nutrients over time, important tissue engineering task for time-dependent drug delivery and sustained release, as well as for encapsulating cells and giving them nutrients through the medium that can diffuse through the gel.

The pores size measurements showed a 0-30 μm diameter range of distribution of pores that represents a suitable range for cells application, in agreement with previous studies (M.

Iliescu, C.D. Hoemann, M.S. Shive, A.Chenite 2008). Natural tissues have pores in the range of nanometer, but macropores are essential to provide space for nutrient diffusion and waste removal, while a denser structure will improve the mechanical properties of scaffolds and enable better cell attachment and intracellular signalling (Loh & Choong 2013).Furthermore it was demonstrated a slight difference in the pre-WU and post-swelling samples in terms of pores diameters (figure 2.8). Mainly, in the post WU, we observed a lower number of pores with diameters below 10μm, compared with the pre-WU samples, where the pores were mostly in the range 0-5μm. These results highlighted as well the salt. In fact in the pre-WU samples, pores were shrinked by the salt placed at the edges that was not present in the post-swelling samples.

However, the mechanical properties that are important features in maintaining the structural stability of the biomaterial are often compromised by the increased porosity. Kelly et al. reported that the native articular cartilage has a compressive Young's modulus ranging from 100-1000 kPa (Kelly et al. 2013). In this experiment, the hydrogels manufactured exhibited lower compressive Young's moduli than that of the native cartilage, but interestingly all the samples showed high values than those found in literature for soft tissue and cartilage regeneration hydrogels. This could be linked to the amount of crosslinking agent that is very influential on the structure of the polymer and on the mechanical properties. In addition to static compression test, the viscoelasticity of the samples was evaluated by stress relaxation test in which the load decreased at fixed strain of 10% in response with time, after an initial 60s strain growth (figure 2.14). The 10% value is in the range in which G' and G" were constant and independent from the strain as found in the strain sweep test. The storage modulus G' remained constant at low strain, but abruptly decreased at around 50% strain and it could be explained as a disruption of interactions inside the structure. In fact links between particles, inside the gel, can be stretched up to a certain maximum and after this point and after this the system can be destroyed [ref]. On the other side, the loss modulus remained constant in the whole range of strain.

The stress-relaxation behaviour of the prepared hydrogels was compared with that of native tissues, since it affects loads transfer, as well as nutrients diffusion. Wagenseil et al. proposed the generalised Maxwell model, consisting in three relaxation times ($\tau_1=1$–10 s, $\tau_2=10$–100 s and $\tau_3>1000$s) for modelling soft biological tissues to evaluate their viscoelastic behaviour. The calculated relaxation times were similar to the values reported in literature for polymeric gels (Wagenseil et al. 2003). These relaxation times are related with the calculated equilibrium

modulus of about 18 kPa ±SD. Theoretically, the confined compression behaviour of poro-elastic materials is determined by equilibrium modulus and Nguyen et al., reported that mechanical properties of cartilaginous biological tissues, such as articular cartilage are in the immature state 0.1 - 0.3 MPa and in mature state of 0.19 - 2.1 MPa respectively, and also meniscus 0.38-0.49 MPa and intervertebral disc (IVD) 0.38 - 1.01 MPa (Nguyen et al. 2012).

Finally, the frequency dependence of the moduli storage and loss moduli is a critical hydrogel characteristic to observe and appreciate the material phase as quite solid-like (G′ ≫ G″) at a high frequency/fast time scale but more liquid-like (G″ > G′) at low frequency/long time scales.(Yan & Pochan 2010)

CH/BGP has been reported by Supper et al, to display a semi-dilute solution rheological behaviour as viscous liquid or unstructured fluid, when measured at low temperature (around 10 °C). In this work, after incubation at 37 °C, rheological frequency sweep test reported a nearly G′ frequency independent behaviour (figure 2.17), confirming previous analysis (Chenite et al. 2001), while G″ increased slightly with frequency, as it is characteristic for hydrogels. The frequency sweep test, confirmed the mechanical strength of the hydrogel, through the value of the storage modulus in the range of kPa, which represents the elastic behaviour of the gel and by the difference between G′ and the loss modulus G′′, reflecting the viscous behaviour of the gel (Supper et al. 2014; Aliaghaei et al. 2012).

The weight loss and heat flow analysis were performed with DSC and TGA analysis to further analyse CH/BGP temperature behaviour, comparing it with the pure elements: CH and BGP. The weight loss in CH/BGP at less than 100 °C, even found in CH and BGP spectra, is due to the loss of free water in samples (figure 2.12) (Deng et al. 2017). After this, there are present two weight loss between 100°C. and 300°C., the first is due to the decomposition of BGP as showed in the DSC by the endothermic BGP peak before 130°C and the second weight loss might be assigned to the loss of water linked to chitosan through hydrogen bonds which will be decreased at high temperature, because of the hydrophobic prominent interaction at high temperature. This second weight loss could be observed at lower temperatures in chitosan samples (around 200°C). Then, bound water began to run off and the weight starts to decrease slowly. Finally, the third stage of degradation, due to the chitosan pyrolysis started by a random split of the glyosidic bonds, followed by further decomposition and elimination in volatile products. It was found that the energy released by chitosan pyrolysis caused exothermic events in DSC curve. The decomposition states of hydrogels started at about 400 °C, which was higher than that of chitosan. At 800 °C, the weight of hydrogels remained about

40% and protonated chitosan remained about 3%. All of these indicated the thermostabilization of chitosan were enhanced by the crosslinking agents (Maity et al. 2016).

Chapter 3. Hydrogel Biological Characterisation

In this section, human TERT immortalised bone marrow stromal cell line (Y201 MSCs) and human articular chondrocytes (hACHs) culture methods are described.

In order to test the system biocompatibility, Y201 MSCs were seeded or encapsulated into the CH/BGP hydrogels and studied in terms of viability (Live/Dead assay), metabolic activity (PrestoBlue assay) and cell morphology (Dapi/Phalloidin immunostaining).

Then, a co-culture model for cartilage regeneration was realised by using the mentioned above hACHs and Y201 MSCs with the aim of *in vitro* mimicking of the real *in vivo* environment. Thus cartilage-like ECM main components formed after co-culturing period was analysed and compared to monocultures. Particularly, histological analysis to have a qualitative assessment of Collagen type II and GAGs production, immunofluorescence analysis for Collagen type II production and CD44 (chondrogenic marker) expression, SEM analysis to investigate cells morphology within the constructs and mechanical analysis (stress-relaxation) were performed.

3.1 Cell culture protocol

3.1.1 Human TERT immortalised bone marrow stromal cell line culture

Human TERT immortalised bone marrow stromal cell line were kindly supplied by Prof P. Genever (York University) at passage 84 and cultured as already described (James et al. 2015). Briefly, cells were grown at 37°C, 5% CO_2, in Dulbecco's Modified Eagle Medium (DMEM, Sigma) with low glucose content, supplemented with 10% fetal bovine serum, 2mM L-glutamine and a 1% penicillin-streptomycin mixture (100U/mL).

After the expansion, cells were used between passage 86 and 90 seeded on the top or embedded into the gel as describe below.

3.1.2 Chondrocytes culture

Human articular chondrocytes (hACHs) were cultured as recommended by the seller (Lonza Biosciences, Switzerland). Cells were kept at 37°C, 5% CO_2 and cultured in Chondrocyte Growth Medium ready-to-use (PromoCell, UK) at 37 °C in a humidified atmosphere incubator containing 5% CO_2 and subcultured to passage 6-7 for the experiments.

3.1.3 Cells seeding and encapsulation

For the cell seeding on the top surface, hydrogel samples (6 mm diameter and 3 height), prepared following the protocol in *par. 2.2.1*, were sterilized after gelification with a UV lamp (256 nm) for 30 min and then 30×10^3 Y201 MSCs were seeded. As control 30×10^3 Y201 were seeded on seeded on glass coverslips (6 mm diameter).

For the cell encapsulation, 200 µL of the CH/BGP solution was poured into a membrane-based cell culture insert (Millicell, membrane pore size of 0.8 µm, Merck, Millipore, Germany) at room temperature and Y201 MSCs were added and mixed gently with the CH/BGP solution at an optimised cellular density of 2×10^6 cell/mL following the consideration reported also by Liu et al (Liu et al. 2018). The inserts containing the prepared solution were placed in 24 multiwell plates and allowed to gellify in the incubator (37°C and 5% CO_2). Finally, after 30-45 minutes fresh DMEM (1 ml) was added into each well.

The medium was refreshed two–three times per week.

3.1.4 Co-culture of MSCs with Chondrocytes

3.1.4.1 Spheroids culture

For spheroids formation, hACHs or Y201 MSCs were trypsinised and counted, respectively at p.5/p.6 for chondrocytes and p.85/p.86 for MSCs. Then, cells were resuspended, centrifuged and seeded in one well of a round bottom 96-wells plate (non-tissue culture treated) at a density of 2×10^5 cells per well (at a concentration of 2×10^5 cells/20µL medium). For the spheroids culture serum free DMEM supplemented with 0.25% Methylcellulose (MC) for Y201 and chondrocytes growth medium supplemented with 0.25% MC for hACHs were used. After 30 minutes of incubation, the respective medium was added to each well in order to achieve 150µL. The experiments were carried out with and without MC in order to assess the utility of this element to obtain a non-necrotic pellet (Zhao et al. 2018; Westendorf & Van Wijnen 2014; James et al. 2015).

3.1.4.2 Co-culture system setup

To set up a direct-contact co-culture system, a chondrocyte spheroid was cultured on the top of a MSCs-laden hydrogel in Chondrocytes growth medium. In order to get consistent results to discuss, three different controls were selected and all the results were compared (figure 3.1) in terms of production of cartilage-like ECM components.

The four systems analysed were:

a) Co-culture (CC): a chondrocytes pellet seeded on Y201 MSCs-laden hydrogel, supplemented with Chondrocytes growth media;

b) Control 1 (CTRL1): a Y201 MSCs pellet seeded on Y201 MSCs-laden hydrogel, supplemented with Chondrocytes growth media;

c) Control 2 (CTRL2): a Y201 MSCs pellet seeded on Y201 MSCs-laden hydrogel, supplemented with Chondrogenic growth media;

d) Control 3 (CTRL3): a chondrocytes pellet seeded on the hydrogel (without cells), supplemented with Chondrocytes growth media.
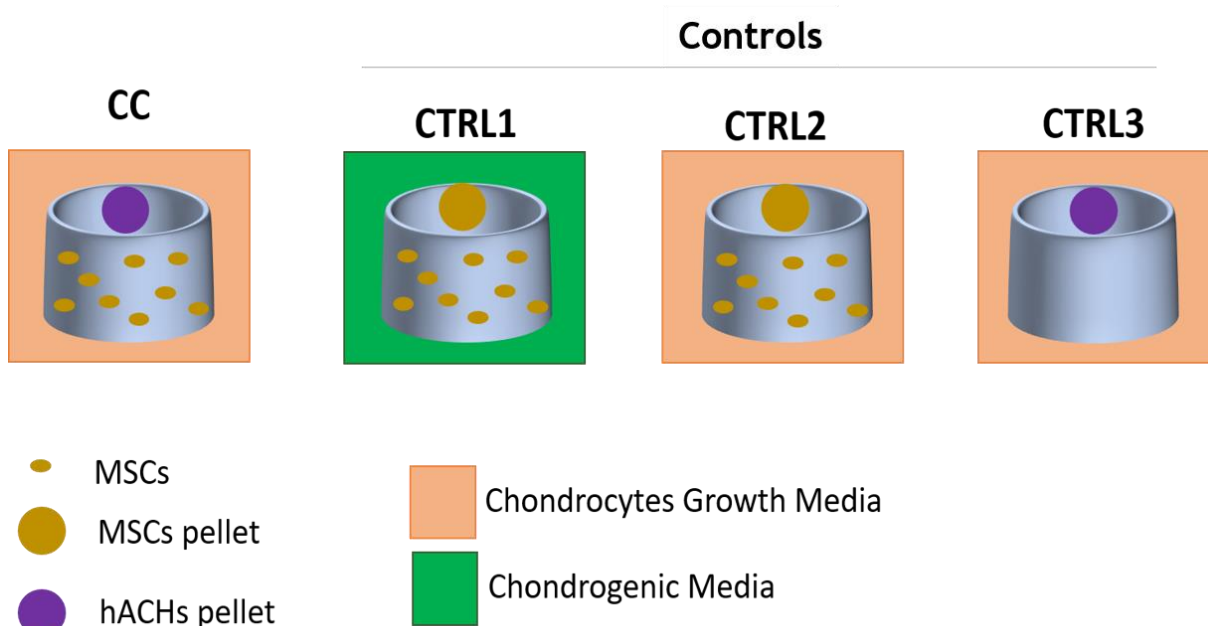
Figure 3.1: Representation of the Co-culture system and controls. CC: Co-culture of MSc encapsulated hydrogel with chondrocytes pellet, in chondrocytes growth media; CTRL1: MSCs encapsulated hydrogel with MSCs pellet, in chondrogenic media; CTRL2: MSCs encapsulated hydrogel with MSCs pellet, in chondrocytes growth media; CTRL3: Empty gels with chondrocytes pellet, in chondrocytes growth media.

3.1.4.3 Construct co-culture manufacturing

After one day of spheroid culture, the hydrogels were prepared following the same procedure reported in *par. 3.1.3*, but using 100µL of gels with the same Y201 MSCs cell density. After formation of the hydrogels, pellets were aspired from the 96-well plate and placed on the top of the respective gels. Chondrocytes growth medium was added to CC, CTRL2 and CTRL3 while chondrogenic media (serum free DMEM with P/S supplemented with 1%ITS+1 (Sigma), 10

ng/mL TGF-β3 (Gibco), 40µg/mL L-Proline (Sigma), 100 nM Dexamethasone (Sigma), 50 µg7mL L-Ascorbic acid-2-phosphate (Sigma) was added to CTRL1.

3.2 Characterisation Methods

3.2.1 Cytotoxicity of the gel

Hydrogel cytotoxicity was evaluated on hydrogel extracts following the international standard ISO 10993 (Goode 2016) (Deng et al. 2017). Briefly, 0.5 ml of CH/BGP solution was poured in a 12-well plate and let gellify at 37 °C in an incubator. Then 2.5 ml DMEM (supplemented with FBS and P/S) was added on the top of each gel and incubated for 24 h. Y201 cells were seeded in a 96- well plate at a density of 5000 cells/well and in a 48-well plate (on 6 mm diameter coverslips) at a density of 30000 cells/well and incubated for 12h. Then, the culture medium was removed and replaced with 100 µl hydrogel extracts. Cytotoxicity has been evaluated after 24 h and 48 h through live/dead on 48-well plate seeded cells coverslip and PrestoBlue on 96-well plate seeded cells.

3.2.1.1 Live/dead

Live/Dead assay (LIVE/DEAD® Cell Imaging Kit, Life Technologies, Thermo Fisher Scientific, UK) was used according to the manufacturer`s instructions. This fluorescence-based kit combines calcein AM and ethidium bromide to yield two-color discrimination of the population of live cells (green) from the dead cells (red) population. Each cell culture condition was washed twice with PBS before incubation with stainings. In brief, 4 µM ethidium homodimer-1 and 10 µM calcein dilute in PBS, were incubated in the dark with the cell-seeded and the cells encapsulated samples for 30 min at 37 °C (Montalbano et al. 2018). For the Live/Dead images, a Countess II FL Automated Cell Counters (ThermoFisher Scientific, UK) was used.

3.2.1.2 PrestoBlue

The PrestoBlue assay was exploited to test the metabolic activity of cells seeded in the 96-well plate both with the extract and with normal media at 24h and 48h of culture. Culture medium was removed at each time point and samples were washed with pre-warmed PBS at 37 °C. PrestoBlue™ reagent (Thermo Scientific, USA) was warmed up and diluted in DMEM (1:10) protected from light; 250µL of solution was added to each well with the gel and incubated for

2.30 hours at 37°C, 5% CO_2. Then, 100μL of each well solution (in duplicate) was transferred to a white bottom 96-well plate and a LS-50B Luminescence Spectrometer (Perkin Elmer, Waltham, MA) was used to measure the fluorescence (560 nm excitation and 590 nm emission). At each time point, after removing the PrestoBlue solution, the samples were washed with PBS twice to delete any residues of PrestoBlue solution, and fresh media was added for the next time point. The obtained values were corrected subtracting the average fluorescence of control wells with only PrestoBlue solution.

3.2.1.3 Transmittance electron microscopy

Morphological assessment was conducted by TEM for investigating the polymer localization and cell structure (organelles and internal structure) using a Phillips CM 100 Compustage (FEI) transmission electron microscope (TEM) (Philips) at HV = 100.0 kV, and digital images were collected using an AMT CCD camera (Deben) with a range of magnification up to 130,000x. Cells encapsulated in the hydrogels were fixed overnight using a pre-warmed solution of 2% glutaraldehyde (TAAB Laboratory Equipment) in sodium cacodylate buffer at 4 °C, followed by a post-fixation with 1% osmium tetroxide (OsO_4) (Agar Scientific). After various dehydration steps, hydrogel were embedded in resin, and cut in ultrathin sections using a diamond knife on a Leica EM UC7 ultra microtome (Leica Microsystems). The sections were stretched with chloroform to eliminate compression, mounted on Pioloform-filmed copper grids (Agar Scientific) and ready to be visualized.

3.2.2 Cells seeding and encapsulation

3.2.2.1 Live/dead

In order to assess cells viability on the top of the gel or dispersed into the gel, the Live/Dead staining was performed, as explained in *par. 3.2.1*. The time point analysed were 1 and 3 days. Samples were imaged after the incubation with the Live/Dead solution at 37°C, immediately using respectively a fluorescence microscope (LEICA DM LB2 Microscope for the cells seeded hydrogel. Analysis of cells encapsulated viability was performed using a Nikon A1R confocal laser, inverted microscope (Nikon, Japan) using constant illumination and capture parameters. In particular, a Galvano scanner was used to acquire 2-5 μm thick z-stacks through the entire thickness of the sample using either 10x (Nikon Plan Apo λ 10x NA 0.45; working distance 4mm, FOV 1.27 x 1.27mm) or 20x (Nikon Plan Apo λ 20x NA 0.75; working distance 1mm, FOV

0.64 x 0.64mm) objectives. Some of the images were acquired as z-stacks, and a maximal projection algorithm was used for 3D reconstruction. Micrographs were then analysed using the NIS-Elements and ImageJ v1.46 software packages.

3.2.2.2 PrestoBlue

For studying the cells metabolic activity, the PrestoBlue assay was exploited for cells seeded on the scaffolds and encapsulated after respectively 1, 3, 7 days of culture and 1 and 3 days, following the protocol of *par. 3.2.1*.

3.2.2.3 Immunostaining

The morphology of the cells was observed by staining their cytoskeleton using rhodamine-phalloidin and the nucleus observed using 4', 6- diamidino-2-phenylindole (DAPI). After 1, 3 and 7 days for the scaffold seeded with cells ,and after 1 and 3 days for the scaffold with cells encapsulated, samples were fixed in pre-warmed 4% w/v paraformaldehyde (PFA) for minimum 15 min at room temperature (or longer at 4°C), washed three times with PBS. Cells were permeabilised using 0.1% v/v Tween20® (Sigma, Life Science) in PBS for three washes. Rhodamine-phalloidin was prepared using 1:100 dilutions of phalloidin-tetramethylrhodamine B isothiocyanate (Sigma) in 0.1% PBS/Tween20® for 20 min at room temperature, covered from light. Residue of phalloidin-rhodamine was removed by washing samples with 0.1% PBS/Tween20® solution three times. Following this, samples were immersed in DAPI solution (1:2500 in 0.1% PBS/Tween20®, Vector Laboratories) for 10 minutes at room temperature protected from light. Then, samples were washed other three times with 0.1% PBS/Tween20® and were imaged using a Nikon A1R inverted confocal microscope at 20x magnification as explained in *par.3.2.2.*1 (Ribeiro et al. 2017).

3.2.2.3 Mechanical analysis

The stress relaxation test were performed after cell culture period, following the protocol used by Bian et al. (Bian et al. 2011), in order to get information about the change in the hydrogel viscoelastic behaviour after Y201 MSCs encapsulation. Briefly, at three different time points (0, 15 and 30 days), samples were removed from the culture, washed with PBS and the experiment was carried out following the protocol explained in *par.2.2.6.2.*

3.2.3 Co-culture assessment

3.2.3.1 Immunofluorescence analysis

The co-culture samples were fixed in pre-warmed 4% w/v PFA for 30 min in the incubator, washed three times with 0.1% PBS/Tween20® for 5 min, blocked for 1 h in PBS supplemented with 2% BSA at 4°C and incubated overnight with primary antibodies: polyclonal Anti-Collagen II (Anti-Col II)(ab34712, abcam,) diluted in 0.1% PBS/Tween20® (1:200) (Berg et al. 2010) and monoclonal Anti-CD44 [EPR18668] (ab189524, abcam,) diluted in 0.1% PBS/Tween20® (1:250), following the product datasheets. Samples were washed twice with 0.1% PBS/Tween20® for 5 min and incubated with Anti-Col II secondary antibody, Alexa Fluor® goat anti-rabbit igG (H+L) (ab150080, abcam) diluted in 0.1% PBS/Tween20® (1:1000) for 1 hour at room temperature. Then, samples were washed twice with 0.1% PBS/Tween20® for 5 min and incubated with Anti-CD44 secondary fluorescein-labelled goat anti-rabbit IgG (H+L) (F2765, Thermo Fisher Scientific) diluted in 0.1% PBS/Tween20® (1:1000), for 1 h. Sample were re-washed twice with 0.1% PBS/Tween20® and DAPI staining for nuclei was performed (as explained in *par. 3.2.2.3*) and imaged using a Nikon A1R confocal laser microscope. Images were acquired at two different time points 7 and 14 days.

3.2.3.2. Histological procedure

For the histological analysis of constructs, all samples were fixed in pre-warmed 10% formalin (24 h), and transferred to 70% Ethanol (in dH_2O) (EtOH) up to seven days. Then, samples were transferred to histology cassettes lined with biopsy sponges and dehydrate in graded ethanol (Fisher) series (80% EtOH for 30 minutes, 95% EtOH for 30 minutes twice and and 100% EtOH 30 minutes twice), followed by two clarification steps in xylene (Fisher) (the first is let overnight and the second one for a couple of hours) (Vemuri et al. 2011). Then, samples were paraffin-embedded (Biobank, Medical School, Newcastle upon Tyne, UK) following routine histological procedures and sectioned in three 5-μm-thick slices. The slices were fixed on glass slides, deparaffined and then stained for the collagen and GAGs production analysis.

- #### *Alcian Blue Assay*

In order to evaluate GAGs production, Alcian Blue acid mucins staining was done. Slides were washed in running water and stained for 20 minutes with Alcian Blue solution (pH 5), prepared by dissolving 5mg of Alcian Blue 8GX (Merck,BDH cat no. 343291G) in 500 ml dH_2O

(Histopatology laboratory, NHS Trust, Newcastle upon Tyne Hospitals). Then, slides were rinsed in running dH_2O.

- ***Sirius Red assay***

The amount of collagen deposited by the cells was investigated using the Sirius Red assay (Jimenez et al. 1985). Sections, were washed in two changes of acidified water, made diluting 0.5 mL of Glacial Acetic Acid in 100 mL of dH_2O. Then, samples were treated with Sirius-red/picric acid solution (Sircol™, Biocolor Ltd., and UK) for 1 hour at room temperature and re-washed in two changes of acidified water to remove the unbound dye. Slides underwent a dehydration process in three rapid changes of absolute alcohol and cleared in Xylene (Fisher, UK) and mounted in DPX Mounting for histology (Sigma Aldrich, UK). Stained slides were covered with a glass slide and imaged with Leica Stereomicroscope (Bright field) and analysed with Leica software.

3.2.3.3 Mechanical behaviour co-culture

The stress relaxation test, explained in *par. 2.2.5.2*, was performed on co-culture and compared with controls , with the aim of evaluating changes in hydrogel mechanical properties with the synergic interaction of hACHs and Y201 MSCs. co-culture samples and controls were tested at 30 days and compared with the hydrogel viscoelasticity parameters at 0 days.

3.2.3.4 Co-culture morphological analysis: SEM

The morphology of the cells within the scaffolds were observed using SEM after 28 days of co-culture. Samples were fixed in pre-warmed 2% Glutaraldehyde overnight, rinsed in PBS twice and dehydrated in ethanol grades: 30 minutes in 25% EtOH, 30 minutes in 50% EtOH, 30 minutes in 75% EtOH, 1 hour in 100% EtOH twice. Samples were stored at 4 °C in 100% EtOH until critical point dried using a BAL-TEC 030 Critical Point Dryer (Leica Geosystems Ltd, Milton Keynes, UK). Finally, gels were mounted on carbon discs (TAAB Laboratory Equipment) and gold-coated using a Polaron E5000 SEM Coating unit (Quorum Technologies Ltd (Polaron Division), East Sussex, UK). After the gold coating using Polaron SEM coating unit with 15 nm of gold samples were imaged at different magnifications. One of each samples was observed.

3.2.4 Statistical analysis

Tests were performed at least in triplicate for each sample. The results were represented as mean ± standard deviation. Differences between groups were determined using One-way analysis of variance (ANOVA) with Turkey's multiple comparison multiple comparison test using levels of statistical significance of $p < 0.05$ (*), $p < 0.01$ (**), $p < 0.001$ (***), and $p < 0.0001$ (****).

3.3 Results

3.3.1 Cytotoxicity analysis

The incubation of MSCs with the hydrogel extract was conducted in order to evaluate the cytotoxicity of CH/BGP gels. From the Live/Dead assay (figure 3.2) it is demonstrated that cells were alive (green stained) after 24h as well as after 48h of incubation with the extract. Moreover, from day 1 to day 2, cells seemed to proliferate and a denser agglomerate of MSCs was visible. Only few dead (red stained) cells were detected. From the Countess analysis >98% of the cells resulted to be alive at both time points. PrestoBlue assay was carried out to test the metabolic activity of cells with the gel extract, compared to the cell cultured with normal media (CTRL). No significative differences were found out between the extract and the CTRL and even between extract samples at 24 hours or 48 hours.

24h   48h
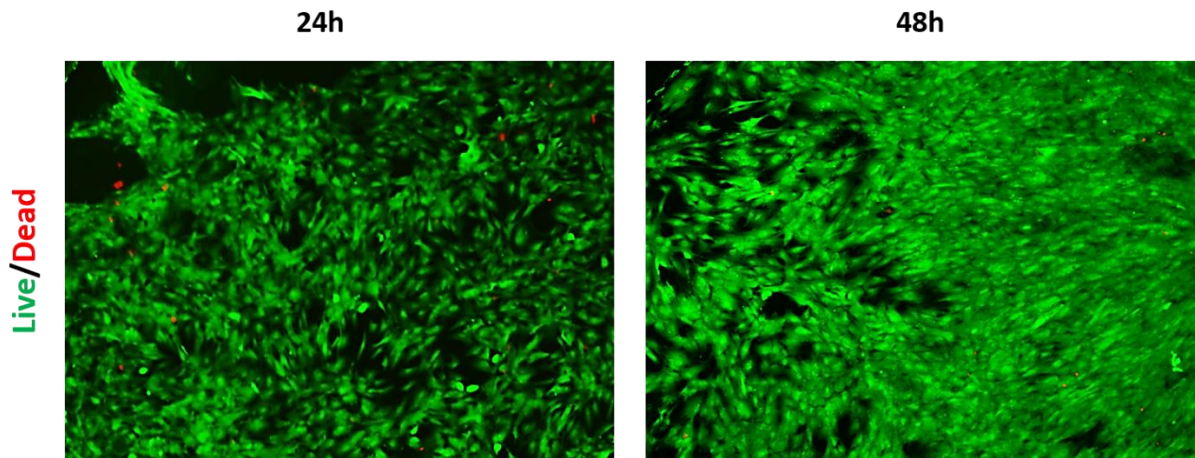
Live/Dead

b)
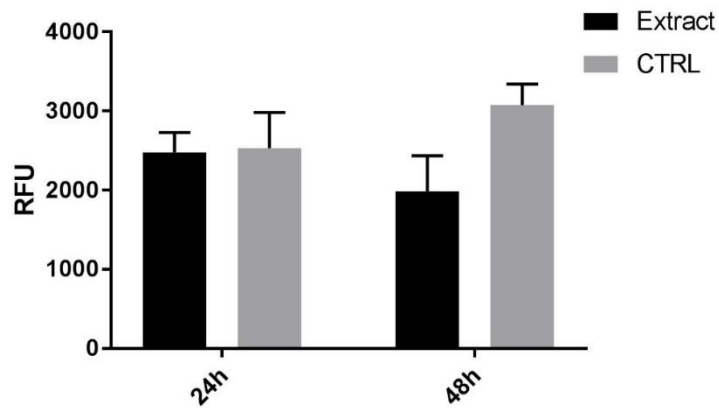
Figure 3.2: Cytotoxicity assay results. a)Live/Dead staining images of MSCs incubated with the gel extract at 24h and 48h (Green for live cells and red for dead cells).b) Metabolic activity of the MSCs incubated with the gel extract or with the normal media as control, at 24 and 48 hours. RFU is referred to relative fluorescence units. No statistical differences were found.

To assess cell and its organelles morphology, salt uptake and organisation, samples were analysed by transmission electron microscopy (figure 3.3). The structure of the cells were not altered after the cell culture in the gel. At the ultrastructural level, MSCs had a large nucleus (N) with abundant chromatin, little marginally condensed heterochromatin and one or more prominent nucleoli (figure 3.3a); cell organelles (endoplasmic reticulum ER, and mitochondria M) were not altered except for the occasional vacuolisation of the cytoplasm. The arrows in the figures indicate the salt internalisation (figure 3.3b), while figure 3.3c shows the endocytosis, before internalizing the salt and creating vacuoles, at the edge of the cell.
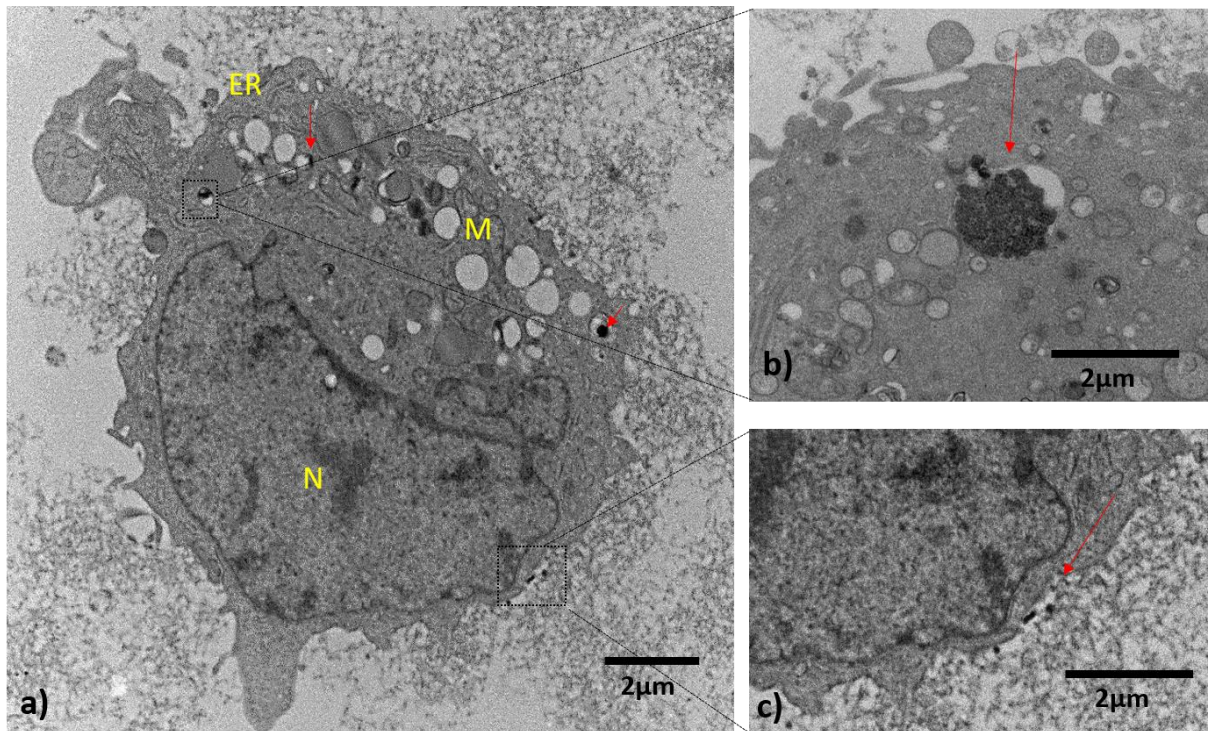
Figure 3.3: Representative TEM pictures of MSCs in the hydrogel after 24h incubation. Red arrows are indicating the salt uptake by cells a) MSC structure, where N labels the nucleus, ER the endoplasmic reticulum and M mitochondria; b) Magnification of a vacuole with salt; c) Endocytosis at cells surface.

3.3.2 Cells seeding viability, morphology and metabolic activity

The biocompatibility of the CH/BGP hydrogel was tested seeding MSCs on the top of the sterilised hydrogel at 1 and 3 days (figure 3.4). In this context, we evaluated the matrices potential to support cellular viability. At 24 h after seeding bright green stained cells were observed and few red cells. At day 3, cells clusterisation was visible, in fact several live cells agglomerate and few dead cell were detected. Additionally, MSCs distribution, morphology, and cytoskeleton organization inside the porous scaffolds were highlighted using Dapi/Phalloidin staining (figure 3.4). The same agglomeration trend found in the Live/Dead images was found with the immunostaining at day 3.
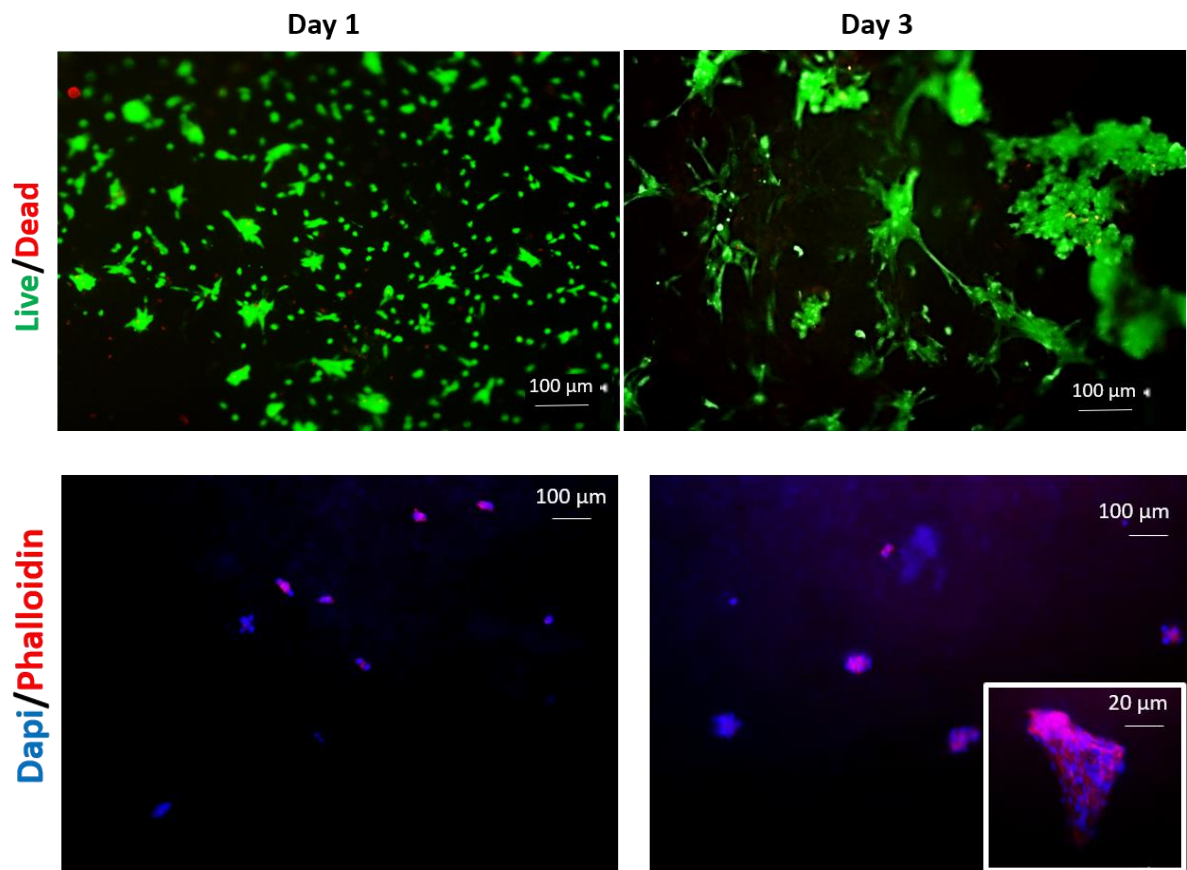
Figure 3.4: Images showing the staining's results at 5x magnification. On the top the Live/Dead at 1 and 3 days, the green stains live cells and the red dead cells. On the bottom Immunostaining at 1 and 3 days, the blue stains nucleus and the Red the F-actin.The insert in the Immunostaining day3 is a 20x magnification.

Metabolic activity analysis, through the PrestoBlue assays demonstrated that the cells metabolic activity when seeded on the top of the scaffold (Figure 3.5) decreased from day 1 to day 7 (from 763.54±46.01 Relative Fluorescence Units (RFU) to 191.63±6.10 RFU). In contrast, the control showed that cells metabolic activity remained stable all over the process (from 789.58±96.4 RFU at day 1 to 723.91±96.26 at day 3).
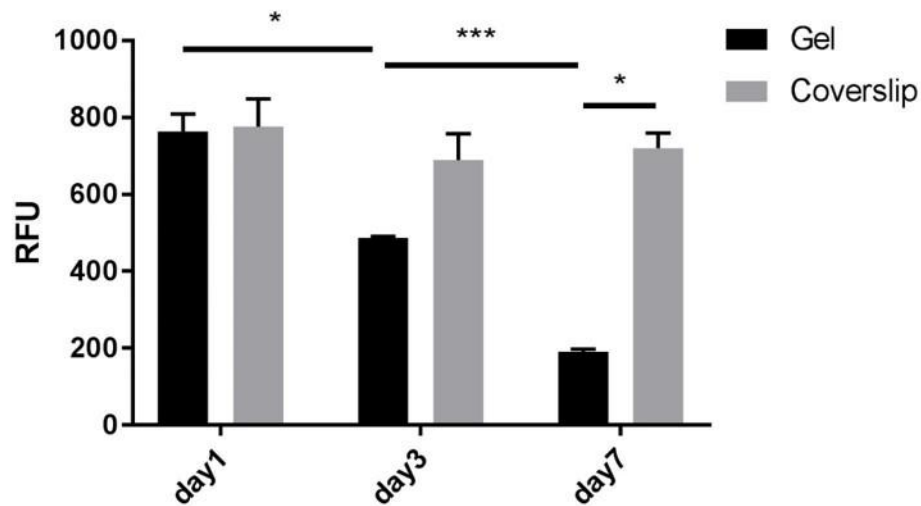
Figure 3.5: PrestoBlue results for cells seeding on the top of the gel at 1, 3 and 7 days, compared with the control (cells seeded on the coverslip). RFU is referred to relative fluorescence units. $p < 0.05$ (*) and $p < 0.001$ (***).

3.3.3 Cells encapsulated viability, metabolic activity and immunostaining

Live/dead staining of MSCs encapsulated in CH/BGP hydrogel showed that after 1 and 3 days in culture, MSCs were viable with a normal, rounded morphology, typical of encapsulated cells (figure 3.6). Few dead cells were observed (red stained).
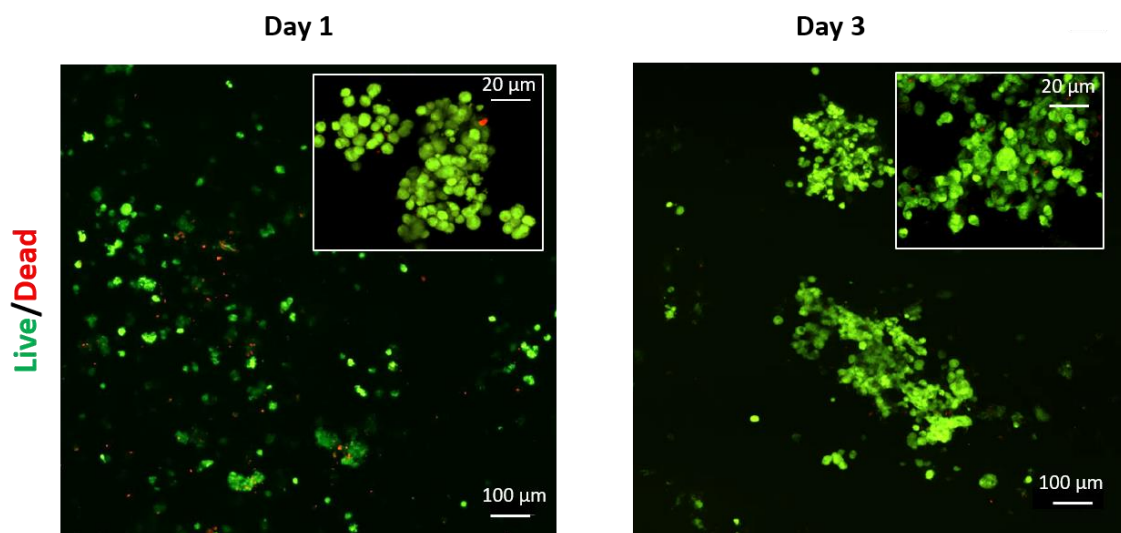
Figure 3.6: Live/Dead images of cells encapsulated in the CH/BGP hydrogel after 1 day and 3 days. The green stains live cells and the red dead cells at 5x magnification. The inserts in each figure are 20x magnification.

DAPI and Rhodamine-phalloidin were used to evaluate the cytoxicity of this formulation (figure 3.7). The rounded shape of nuclei and the staining of the cytoskeleton suggested that

the thermosensitive hydrogels were compatible without visible cytotoxicity. Moreover, materials mixing and gelification process did not adversely affect the encapsulated cell viability.

Day 1   **Day 3**
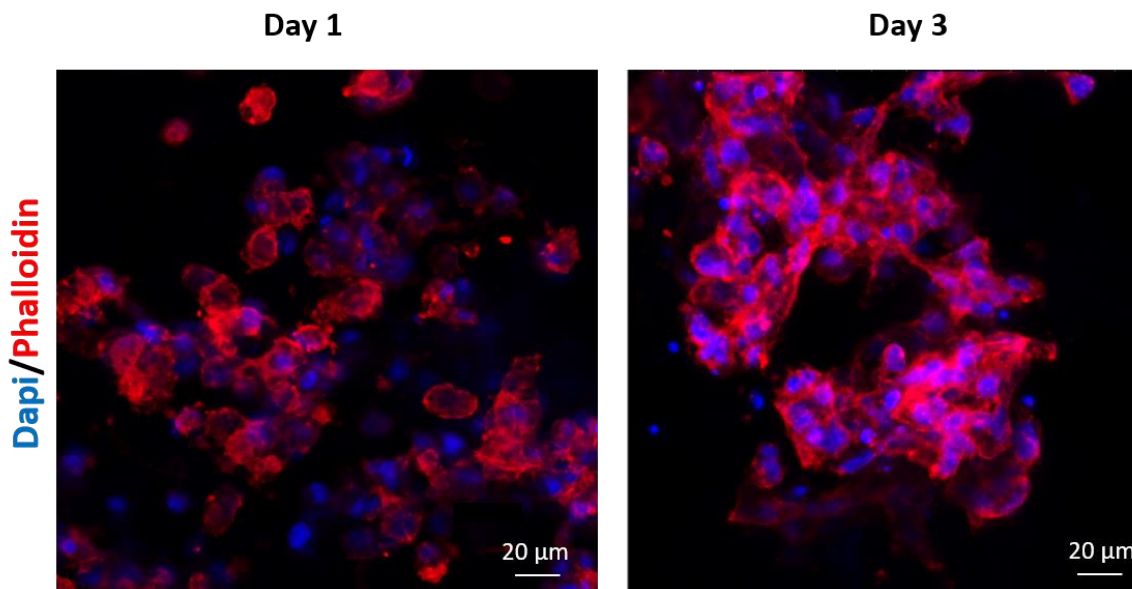
Figure 3.7: Immunostaining images of cells encapsulated in the CH/BGP hydrogel after 1 day and 3 days. The blue stains nuclei and the red the cytoskeleton 20x magnification.

For the MSCs-laden hydrogel, the metabolic activity resulted to be non-statistically different from day 1 to day 7 (1230±150 RFU to 800±105 RFU) (figure 3.8).
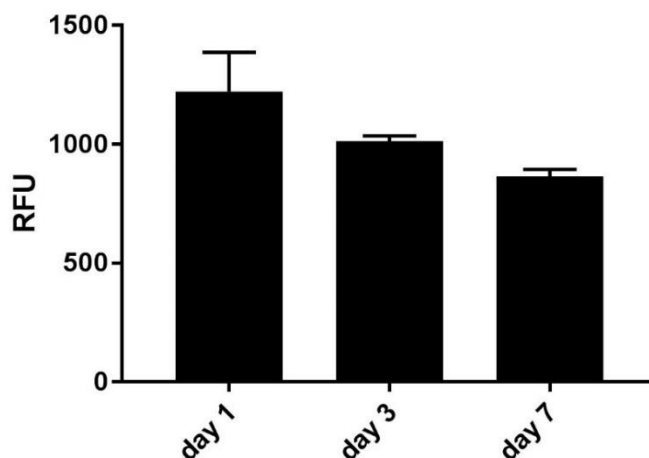
Figure 3.8: PrestoBlue results for cells encapsulated in the hydrogel at 1, 3 and 7 days. RFU is referred to relative fluorescence units. No statistical differences were revealed. No statistical differences were found.

Mechanical testing indicated that hydrogel constructs exhibited significant increases in peak stress after 30 days of MSCs culture; in fact significant differences from day 15 (40±4.2 kPa) to day 30 (57.7±7.6 kPa) were obtained (p <0.05)(figure 3.9). On the other side, the equilibrium Young's moduli didn't exhibit increase from day 0 to day 30, showing the hydrogel was mechanically stable over time, attaining an equilibrium moduli (E_Y) of around 22.6±5.1 kPa at day 15 and 16.0±2.8 kPa at day 30 (figure 3.9).
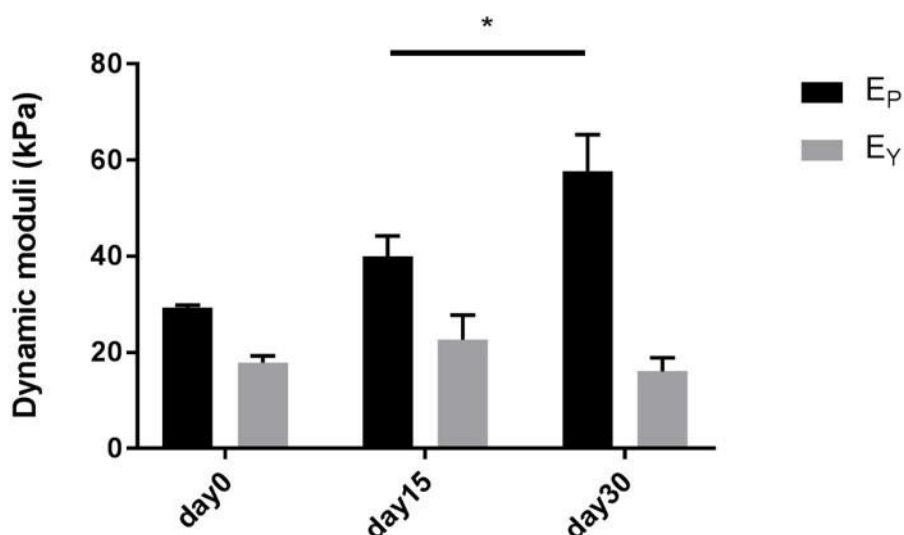
Figure 3.9: Peak stress and equilibrium Young's moduli obtained for the hydrogel with MSCs encapsulated, over time (0, 15 and 30 days). p < 0.05.

3.3.4 Co-culture analysis

Figure 3.10 shows the spheroid in the 96-round bottom well after 24h of incubation: the chondrocytes' spheroids shape evidenced a more compact and rounded-like (figure 3.10a) shape than the mesenchymal stem cells (figure 3.10b). Before assessing the experiment, the formation of the hACHs and MSCs spheroids and their vitality were experimented both in presence and in absence of the methacrylate. From those analysis it was found that the MC addition supports the maintenance of a viable, compact and non-necrotic pellet, in contrast with the results obtained without MC (data not shown).
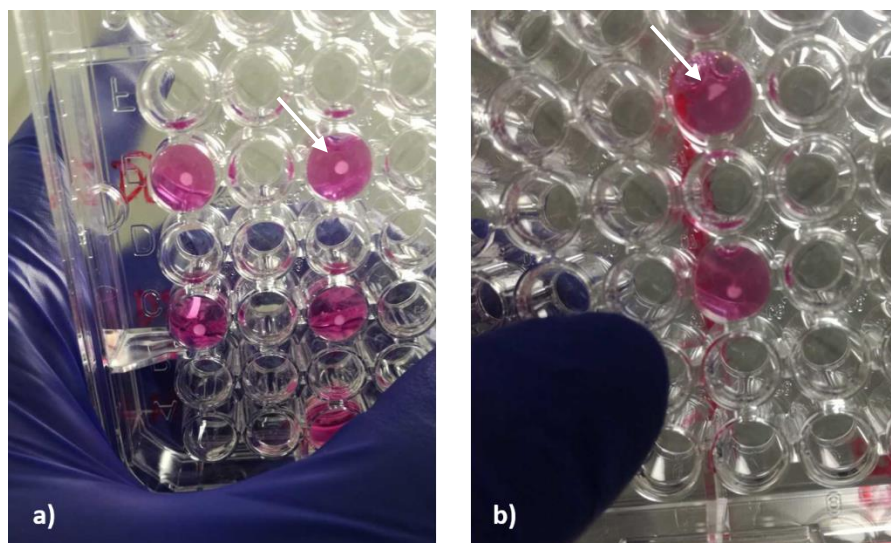
Figure 3.10: Pictures taken from the bottom of the 96-round bottom well of the 2×10^5 cells spheroids. (a) Chondrocytes spheroids were cultured in chondrocytes growth media supplemented with 0.25% MC and (b) MSCs in serum free DMEM supplemented with 0.25% MC. Arrows are indicating the spheroids.

3.3.4.1 Immunofluorescence analysis

Immunofluorescence analysis were performed after 7 and 14 days. The figure 3.11 shows the images related to the co-culture at day 7 and the related controls. In particular, figures a-d) show the pellet area, figure e-h show the area surrounding the pellet . It was evident that the chondrocyte spheroid were characterised by a round-like shape (the nuclei were stained with DAPI), with a larger diameter than MSCs pellet and moreover, it resulted integral after 7 days of culture both in co-culture (figure 3.11a) and in CTRL3 (figure 3.11d). On the other hand, MSCs spheroid appeared to be smaller, although it maintained a stable structure in CTRL1 (figure 3.11b) or completely damaged in CTRL 2 (figure 3.11c).

On the other hand, around the pellet area, in the case of co-culture (figure 3.11e), several cells were dispersed within the gel, that could be recognised as MSCs entrapped into the gel or chondrocytes migrated from the pellet. Same behaviour was visible in samples with the chondrocyte pellets lying on the empty hydrogel (CTRL3) (figure 3.11h). With regard to samples with only MSCs (spheroids and encapsulated in the hydrogel), in the case of CTRL1 no cells dispersed within the gel were visible, suggesting that all the cells were agglomerated into

the pellet (figure 3.11f), while in the case of CTRL2, there were visible cells dispersed into the gel (figure 3.11g), that could be attributed as pellet fragments (figure 3.11c).

Analysing and comparing the presence of CD44 chondrogenic marker (green staining): for the co-culture, CD44 was present within the spheroid and inside the gel (figure 3.11 a, e); while for CTRL1 (figure 3.11 b, f) and CTRL3 (figure 3.11d, h) is the chondrogenic marker was present only on the surface of the pellet and in large quantities inside the gel respectively; then for CTRL2 a very small quantity of CD44 was evidenced both around the pellet and in the gel (figure 3.11c, g).

Finally, the production of collagen type II was analysed, showing that the greatest presence of collagen was found in the co-culture system, as the protein was present both inside the spheroid (figure3.11a) and into the gel (figure 3.11e). Among the controls, it was noticeable the presence of Col II in all three gels (figure 3.11f, g, h), or on spheroids surface, but not inside the three spheroids (Fig 3.10b, c, d).

The results obtained on day 7 were compared with those obtained at day 14. In particular, we noted the integrity of chondrocyte pellets in the case of co-culture, a higher production of Col II and a larger quantity of CD44 (fig 3.11i). In the case of CTRL2, where the MSCs were in the chondrogenic medium (figure 3.11j), the spheroid was intact, the presence of CD44, as well as of Col II was similar to the 7 days (fig 3.11g); for CTRL2 (figure 3.11k), the spheroid was damaged, the production of CD44 was slightly increased compared to 7 days (fig 3.11g) and the amount of Col II was not particularly different in intensity. Finally, as far as concerned CTRL3, it was possible to notice a very high presence of CD44, higher than at day 7 (figure 3.11h) and of cells dispersed within the gel (figure 3.11l) with a minimal production of new collagen.

Day 7

Co-culture | **CTRL1** | **CTRL2** | **CTRL3**

Coll II/DAPI/CD44

Day 14

Coll II/DAPI/CD44
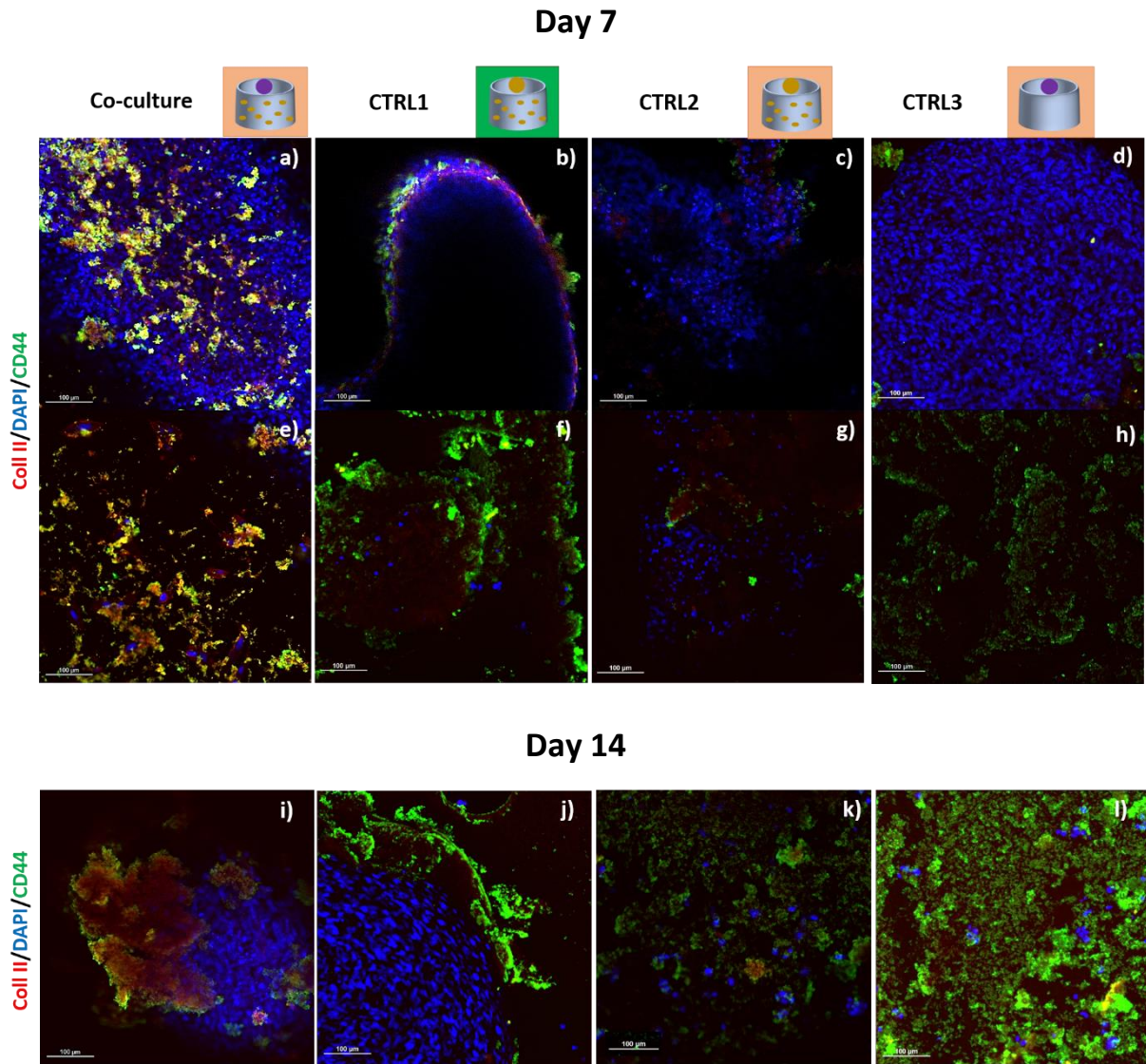
Figure 3.11: Immunofluorescence staining's: Red for Col II, Blue for DAPI and Green for CD44. Results obtained at 7 (a-h) and 14 (i-l) days for Co-culture (hACHs spheroid on MSCs-laden hydrogen), CTRL1 (MSCs spheroid on MSCs-laden hydrogel in chondrogenic media), CTRL2 (MSCs spheroid on MSCs-laden hydrogel in chondrocytes growth media) and CTRL3 (hACHs spheroid on empty hydrogel). At day 7, spheroid images were captured (a-d) and hydrogel images (e-h) for all four cases. At day 14, only relevant images in order to understand the culture behaviour were taken.

In addition, for the co-culture. Figure 3.12 shows the 3D volumetric stack, captured from day 7 to day 28 It was clear the increase in production of collagen over time. Moreover, from day 7 to day 14, the chondrocyte pellet was more compact, while at day 28 it was completely no longer visible, probably covered by the great presence of collagen that was produced. The formation of new collagen seemed to start from the spheroid and then enlarging and spreading inside the gel from the time point 7 to time point 28 days.
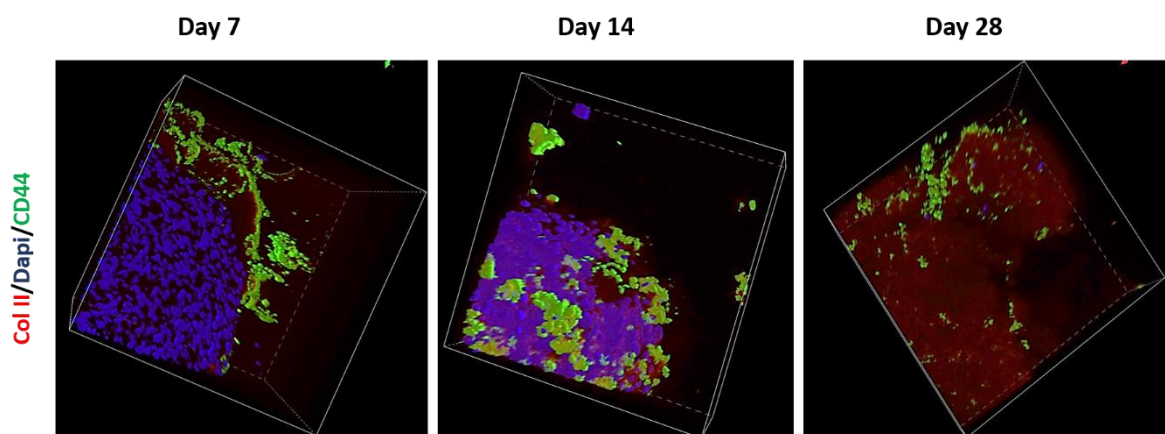
Figure 3.12: Confocal microscopy volume stack of the co-culture. Staining: Cells nuclei in the gel (DAPI, blue), collagen II (red) and CD44-chondrogenic marker (green) at three time points (7, 14 and 28 days).

3.3.4.2 Histological analysis

Histological analysis at 30 days are shown in figure 3.13 (Figure S3?? Shows the analysis at 7 days). After 4 weeks of co-culture of hACHs spheroid on a MSCs-laden hydrogel in chondrocytes proliferation medium, of the production of GAGs and collagen were clearly visible (figure 3.13g,k), compared to the controls. In fact in CTRL1, CTRL2 and CTRL3 GAGs were mainly found surrounding the hACHs (CTRL3) and MSCs (CTRL1 and CTRL2) spheroids (red arrows in figure 3.13g,h,I,j,m indicates the pellets). In CTRL3 the collagen was spread all over the gel; however its amount was lower and more fragmented respect with the results of the co-culture. Furthermore, the cartilage production in CTRL 1 was higher than in CTRL 2 and it was concentrated around the pellet, confirming the immunofluorescence results at day 14.
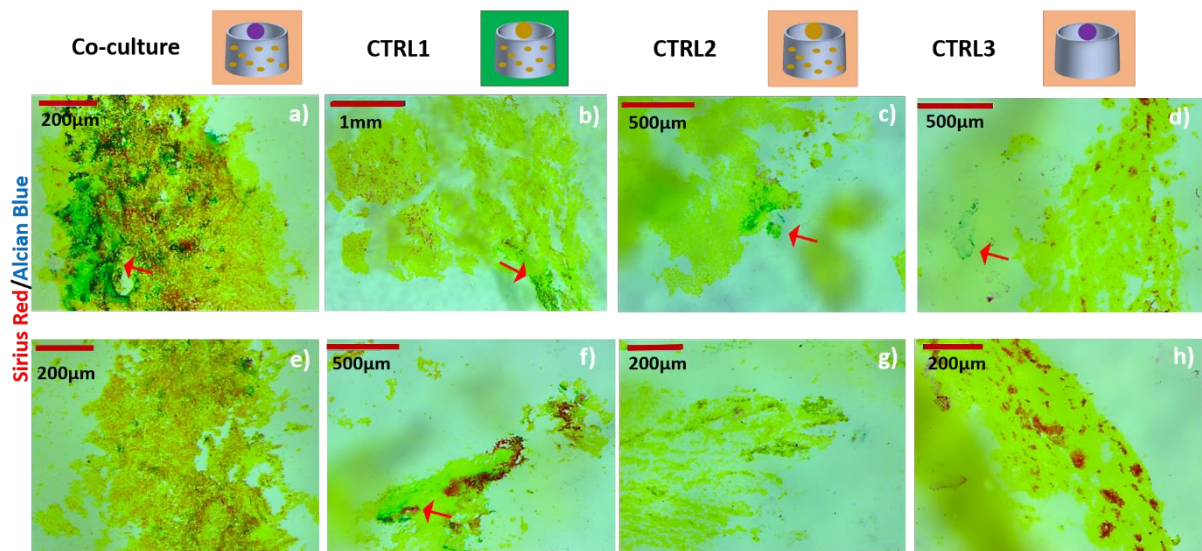
Figure 3.13: Histological sections of the constructs after 28 days of culture. Co-culture of hACHs pellet on a MSCs-laden hydrogel (a,e); MSCs pellet on a MSCs-laden hydrogel in Chondrogenic media (b,f); MSCs pellet on a MSCs-laden hydrogel in Chondrocytes growth media (c,g); hACHs pellet on the empty hydrogel(d,h). GAGs were visualized by Alcian blue staining and Collagen by Sirius red staining. Red arrows are indicating the spheroids in each sample. In the bottom row we have a magnification of the top images.

3.3.4.3 Mechanical behaviour

Viscoelastic behaviour was studied with the stress-relaxation analysis when the co-culture was assessed. In particular the equilibrium moduli was analysed (figure 3.14). The results obtained after 30 days of culture in the four different cases (co-culture, CTRL1, CTRL2 and CTRL3) were compared with the hydrogel viscoelastic response at day 0.

The co-culture showed the highest E_Y, which reached the value of 29.5 ±2.5 kPa, resulting statistically different from the hydrogel E_Y of 17±0.8 kPa at day 0 (p<0.05). The controls didn't show significant differences from the hydrogel at day0.
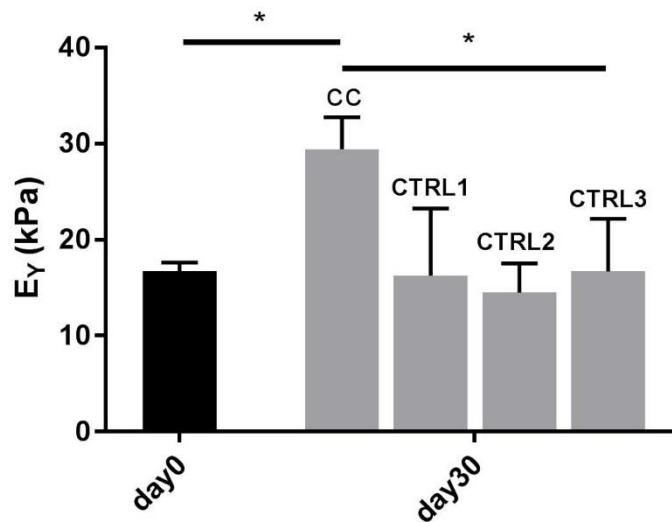
Figure 3.14: Stress relaxation test analysis for the co-culture (CC) of a hACHs spheroid on a MSCs-laden hydrogel and the three controls: MSCs spheroid on a MSCs-laden hydrogel in chondrogenic media (CTRL1), MSCs spheroid on a MSCs-laden hydrogel in chondrocytes growth media (CTRL2), hACHs spheroid on an empty hydrogel (CTRL3) after 30 days of culture, compared with the day0 (hydrogel alone). $p < 0.05$ (*).

3.3.4.4 Co-culture morphological analysis

The morphology of the cell-laden hydrogels was examined using SEM after 45 days of culture (figure 3.15). The analysis was conducted for the co-culture as well as for the controls (CTRL1, CTRL2, and CTRL3). Electron microscope images of the hydrogels showed a porous structure even after the cells culture, confirming the results found in the morphological analysis in the previous chapter, in absence of cells. The investigation of the constructs surface and cross-sections revealed the presence of numerous cells entrapped within the matrix. The co-culture images (figure 3.15a,b) show the chondrocytes cells (indicated by white arrows), distributed within the pores of the matrix and exhibited a round-shaped morphology with a diameter <20µm. A similar structure with round-shaped cells was found for CTRL3, where the hACHs spheroids was cultured on an empty gel (figure 3.15g,h). In the inserts of figure 3.15b and 3.15h, it was shown a fiber-like matrix dispersed within the cells. On the other side, in the CTRL1 (figure 3.15c,d) and CTRL2 (figure3.15e,f) a spread-like cell morphology was found (indicated by the white arrows). Moreover, the same fiber-like matrix found in the co-culture and CTRL 3, was found in CTRL1, while a less fibrous one was found for CTRL2, with more bulges.
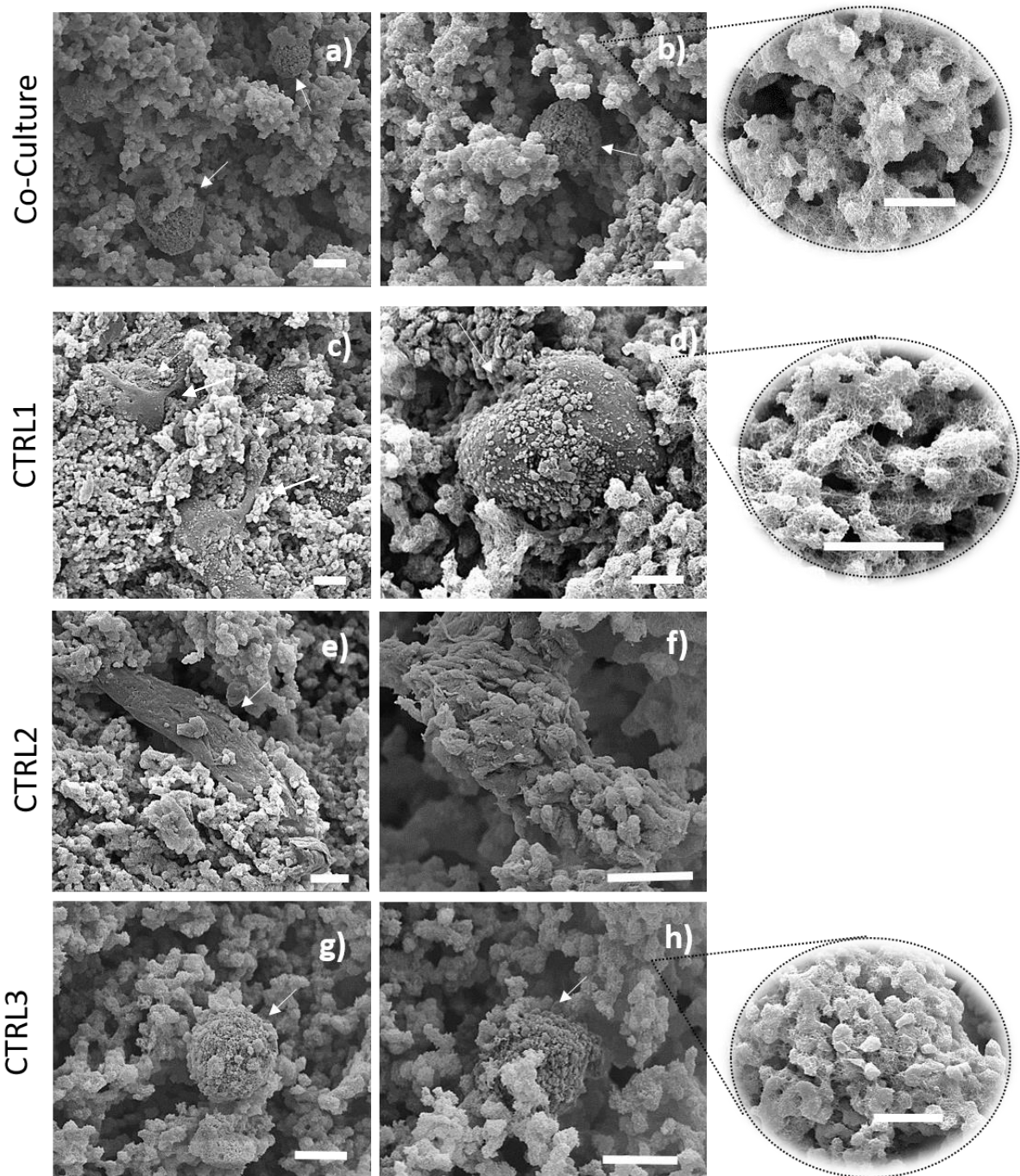
Figure 3.15: Scanning Electron Microscopy (SEM) micrographs of cells-laden hydrogels surface and cross-sections at 45 days post-culture. In particular four different samples are examined: co-culture of hACHs spheroid on MSCs-laden hydrogel (a-b), CTRL1: MSCs pellet on a MSCs-laden hydrogel in Chondrogenic media (c,d); CTRL2: MSCs pellet on a MSCs-laden hydrogel in Chondrocytes growth media (e,f); CTRL3: hACHs pellet on the empty hydrogel (g,h). The inserts in figures b,d,h report the matrix morphologies. White arrows are indicating the cells in each images. Scale bar: 10µm.

3.4 Discussion

Cell-based hydrogel scaffold therapy is one of the main strategies being investigated in cartilage regeneration. Several materials have been evaluated in literature and among them the chitosan. These studies are focused on the influence of hydrogels to provide an appropriate biochemical and biomechanical environment for cells viability and hyaline-type cartilage regeneration (Sánchez-Téllez et al. 2017)

In this work, a thermosensitive hydrogel has been studied and investigated based on chitosan and β-glycerophosphate, thanks to its capability to undergo the sol/gel transition at body temperature in 5-10 minutes. This short gelation time makes it possible to inject the gel *in vivo* during surgery and has made this hydrogel very interesting.

The cytocompatibility of the proposed thermosensitive system was evaluated incubating MSCs with hydrogel extracts for testing if the high amount of BGP salt (16% w/v) could affect MSCs viability or their metabolic activity (figure 3.2). The results demonstrated that the extract did not influence negatively the cell metabolism (just few dead cells were observed at 24 hours), indicating that the hydrogels had no cytotoxic effect on cells activity behaviour. However, these results are in contrast with some research reported literature, where they found that cell viability was affected by BGP solution in a dose-dependent manner, due to a rapid release of BGP when immersed in medium, leading to hypertonicity of the medium. In order to overcome these problems, some different composition were tested, such as $NaHCO_3$ and phosphate buffer combined with BGP as proposed by Deng et al. (Deng et al. 2017). Generally, the cytotoxicity of the extracts from chitosan (at a concentration less than 2% w/v) mixed with more than 10% w/v BGP can affect the cell viability, while with 2% chitosan ionically crosslinked with BGP higher than 15% (w/v) shows similar outcomes (Ahmadi & De Bruijn 2008). In this dissertation the concentration of BGP was 16% (w/v) while the CH concentration was 2.5% (w/v) without showing any cytotoxicity effects.

To further investigate the toxicity of hydrogel extracts, morphology of MSCs inside the gel, was investigated through TEM analysis (figure 3.3). TEM images revealed intact mitochondria, organelles responsible of cell metabolic activity (confirming the results observed via PrestoBlue assay) and endoplasmic reticulum, responsible of photosynthesis. On the other side, condensed osmophilic cytoplasm, and numerous large cytoplasmic inclusions that were membrane- bound vacuoles characteristic of autophagy were present. In apoptotic cells with

unfragmented nuclei, the nuclear chromatin was segregated into sharply circumscribed dense masses and swollen electron-dense mitochondria (Kressel & Groscurth 1994). Endocytosis occurred at the cell surface and involved the internalization of the salt into the cell in vacuoles. Phagocytosis is a stepwise endocytic process, involving particles uptake into triggered cell surface membrane cup-shaped deformations that usually encircle the particle, resulting in phagosomes (Kumari et al. 2010). The association of autophagic vacuoles with cell death has been observed in developing animals, but it has not been clear whether the process serves to rescue or condemn the cell (Yu 2004). From the Live/Dead and the PrestoBlue analyses, vacuolisation process did not interfere negatively with cells viability that could be due to the consequent formation of a large autophagosome expelled through exocytosis.

Further biological assessment was performed to confirm the biocompatibility of the construct after seeding MSCs were seeded on the top of the CH/BGP hydrogel. Live/Dead showed only few dead cells on the surface (maybe due to a lack in their adhesion) (figure 3.4) while the immunostainings of MSCs nucleus (DAPI) and cytoskeleton (Phalloidin) (figure 3.6) evidenced the tendency of these cells to agglomerate and to penetrate inside the gel. This can be considered an interesting result obtained thanks to the structure of the hydrogel and its interconnected porosity, discussed in the previous chapter. Hydrogel structure and its morphology, enabled cells to migrate inside the gel and to communicate between each other. It has been reported in literature that the tendency to agglomerate may allow cells differentiation. From the metabolic activity analysis (figure 3.5), cells activity appeared not significantly different between day 1 and day 3, but slightly decreased after 7 days. This phenomena could be related to the starting of cells differentiation, that did not imply their proliferation (DeLise et al. 2000).

Final cytocompatibility tests was performed on the MSCs-laden hydrogel systems (figure 3.6). This specific study can be considering very challenging and propaedeutic for the second part of the biological assessment, because we aim to apply the proposed CH/BGP system in cell therapy based on the injection of the cells-embedded hydrogel in sol state in the desired site in order to repair/regenerate it. Cells resulted to remain alive and to survive during the sol/gel transition process. Furthermore, as previously mentioned, the Prestoblue assay confirmed the stability of the metabolic activity (figure 3.8), suggesting a tendency of the hydrogel to not improve the proliferation but probably to stimulate the differentiation of the cells, whose begin the process of chondrogenesis.

Some works in literature reported the use of the CH/BGP hydrogel for osteogenic differentiation of MSCs, but the pores diameter obtained in this work, ranging from few to30 µm suggested that the application in cartilage tissue engineering was more suitable for this construct. In fact the pore size needed for the bone tissue ingrowth is at least 100 µm (Schliephake et al. 1991).

MSCs have emerged as a clinically relevant cell source for regenerative medicine, especially for cartilage repair. In contrast to chondrocytes, which undergo de-differentiation with expansion *in vitro*, MSCs are readily isolated from patients and expanded for use (Eslaminejad 2014). This cells have been reported to undergo chondrogenesis and deposit a cartilage specific matrix in a variety of natural and synthetic scaffold materials in the presence of the appropriate growth factors (GFs) (Bian et al. 2011). Although the above-mentioned CH/BGP hydrogel demonstrated to represent a stable and biocompatible 3D environment for MSCs viability, its therapeutic and functional efficiency in cartilage regeneration needs to be proved. Last decade studies indicated that paracrine factors released by articular chondrocytes are able to induce the chondrogenesis of MSCs (Ahmed et al. 2007; Lettry et al. 2010; Bian et al. 2011; Tsuchiya et al. 2004). *In vitro* chondrogenic differentiation of these precursor cells usually require cues from growth and signalling factors, provided *in vivo* by surrounding tissues and cells, to initiate and maintain chondrogenic differentiation status of MSCs. Therefore, the final objective of this study was to assess whether the addition of articular chondrocytes, the only cartilage cell type, to MSCs cultures influenced the properties of tissue-engineered cartilage when co-cultured in CH/BGP hydrogels *in vitro* (Ahmed et al. 2007).

In particular a close-contact co-culture of hACHs spheroid on a MSCs-laden hydrogel was designed and manufactured (figure 3.1). This system was created taking in consideration the correlation between of a spheroid and chondrocytes issues of de-differentiation, when 2D culture and their seeding density directly that can cause morphological and cytoskeletal changes to the naturally spherical chondrocytes (Kelsea 2014). Phenotypically, de-differentiation involves a decrease in expression of chondrocyte markers, such as Col II, aggrecan and an increase in expression of fibroblastic markers. This is a critical problem for cartilage tissue engineering because de-differentiated chondrocytes in fibroblasts are not able anymore to produce hyaline cartilage (Watt 1988; Hubka et al. 2014). In this work, Col II and GAGs production, main elements of the articular cartilage and CD44 expression were analysed and compared with the controls described before: CTRL1- MSCs pellet on a MSCs-

laden hydrogel in chondrogenic media; CTRL2- MSCs pellet on a MSCs-laden hydrogel and CTRL3- hACHs pellet on an empty hydrogel both in chondrocytes growth media. CTRL2 and CTRL3 were considered to evaluate if the growth factors present in the media could influence comparably with the influence of the chondrocytes in close-contact and their signalling to MSCs.

Immunofluorescence analysis was performed at day 7 and day 14 of culture (figure 3.11). Co-culture and chondrocyte control in the empty gel (CTRL3) showed a bigger pellet that could be due to the size of the chondrocytes, with a diameter of about 16 μm (Bush & Hall 2003), compared to that of the mesenchymal stem cells of about 12-13μm (Ge et al. 2014). Moreover, in the co-culture, many cells have been observed in the proximity of the spheroid, rather than in the area of the hydrogel distant from the spheroid (figure 3.11e) and at 14 days all the nuclei appeared all agglomerated in the spheroid, suggesting a communication and migration of MSCs to hACHs spheroid. On the other hand, CD44, that is an isomeric family of surface molecules expressed on different of cell types, including chondrocytes, was widely present in the co-culture at day 7 and day 14, and in both cases mostly present around or into the spheroid. The same behaviour was observed for the Col II expression, which increased from day 1 to day 28 (figure 3.11) from the pellet to the gel, covering all the spheroid surface and the gel volume. CTRL1 showed that the spheroid maintained its shape at day 7 and day 14 (figure 3.11b, j) while the CD44 expression resulted to the chondrogenic differentiation of MSCs in presence of chondrogenic media (supplemented with the chondrogenic factor TGF-β3) together with a minimal production of Col II production, evidently in less amount less than in the co-culture. Despite CTRL2 presented a spheroid with a compromised round shape since day 7, maybe since in chondrocytes growth media included not enough biochemical cues that allowed cells to migrate and aggregate. Furthermore, the CD44 expression at day 7 was minimal, since the differentiation in chondrocytes did not occurred.

Finally, CTRL3, where the chondrocytes pellet was seeded on the acellularized hydrogel, presented an intact spheroid up to 7 days, while its disaggregation occurred at 14 days and this could be related to the fact that chondrocytes spheroids is lying on an empty gel and without the synergic interaction with MSCs the spheroid is not able to survive. Moreover the Col II resulted to be expressed more at day 7 than day 14, where CD44 was more relevant.

According the histological analysis, hACHs/MSCs co-culture showed a GAGs accumulation enhancement compared to controls, confirming the immunofluorescence analysis trend

obtained up to 14 days (figure 3.13). The GAGs content appeared diffused throughout the sections, while in all three controls, if present, it appeared only surrounding the spheroid. The collagen content, also, resulted very different in the 4 samples: the co-culture demonstrated a high production of collagen at 28 days, while CTRL3 demonstrated a fragmented production of collagen in the gel. For the CTRL1 in chondrogenic media, collagen was produced and most of this was concentrated around the pellet that confirmed that the chondrogenesis and collagen production started from the MSCs aggregates. For the CTL2 in chondrocytes growth media, the production of collagen was reduced respect with CTRL1; this result confirmed that the ready-to-use growth media could lack of some factors that were, instead, present in the chondrocytes growth media. The increased production of collagen and GAGs of the co-culture respect to the CTRL2 of MSCs alone cultured in chondrogenic media, could be due to that only soluble factors are not sufficient to support chondro-induction, while the chondrocytes/MSCs direct contact can stimulate this phenomena (Richardson et al. 2008). Other studies, indeed, reported that it depends on soluble factors concentration (Bian et al. 2011).

Finally, mechanical testing indicated that mixed constructs seeded with a combination of MSCs and chondrocytes exhibited significant increase in equilibrium moduli over time from 17.0±0.8kPa to 29.0±2.5kPa, whereas this value in all other controls remained relatively unchanged for up to 30 days of culture (figure 3.14). These results are in accordance with previously obtained (Bian et al. 2011). Moreover, the equilibrium Young's moduli of the co-culture were significantly higher than the negative control (CTRL3) of only chondrocytes.

These results showed that the mechanical properties of cartilage are generally positively correlated to the GAGs and Col II content and, therefore, the increase in the equilibrium Young's modulus of the constructs can be attributed to the cartilage matrix produced in the co-culture.

After 45 days of culture, the morphology of the four-different kind of samples (co-culture, CTRL1, CTRL2, CTRL3) was analysed by SEM (figure 3.15). Round shaped chondrocytes were found uniformly distributed in the CH/BGP hydrogel after *in vitro* culture, in the case of co-culture and CTRL3 (made only of a chondrocytes spheroid in an empty gel). The cells resided in the cavities or by the edges of the cavities, encapsulated within the chitosan hydrogel. The existence of the cavities reflects the living spaces preserved by the cells, which resides in lacunae *in vivo* and moreover, collagen fibers secreted by the cells bridged between the cell and the hydrogel, demonstrating that there is an effective interaction between cells and the

hydrogel (Hong et al. 2007). Moreover, chondrocytes appeared to interact with fibers and it could be as a result of electrostatic interactions between cationic surface of chitosan amines and negatively charged cell membrane (Mohabatpour et al. 2016). The matrix produced by the chondrocytes (insert in figure 3.15b and 3.15h) resulted to be very similar to the hyaline type present *in vivo*, produced by chondrocytes, meaning that the hydrogel scaffold represents a good environment for cartilage production by cells.

In MSCs controls, the usual MSCs spread-shape was visible (Suzawa et al. 2015; Liu et al. 2018), while, only in the control cultured in chondrogenic media, the hyaline-like matrix was observed, confirming the results obtained previously, indicating the importance of the growth factor to obtain chondrogenic differentiation of MSCs and subsequent cartilage matrix production.

The examination of these cross-sections at 45 days post-seeding showed that both cells (hACHs and MSCs) remained viable in these matrices, maintaining their normal morphology and seemed to progressively produce and organize their own extracellular matrix predicting a potential clinical application of the hydrogel (Mohabatpour et al. 2016)

Chapter 4. General Conclusions and Future Directions

A reliable approach to reconstruct durable and fully functional articular cartilage tissue is required for effective clinical therapies. Here, injectable hydrogels together with cell-based therapies offer new treatment strategies in cartilage repair.

In this work, a thermosensitive chitosan/ β-glycerophosphate hydrogel for cartilage regeneration. has been investigated.

The studied hydrogel resulted to have a porous interconnected structure, optimal for nutrient uptake and release, with appropriate biochemical and mechanical properties suitable for delivery of cells in order to regenerate the damaged tissues. Moreover, since this formulation is in liquid state at room temperature, MSCs can be homogenously distributed within the solution and the formulation can be administrated to injured sites in a minimally invasive manner. After being applied to the defective tissue, the solution forms a 3D structure at 37 ^{o}C in around 5min, with mechanical properties close to those found in literature for other hydrogels. Chitosan with its cationic characteristic offers a promising scaffold or carrier in tissue engineering applications, since this feature enables it to adhere to most body tissues which contain a net negative charge due to the presence of GAGs in their ECM. This is a key feature, in fact for an effective tissue regeneration, the system needs to be bonded to the surrounding tissue and at the same time needs to be mechanically stable.

To establish cytocompatibility of the CH/BGP preparations and demonstrating the absence of any toxic elements compromising cell viability, MSCs were firstly seeded and consequently encapsulated within the hydrogel, showing good results in terms of viability and metabolic activity. Moreover, the hydrogel showed to be conducive to the chondrogenesis of MSCs when in contact with the human chondrocytes, leading to the formation of neocartilage *in vitro*.

In fact, in order to mimic the real environment, a co-culture of hMSCs embedded in the gel and chondrocytes seeded on the top of the gel in a spheroid shape to avoid de-differentiation, has been developed and analysed, resulting in a physically stable and biologically dynamic environment for MSCs chondrogenesis, leading to the production of a hyaline type cartilage structure *in vitro*. Moreover, this work was being performed using human articular chondrocytes and natural-based and engineered hydrogel system, in an attempt to provide specific insight into clinical applicability.

In conclusion, our findings demonstrate that co-culturing human MSCs with human articular chondrocytes in chitosan-based hydrogels can enhance the mechanical properties and cartilage specific ECM content of tissue-engineered cartilage.

The findings from this study are potentially of clinical significance. When treating local cartilage defects of small dimensions but of irregular geometry, the advantage of this thermosensitive chitosan- system is that the defects can be repaired with the hydrogel solution seeded with autologous MSCs and injected. This allows close contact between the implanted MSCs and the articular chondrocytes in the surrounding host tissue, effectively forming a co-culture system *in vivo*. As suggested by findings from this study, the interactions between these two populations of cells could result in enhanced chondrogenesis.

This work presents some aspects that can surely be deeply investigated in the future.

From the physico-chemical point of view, an injectability analysis must be performed to confirm the clinical application as injectable hydrogel for cell therapy. On the other side from the biological point of view, in particular regarding the co-culture, a quantitative analysis should be performed, as for example a quantitative real-time RT-PCR to quantify expression levels of collagen type II or GAGs content, by biochemical assays (spectrophotometrically using dimethyl methylene blue). Furthermore MSCs were found to induce chondrocytes proliferation (Hubka et al. 2014; Acharya et al. 2012), which is rather unconventional in chondrocyte culture, by-product of de-differentiation and this could be analysed using two different dyes for chondrocytes and MSCs and qualitatively observing their migration and behaviour inside the construct.

4.1 3D printing and beyond

Despite significant advances using various approaches including tissue engineering, repair of articular cartilage remains a major challenge. Furthermore, current 3D approaches with cell-laden biomaterials, like the CH/BGP hydrogel studied in this work, are a significant step forward from conventional two-dimensional methods. However, for clinical translation, these tissues engineered constructs often require large numbers of cells with more complex structural hierarchies. AC structure is very complex, in fact it is composed by layer with different composition and even the cells shape is different from the deepest layer in contact with the bone, to the surface. The closer the *in vitro* model allows the reproduction of the *in vivo* AC tissue complexity the more value the model will acquire. This concept helped to

overturn the way TE was conceived, opening new doors to the development of 3D printing technology as ''bottom-up" or additive manufacturing strategy to more precisely control the structure of the material scaffold, allowing the fabrication of multi-layered structures and cost and time effective rapid prototyping. Bio fabrication, intended as the use of 'bioink' to print living cells within a material construct, is an evolving aspect of 3D printing technology. This is one of the major advantages of 3D bioprinting technologies whereby well- defined geometries with gradient composition of biomaterials and cells can be achieved during construct manufacturing with complex structural features. There is still much work to be done before obtaining a bioink with printable rheological properties and optimal mechanical and biological properties for cell survival, adhesion and tissue-specific function, but the first attempts are encouraging and can open the doors to a future work on cartilage regeneration (figure 3.16) (Duarte Campos et al. 2012; Schon et al. 2017; Zhang et al. 2017; Mouser et al. 2017; Apelgren et al. 2017).
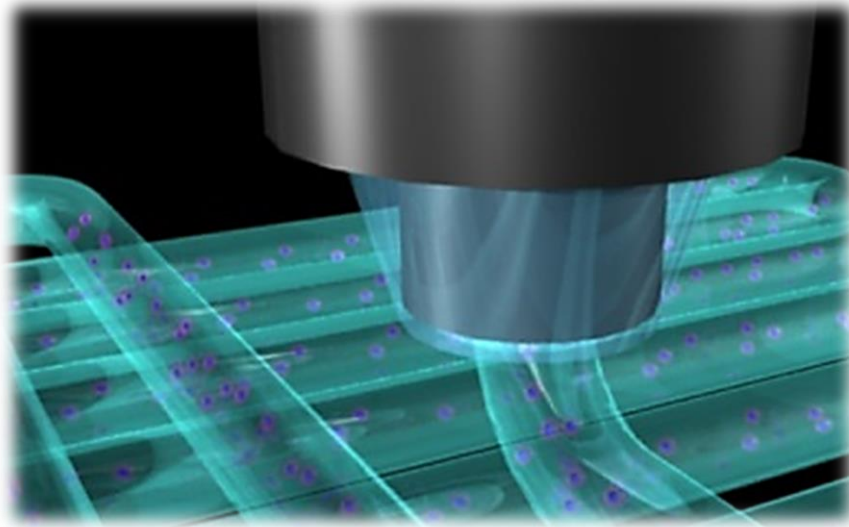
Figure 3.16: Future prospective: 3D printing of a bioink composed by hydrogel and cells in order to reproduce the cartilage architecture (Costantini et al. 2016).

Supplementary

a) Figures
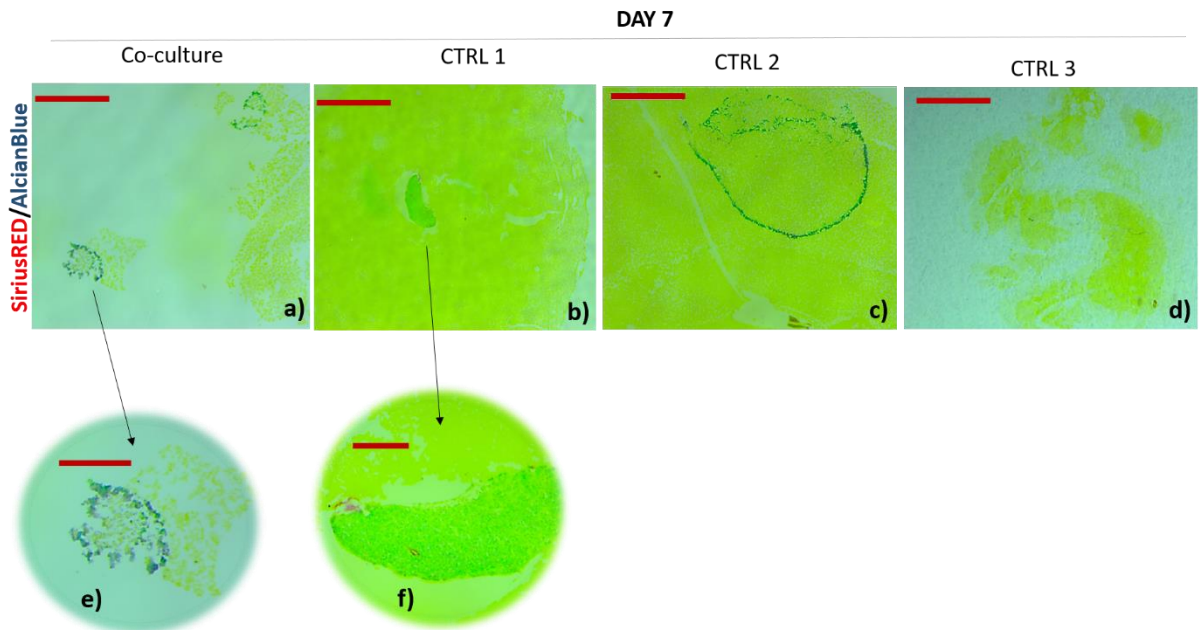
Figure S1: Histological analysis of the Co-culture at day 7.

b) Matlab

In order to fit a third order exponential decay curve that obeys the generalized Maxwell model, the following Matlab code was designed. Three time constants were calculated by running the code.

```
%This code fits a third order exponential decay equation to the
%experimental data
%Tau 1, Tau2, and Tau3 are the three relaxation time constants
%x is the column vector corresponding to time. Time starts at the point where the peak stress
is reatched.
%y is the column vector corresponding to stress. Values are taken after a strain of 10% is
reached.
x =[0:0.5:1000.5]';
y= Filename(:,2);
ft2 = fittype('a1*exp(-xx1/tau1)+b1*exp(-xx1/tau2)+c1*exp(-xx1/tau3)+d1',...
        'dependent','yy1','independent','xx1',...
        'coefficients',{'tau1','tau2','tau3','a1','b1','c1','d1'})
fitobject1 = fit(x,y,ft2,'StartPoint',[500 70 10 1 1 1 1])
plot(fitobject1)
hold on
plot(x,y)
legend('Fitted Curve','Experimental Data'),xlabel('Time (s)'),ylabel('Stress MPa)'),
title('Hydrogel Stress Relaxation')
```

Another Matlab code was designed to fit a first order decay curve that helped to determine the viscosity of each hydrogel composition through the value of the time constant given as an output after running the code.

```
%This code fits a first order exponential decay equation to the
%experimental data
%Tau 1, Tau2, and Tau3 are the three relaxation time constants
%x is the column vector corresponding to time. Time starts at the point where the peak stress
is reatched.
%y is the column vector corresponding to stress. Values are taken after a strain of 10% is
reached.
x =[0:0.5:1000.5]';
y= G100stressrelax04(:,2);
ft2 = fittype('a1*exp(-x/tau)',...
        'dependent','y','independent','x',...
        'coefficients',{'tau','a1'})

fitobject1 = fit(x,y,ft2)
plot(fitobject1)
hold on

plot(x,y)
legend('Fitted Curve','Experimental Data'),xlabel('Time (s)'),ylabel('Stress MPa'),
title('Hydrogel Stress Relaxation')
```

References

Acharya, C. et al., 2012. Enhanced chondrocyte proliferation and mesenchymal stromal cells chondrogenesis in coculture pellets mediate improved cartilage formation. *Journal of Cellular Physiology*, 227(1), pp.88–97.

Agency, E.M., 2009. Ic in Od Uc T N O Lo Ng Er Au T Ho Ris in Pr Od Uc T N O Ng Er Ho Ed. , (October 2004), pp.1–2.

Ahmadi, R. & De Bruijn, J.D., 2008. Biocompatibility and gelation of chitosan-glycerol phosphate hydrogels. *Journal of Biomedical Materials Research - Part A*, 86(3), pp.824–832.

Ahmed, N. et al., 2007. Soluble signalling factors derived from differentiated cartilage tissue affect chondrogenic differentiation of rat adult marrow stromal cells. *Cellular Physiology and Biochemistry*, 20(5), pp.665–678.

Alexopoulos, L.G. et al., 2005. Osteoarthritic changes in the biphasic mechanical properties of the chondrocyte pericellular matrix in articular cartilage. *Journal of Biomechanics*, 38(3), pp.509–517.

Alford, J.W. & Cole, B.J., 2005. Cartilage Restoration, Part 1: Basic Science, Historical Perspective, Patient Evaluation, and Treatment Options. *The American Journal of Sports Medicine*, 33(2), pp.295–306. Available at: https://doi.org/10.1177/0363546504273510.

Aliaghaei, M. et al., 2012. Investigation of gelation mechanism of an injectable hydrogel based on chitosan by rheological measurements for a drug delivery application. *Soft Matter*, 8(27), pp.7128–7137.

Annabi, N. et al., 2010. Controlling the Porosity and Microarchitecture of Hydrogels for Tissue Engineering. *Tissue Engineering Part B: Reviews*, 16(4), pp.371–383. Available at: http://www.liebertonline.com/doi/abs/10.1089/ten.teb.2009.0639.

Anon, Adult human chondrocytes cultured in alginate form a matrix similar to native human articular cartilage. *American journal of physiology.*, 271(3 40-3), pp.C742--C752.

Antoine, E.E., Vlachos, P.P. & Rylander, M.N., 2014. Review of Collagen I Hydrogels for Bioengineered Tissue Microenvironments: Characterization of Mechanics, Structure, and Transport. *Tissue Engineering Part B: Reviews*, 20(6), pp.683–696. Available at: https://doi.org/10.1089/ten.teb.2014.0086.

Apelgren, P. et al., 2017. Chondrocytes and stem cells in 3D-bioprinted structures create human cartilage in vivo. *PLoS ONE*, 12(12), pp.1–16.

Armiento, A.R. et al., 2018. Biomaterials for articular cartilage tissue engineering: Learning from biology. *Acta Biomaterialia*, 65, pp.1–20. Available at: https://doi.org/10.1016/j.actbio.2017.11.021.

Assaad, E., Maire, M. & Lerouge, S., 2015. Injectable thermosensitive chitosan hydrogels with controlled gelation kinetics and enhanced mechanical resistance. *Carbohydrate Polymers*, 130, pp.87–96. Available at: http://dx.doi.org/10.1016/j.carbpol.2015.04.063.

Aung, A. et al., 2011. Osteoarthritic chondrocyte-secreted morphogens induce chondrogenic differentiation of human mesenchymal stem cells. *Arthritis and Rheumatism*, 63(1), pp.148–158.

Bae, J.W. et al., 2014. In situ formation of enzyme-free hydrogels via ferromagnetic microbead-assisted enzymatic cross-linking. *Chemical Communications*, 50(89), pp.13710–13713.

Bae, W.C. et al., 2008. Wear-lines and split-lines of human patellar cartilage: relation to tensile biomechanical properties. *Osteoarthritis and Cartilage*, 16(7), pp.841–845.

Ben-Yishay, A. et al., 1995. Repair of Articular Cartilage Defects with Collagen-Chondrocyte Allografts. *Tissue Engineering*, 1(2), pp.119–133. Available at: http://search.proquest.com/docview/215615935/.

Bentley, G. & Greer III, R.B., 1971. Homotransplantation of Isolated Epiphyseal and Articular Cartilage Chondrocytes into Joint Surfaces of Rabbits. *Nature*, 230, p.385. Available at: http://dx.doi.org/10.1038/230385a0.

Benya, P.D. & Shaffer, J.D., 1982. Dedifferentiated chondrocytes reexpress the differentiated collagen phenotype when cultured in agarose gels. *Cell*, 30(1), pp.215–224.

Berg, V. et al., 2010. Human articular chondrocytes express ChemR23 and chemerin; ChemR23 promotes inflammatory signalling upon binding the ligand chemerin21-157. *Arthritis Research and Therapy*, 12(6), p.R228. Available at: http://arthritis-research.com/content/12/6/R228.

Bhosale, A.M. & Richardson, J.B., 2008. Articular cartilage: Structure, injuries and review of management. *British Medical Bulletin*, 87(1), pp.77–95.

Bian, L. et al., 2011. Coculture of Human Mesenchymal Stem Cells and Articular Chondrocytes Reduces Hypertrophy and Enhances Functional Properties of Engineered Cartilage. *Tissue Engineering Part A*, 17(7–8), pp.1137–1145. Available at: http://www.liebertonline.com/doi/abs/10.1089/ten.tea.2010.0531.

Boere, K.W.M. et al., 2014. Covalent attachment of a three-dimensionally printed thermoplast to a gelatin hydrogel for mechanically enhanced cartilage constructs. *Acta Biomaterialia*, 10(6), pp.2602–2611. Available at: http://dx.doi.org/10.1016/j.actbio.2014.02.041.

Boffito, M. et al., 2015. Thermosensitive block copolymer hydrogels based on poly(E-caprolactone) and polyethylene glycol for biomedical applications: State of the art and future perspectives. *Journal of Biomedical Materials Research - Part A*, 103(3), pp.1276–1290.

Bonifacio, M.A. et al., 2018. Antibacterial effectiveness meets improved mechanical properties: Manuka honey/gellan gum composite hydrogels for cartilage repair. *Carbohydrate Polymers*, 198(April), pp.462–472. Available at: https://doi.org/10.1016/j.carbpol.2018.06.115.

Bornes, T.D. et al., 2015. Hypoxic culture of bone marrow-derived mesenchymal stromal stem cells differentially enhances in vitro chondrogenesis within cell-seeded collagen and hyaluronic acid porous scaffolds. *Stem Cell Research and Therapy*, 6(1). Available at: ???

Brittberg, M. et al., 1994. Treatment of Deep Cartilage Defects in the Knee with Autologous Chondrocyte Transplantation. *New England Journal of Medicine*, 331(14), pp.889–895. Available at:

https://doi.org/10.1056/NEJM199410063311401.

Brix, M.O. et al., 2014. Treatment of full-thickness chondral defects with hyalograft C in the Knee: Long-term results. *American Journal of Sports Medicine*, 42(6), pp.1426–1432.

Buckwalter, J.A., 1998. Articular Cartilage: Injuries and Potential for Healing. *Journal of Orthopaedic & Sports Physical Therapy*, 28(4), pp.192–202. Available at: http://www.jospt.org/doi/10.2519/jospt.1998.28.4.192.

Buckwalter, J.A. & Mankin, H.J., 1998. Articular cartilage: tissue design and chondrocyte-matrix interactions. *Instructional course lectures*, 47, pp.477–486.

Buckwalter, J.A. & Mankin, H.J., 1997. Articular cartilage. Part I: Tissue design and chondrocyte-matrix interactions. *Journal of Bone and Joint Surgery - Series A*, 79(4), pp.600–611. Available at: https://www.scopus.com/inward/record.uri?eid=2-s2.0-0030923403&partnerID=40&md5=53a2a597248d02bdd1f626f95ef732e3.

Buschmann, M.D. et al., 1992. Chondrocytes in agarose culture synthesize a mechanically functional extracellular matrix. *Journal of orthopaedic research.*, 10(6), pp.745–758.

Bush, P.G. & Hall, A.C., 2003. The volume and morphology of chondrocytes within non-degenerate and degenerate human articular cartilage. *Osteoarthritis and Cartilage*, 11(4), pp.242–251.

Cao, L. et al., 2013. An injectable hydrogel formed by in situ cross-linking of glycol chitosan and multi-benzaldehyde functionalized PEG analogues for cartilage tissue engineering†. *Journal of Materials Chemistry B*, 1(35), pp.1–41.

Cao, L. et al., 2015. An injectable hydrogel formed by in situ cross-linking of glycol chitosan and multi-benzaldehyde functionalized PEG analogues for cartilage tissue engineering. *Journal of Materials Chemistry B*, 3(7), pp.1268–1280.

Casscells, S.W., 1990. Articular cartilage and knee joint function: Basic science and arthroscopy. *Arthroscopy*, 6(2), p.167. Available at: https://doi.org/10.1016/0749-8063(90)90051-E.

Chalovich, J.M. & Eisenberg, E., 2013. NIH Public Access. *Magn Reson Imaging*, 31(3), pp.477–479.

Chen, C. et al., 2013. Performance optimization of injectable chitosan hydrogel by combining physical and chemical triple crosslinking structure. *Journal of Biomedical Materials Research - Part A*, 101 A(3), pp.684–693.

Chen, C. et al., 2012. Preparation and properties of an injectable thermo-sensitive double crosslinking hydrogel based on thiolated chitosan/beta-glycerophosphate. *Journal of Materials Science*, 47(5), pp.2509–2517. Available at: https://doi.org/10.1007/s10853-011-6075-6.

Chen, F.H., Rousche, K.T. & Tuan, R.S., 2006. Technology insight: Adult stem cells in cartilage regeneration and tissue engineering. *Nature Clinical Practice Rheumatology*, 2(7), pp.373–382.

Cheng, C.W., Solorio, L.D. & Alsberg, E., 2014. Decellularized tissue and cell-derived extracellular matrices as scaffolds for orthopaedic tissue engineering. *Biotechnology Advances*, 32(2), pp.462–484. Available at: http://dx.doi.org/10.1016/j.biotechadv.2013.12.012.

Cheng, Y.H. et al., 2010. Thermosensitive Chitosan – Gelatin – Glycerol Phosphate Hydrogels as a Cell Carrier for Nucleus Pulposus Regeneration: An In Vitro Study. *Tissue Engineering Part A*, 16(2), pp.695–703.

Chenite, a et al., 2001. Rheological characterisation of thermogelling chitosan / glycerol-phosphate solutions. *Carbohydrate Polymers*, 46, pp.39–47.

Chenite, A. et al., 2000. Novel injectable neutral solutions of chitosan form biodegradable gels in situ. *Biomaterials*, 21(21), pp.2155–2161.

Cho, I.S. et al., 2016. Synthesis and characterization of a new photo-crosslinkable glycol chitosan thermogel for biomedical applications. *Carbohydrate Polymers*, 144, pp.59–67. Available at: http://dx.doi.org/10.1016/j.carbpol.2016.02.029.

Cho, J. et al., 2006. Chitosan and glycerophosphate concentration dependence of solution behaviour and gel point using small amplitude oscillatory rheometry. *Food Hydrocolloids*, 20(6), pp.936–945.

Cho, J. et al., 2005. Physical gelation of chitosan in the presence of β-glycerophosphate: The effect of temperature. *Biomacromolecules*, 6(6), pp.3267–3275.

Coleman, R.M. et al., 2013. The Therapeutic Effect of Bone Marrow-Derived Stem Cell Implantation After Epiphyseal Plate Injury Is Abrogated by Chondrogenic Predifferentiation. *Tissue Engineering Part A*, 19(3–4), pp.475–483. Available at: http://online.liebertpub.com/doi/abs/10.1089/ten.tea.2012.0125.

Costantini, M. et al., 2016. 3D bioprinting of BM-MSCs-loaded ECM biomimetic hydrogels for in vitro neocartilage formation. *Biofabrication*, 8(3).

Crompton, K.E. et al., 2007. Polylysine-functionalised thermoresponsive chitosan hydrogel for neural tissue engineering. *Biomaterials*, 28(3), pp.441–449.

Dahlin, R.L. et al., 2014. Chondrogenic Phenotype of Articular Chondrocytes in Monoculture and Co-Culture with Mesenchymal Stem Cells in Flow Perfusion. *Tissue Engineering Part A*, 20(21–22), pp.2883–2891. Available at: http://online.liebertpub.com/doi/abs/10.1089/ten.tea.2014.0107.

Dang, Q.F. et al., 2012. Design and evaluation of a highly porous thermosensitive hydrogel with low gelation temperature as a 3D culture system for Penaeus chinensis lymphoid cells. *Carbohydrate Polymers*, 88(1), pp.361–368. Available at: http://dx.doi.org/10.1016/j.carbpol.2011.12.014.

DeLise, A.M., Fischer, L. & Tuan, R.S., 2000. Cellular interactions and signaling in cartilage development. *Osteoarthritis and Cartilage*, 8(5), pp.309–334.

Deng, A. et al., 2017. Enhanced gelation of chitosan/β-sodium glycerophosphate thermosensitive hydrogel with sodium bicarbonate and biocompatibility evaluated. *Materials Science and Engineering C*, 78, pp.1147–1154. Available at: http://dx.doi.org/10.1016/j.msec.2017.04.109.

Derry, S.S., Moore, R.A.R.A. & Rabbie, R.R., 2011. Topical NSAIDs for chronic musculoskeletal pain in adults. *Cochrane database of systematic reviews (Online)*, 9(9), pp.CD007400-CD007400. Available at: http://eutils.ncbi.nlm.nih.gov/entrez/eutils/elink.fcgi?dbfrom=pubmed&id=22972108&retmode=ref&cmd=prlinks%5

Cnpapers2://publication/doi/10.1002/14651858.CD007400.pub2.

Diduch, D.R. et al., 2000. Marrow stromal cells embedded in alginate for repair of osteochondral defects. *Arthroscopy: The Journal of Arthroscopic & Related Surgery*, 16(6), pp.571–577.

Duarte Campos, D.F. et al., 2012. Supporting Biomaterials for Articular Cartilage Repair. *Cartilage*, 3(3), pp.205–221.

Eslaminejad, M.B., 2014. Mesenchymal stem cells as a potent cell source for articular cartilage regeneration. *World Journal of Stem Cells*, 6(3), p.344. Available at: http://www.wjgnet.com/1948-0210/full/v6/i3/344.htm.

Estrela, C. et al., 2011. Mesenchymal stem cells in the dental tissues: Perspectives for tissue regeneration. *Brazilian Dental Journal*, 22(2), pp.91–98.

Etxabide, A. et al., 2018. Lactose-crosslinked fish gelatin-based porous scaffolds embedded with tetrahydrocurcumin for cartilage regeneration. *International Journal of Biological Macromolecules*, 117, pp.199–208. Available at: https://doi.org/10.1016/j.ijbiomac.2018.05.154.

Federico, S. & Herzog, W., 2008. On the permeability of fibre-reinforced porous materials. *International Journal of Solids and Structures*, 45(7–8), pp.2160–2172.

Filardo, G. et al., 2016. Stem cells in articular cartilage regeneration. *Journal of Orthopaedic Surgery and Research*, 11(1). Available at: http://dx.doi.org/10.1186/s13018-016-0378-x.

Florian Hildner, Ph.D., Sebastian Concaro, M.D., Anja Peterbauer, M.Sc., Susanne Wolbank, Ph.D., Martin Danzer, Ph.D., Anders Lindahl, M.D., P.D. & Paul Gatenholm, Ph.D., Heinz Redl, Ph.D., and Martijn van Griensven, M.D., P.D., 2009. Human Adipose-Derived Stem Cells Contribute to Chondrogenesis in Coculture with Human Articular Chondrocytes. *Tissue Engineering Part A*, 15(12).

Fragonas, E. et al., 2000. Articular cartilage repair in rabbits by using suspensions of allogenic chondrocytes in alginate. *Biomaterials.*, 21(8), pp.795–801.

Francis Suh, J.K. & Matthew, H.W.T., 2000. Application of chitosan-based polysaccharide biomaterials in cartilage tissue engineering: A review. *Biomaterials*, 21(24), pp.2589–2598.

Freeman, R., 1968. The permeability of articular cartilage. *The Journal of bone and joint surgery.*, 50, pp.1260–1.

G.Tahrir, F., Ganji, F. & Ahooyi, T., 2015. Injectable Thermosensitive Chitosan/Glycerophosphate-Based Hydrogels for Tissue Engineering and Drug Delivery Applications: A Review. *Recent Patents on Drug Delivery & Formulation*, 9(2), pp.107–120. Available at: http://www.eurekaselect.com/openurl/content.php?genre=article&issn=1872-2113&volume=9&issue=2&spage=107.

Ganji, F., Abdekhodaie, M.J. & Ramazani, A., 2007. Gelation time and degradation rate of chitosan-based injectable hydrogel. *Journal of Sol-Gel Science and Technology*, 42(1), pp.47–53.

Gao, C. et al., 2013. Development and characterization of injectable chitosan-based hydrogels containing dexamethasone/rhBMP-2 loaded hydroxyapatite nanoparticles. *Materials Letters*, 93, pp.312–315. Available at: http://www.sciencedirect.com/science/article/pii/S0167577X12016850.

Ge, J. et al., 2014. The Size of Mesenchymal Stem Cells is a Significant Cause of Vascular Obstructions and Stroke. *Stem Cell Reviews and Reports*, 10(2), pp.295–303. Available at: https://doi.org/10.1007/s12015-013-9492-x.

Gerhardt, L.-C. & Boccaccini, A.R., 2010. Bioactive Glass and Glass-Ceramic Scaffolds for Bone Tissue Engineering. *Materials*, 3(7), pp.3867–3910. Available at: http://www.mdpi.com/1996-1944/3/7/3867/.

Glyn-Jones, S. et al., 2015. Osteoarthritis. *The Lancet*, 386(9991), pp.376–387.

Goa, K.L. & Benfield, P., 1994. Hyaluronic Acid. *Drugs.*, 47(3), pp.536–566.

Goode, J., 2016. Use of International Standard ISO 10993-1, Biological evaluation of medical devices - Part 1: Evaluation and testing within a risk management process. *Department of Health and Human Services Food and Drug Administration*, p.68. Available at: https://www.fda.gov/downloads/medicaldevices/deviceregulationandguidance/guidancedocuments/ucm348890.pdf.

Gooding, C.R. et al., 2006. A prospective, ranomised study comparing two techniques of autologous chondrocyte implantation for osteochondral defects in the knee: Periosteum covered versus type I/III collagen covered. *The Knee*, 13(3), pp.203–210. Available at: http://www.sciencedirect.com/science/article/pii/S0968016006000354.

Gudbergsen, H. et al., 2012. Weight loss is effective for symptomatic relief in obese subjects with knee osteoarthritis independently of joint damage severity assessed by high-field MRI and radiography. *Osteoarthritis and Cartilage*, 20(6), pp.495–502.

Guilak, F., 2000. The deformation behavior and viscoelastic properties of chondrocytes in articular cartilage. In *Biorheology*. pp. 27–44.

Hamedi, H. et al., 2018. Chitosan based hydrogels and their applications for drug delivery in wound dressings: A review. *Carbohydrate Polymers*, 199(March), pp.445–460. Available at: https://linkinghub.elsevier.com/retrieve/pii/S0144861718307690.

Han, H.D. et al., 2008. A chitosan hydrogel-based cancer drug delivery system exhibits synergistic antitumor effects by combining with a vaccinia viral vaccine. *International Journal of Pharmaceutics*, 350(1), pp.27–34. Available at: http://www.sciencedirect.com/science/article/pii/S0378517307006941.

Harley, B.A. et al., 2006. Fabricating tubular scaffolds with a radial pore size gradient by a spinning technique. *Biomaterials*, 27(6), pp.866–874.

Hendriks, J., Riesle, J. & van Blitterswijk, C.A., 2007. Co-culture in cartilage tissue engineering. *Journal of Tissue Engineering and Regenerative Medicine*, 1(3), pp.170–178.

Heng, B.C., Cao, T. & Lee, E.H., 2004. Directing Stem Cell Differentiation into the Chondrogenic Lineage In Vitro. *Stem Cells*, 22(7), pp.1152–1167. Available at: http://doi.wiley.com/10.1634/stemcells.2004-0062.

Hennink, W.E. & van Nostrum, C.F., 2012. Novel crosslinking methods to design hydrogels. *Advanced Drug Delivery Reviews*,

64(SUPPL.), pp.223–236. Available at: http://dx.doi.org/10.1016/j.addr.2012.09.009.

Higham, A.K. et al., 2014. Photo-activated ionic gelation of alginate hydrogel: Real-time rheological monitoring of the two-step crosslinking mechanism. *Soft Matter*, 10(27), pp.4990–5002.

Hong, Y. et al., 2007. Covalently crosslinked chitosan hydrogel: Properties of in vitro degradation and chondrocyte encapsulation. *Acta Biomaterialia*, 3(1), pp.23–31.

Hsu, C.W. et al., 2013. Combined Effects of Bone Marrow-Derived Mesenchymal Stem Cells and PLGA-PEG-PLGA Scaffolds on Repair of Articular Cartilage Defect. *Advanced Materials Research*, 815, pp.345–349.

Huang, C.P. et al., 2009. Engineering microscale cellular niches for three-dimensional multicellular co-cultures. *Lab on a Chip*, 9(12), pp.1740–1748.

Hubka, K.M. et al., 2014. Enhancing Chondrogenic Phenotype for Cartilage Tissue Engineering: Monoculture and Coculture of Articular Chondrocytes and Mesenchymal Stem Cells. *Tissue Engineering Part B: Reviews*, 20(6), pp.641–654. Available at: http://online.liebertpub.com/doi/abs/10.1089/ten.teb.2014.0034.

Hunziker, E.B., 2002. Articular cartilage repair: Basic science and clinical progress. A review of the current status and prospects. *Osteoarthritis and Cartilage*, 10(6), pp.432–463.

Hunziker, E.B., 2009. The elusive path to cartilage regeneration. *Advanced Materials*, 21(32–33), pp.3419–3424.

James, S. et al., 2015. Multiparameter Analysis of Human Bone Marrow Stromal Cells Identifies Distinct Immunomodulatory and Differentiation-Competent Subtypes. *Stem Cell Reports*, 4(6), pp.1004–1015. Available at: http://dx.doi.org/10.1016/j.stemcr.2015.05.005.

Jarry, C. et al., 2002. Irradiating or Autoclaving Chitosan/Polyol Solutions: Effect on Thermogelling Chitosan-β-glycerophosphate Systems. *Chemical & Pharmaceutical Bulletin*, 50(10), pp.1335–1340. Available at: http://joi.jlc.jst.go.jp/JST.JSTAGE/cpb/50.1335?from=CrossRef.

Jayasuriya, C.T. et al., 2016. The influence of tissue microenvironment on stem cell–based cartilage repair. *Annals of the New York Academy of Sciences*, 1383(1), pp.21–33.

Jimenez, W. et al., 1985. Measurement of fibrosis in needle liver biopsies: Evaluation of a colorimetric method. *Hepatology : official journal of the American Association for the Study of Liver Diseases.*, 5(5), pp.815–818.

Jin, R. et al., 2010. Enzymatically Crosslinked Dextran-Tyramine Hydrogels as Injectable Scaffolds for Cartilage Tissue Engineering. *Tissue Engineering Part A*, 16(8), pp.2429–2440. Available at: http://www.liebertonline.com/doi/abs/10.1089/ten.tea.2009.0764.

Kaga, S. et al., 2016. Synthesis and functionalization of dendron-polymer conjugate based hydrogels via sequential thiol-ene "click" reactions. *Journal of Polymer Science, Part A: Polymer Chemistry*, 54(7), pp.926–934.

Kaji, H. et al., 2011. Engineering systems for the generation of patterned co-cultures for controlling cell–cell interactions. *Biochimica et Biophysica Acta (BBA) - General Subjects*, 1810(3), pp.239–250. Available at: http://www.sciencedirect.com/science/article/pii/S0304416510001728.

Kalamegam, G. et al., 2018. A Comprehensive Review of Stem Cells for Cartilage Regeneration in Osteoarthritis. *Advances in experimental medicine and biology*. Available at: http://www.ncbi.nlm.nih.gov/pubmed/29725971.

Kang, H. et al., 2014. In vivo cartilage repair using adipose-derived stem cell-loaded decellularized cartilage ECM scaffolds. *Journal of tissue engineering and regenerative medicine.*, 8(6), pp.442–453.

Kariminekoo, S. et al., 2016. Implications of mesenchymal stem cells in regenerative medicine. *Artificial Cells, Nanomedicine and Biotechnology*, 44(3), pp.749–757.

Kelly, T.A.N. et al., 2013. Tissue-engineered articular cartilage exhibits tension-compression nonlinearity reminiscent of the native cartilage. *Journal of Biomechanics*, 46(11), pp.1784–1791. Available at: http://dx.doi.org/10.1016/j.jbiomech.2013.05.017.

Khodaverdi, E. et al., 2012. In Vitro Insulin Release from Thermosensitive Chitosan Hydrogel. *AAPS PharmSciTech*, 13(2), pp.460–466. Available at: http://www.springerlink.com/index/10.1208/s12249-012-9764-9.

Kim, H.J. & Park, J.-S., 2017. Usage of Human Mesenchymal Stem Cells in Cell-based Therapy: Advantages and Disadvantages. *Development & Reproduction*, 21(1), pp.1–10. Available at: http://www.ksdb.org/archive/view_article?pid=dr-21-1-1.

Kim, S. et al., 2010. A chitosan/β-glycerophosphate thermo-sensitive gel for the delivery of ellagic acid for the treatment of brain cancer. *Biomaterials*, 31(14), pp.4157–4166. Available at: http://dx.doi.org/10.1016/j.biomaterials.2010.01.139.

Klouda, L., 2015. Thermoresponsive hydrogels in biomedical applications A seven-year update. *European Journal of Pharmaceutics and Biopharmaceutics*, 97, pp.338–349.

Kressel, M. & Groscurth, P., 1994. Distinction of apoptotic and necrotic cell death by in situ labelling of fragmented DNA. *Cell & Tissue Research*, 278(3), pp.549–556.

Kubosch, E.J. et al., 2016. The trans-well coculture of human synovial mesenchymal stem cells with chondrocytes leads to self-organization, chondrogenic differentiation, and secretion of TGFβ. *Stem Cell Research and Therapy*, 7(1), pp.1–11. Available at: http://dx.doi.org/10.1186/s13287-016-0322-3.

Kumari, S., Mg, S. & Mayor, S., 2010. Endocytosis unplugged: Multiple ways to enter the cell. *Cell Research*, 20(3), pp.256–275. Available at: http://dx.doi.org/10.1038/cr.2010.19.

Kuo, K.-C. et al., 2015. Bioengineering vascularized tissue constructs using an injectable cell-laden enzymatically crosslinked collagen hydrogel derived from dermal extracellular matrix. *Acta Biomaterialia*, 27, pp.151–166. Available at: http://www.sciencedirect.com/science/article/pii/S1742706115300969.

Kwon, J.S. et al., 2012. Chitosan-based hydrogels to induce neuronal differentiation of rat muscle-derived stem cells. *International Journal of Biological Macromolecules*, 51(5), pp.974–979. Available at: http://dx.doi.org/10.1016/j.ijbiomac.2012.08.007.

Lavertu, M., Filion, D. & Buschmann, M.D., 2008. Heat-Induced Transfer of Protons from Chitosan to Glycerol Phosphate Produces Chitosan Precipitation and Gelation. *Biomacromolecules*, 9(2), pp.640–650. Available at: https://doi.org/10.1021/bm700745d.

Lee, N.K. et al., 2009. Comparison of the synthetic biodegradable polymers, polylactide (PLA), and polylactic-co-glycolic acid (PLGA) as scaffolds for artificial cartilage. *Biotechnology and Bioprocess Engineering*, 14(2), pp.180–186.

Lettry, V. et al., 2010. Coculture of equine mesenchymal stem cells and mature equine articular chondrocytes results in improved chondrogenic differentiation of the stem cells. *The Japanese journal of veterinary research*, 58(1), pp.5–15.

Li, F. et al., 2018. Cartilage tissue formation through assembly of microgels containing mesenchymal stem cells. *Acta Biomaterialia*. Available at: http://www.sciencedirect.com/science/article/pii/S1742706118304094.

Li, F. et al., 2012. Human Placenta-Derived Mesenchymal Stem Cells with Silk Fibroin Biomaterial in the Repair of Articular Cartilage Defects. *Cellular Reprogramming*, 14(4), pp.334–341.

Li, J. et al., 2012. Dynamic compression of rabbit adipose-derived stem cells transfected with insulin-like growth factor 1 in chitosan/gelatin scaffolds induces chondrogenesis and matrix biosynthesis. *Journal of Cellular Physiology*, 227(5), pp.2003–2012.

Li, L.P., Buschmann, M.D. & Shirazi-Adl, A., 2003. Strain-rate Dependent Stiffness of Articular Cartilage in Unconfined Compression. *Journal of Biomechanical Engineering*, 125(2), pp.161–168. Available at: http://dx.doi.org/10.1115/1.1560142.

Liang, Y. & Kiick, K.L., 2016. Liposome-Cross-Linked Hybrid Hydrogels for Glutathione-Triggered Delivery of Multiple Cargo Molecules. *Biomacromolecules*, 17(2), pp.601–614. Available at: https://doi.org/10.1021/acs.biomac.5b01541.

Liu, T. et al., 2018. Encapsulation of mesenchymal stem cells in chitosan/β-glycerophosphate hydrogel for seeding on a novel calcium phosphate cement scaffold. *Medical Engineering and Physics*, 56, pp.9–15. Available at: https://doi.org/10.1016/j.medengphy.2018.03.003.

Loh, Q.L. & Choong, C., 2013. Three-Dimensional Scaffolds for Tissue Engineering Applications: Role of Porosity and Pore Size. *Tissue Engineering Part B: Reviews*, 19(6), pp.485–502. Available at: http://online.liebertpub.com/doi/abs/10.1089/ten.teb.2012.0437.

Lories, R.J. & Luyten, F.P., 2018. *Overview of Joint and Cartilage Biology*,

Lutz, W., Sanderson, W. & Scherbov, S., 2008. The coming acceleration of global population ageing. *Nature*, 451, p.716. Available at: http://dx.doi.org/10.1038/nature06516.

M. Iliescu, C.D. Hoemann, M.S. Shive, A.Chenite, M.D.B., 2008. Ultrastructure of Hybrid Chitosan–Glycerol Phosphate Blood Clots by Environmental Scanning Electron Microscopy. *Microscopy Research and Technique2*, 71, pp.236–247.

Magnusson, P.B., 1941. Joint debridement: Surgical treatment of degenerative arthirtis. *Surg Gynaecol Obstet*, 73, pp.1–9.

Mahmoudifar, N. & Doran, P.M., 2010. Chondrogenic differentiation of human adipose-derived stem cells in polyglycolic acid mesh scaffolds under dynamic culture conditions. *Biomaterials*, 31(14), pp.3858–3867. Available at: http://dx.doi.org/10.1016/j.biomaterials.2010.01.090.

Maity, S. et al., 2016. A dynamic chitosan-based self-healing hydrogel with tunable morphology and its application as an isolating agent. *RSC Advances*, 6(84), pp.81060–81068.

Man, G.S. & Mologhianu, G., 2014. Osteoarthritis pathogenesis - a complex process that involves the entire joint. *Journal of medicine and life*, 7(1), pp.37–41. Available at: /pmc/articles/PMC3956093/?report=abstract.

Marquass, B. et al., 2011. Matrix-associated implantation of predifferentiated mesenchymal stem cells versus articular chondrocytes: In vivo results of cartilage repair after 1 year. *American Journal of Sports Medicine*, 39(7), pp.1401–1412.

Matsusue, Y., Yamamuro, T. & Hama, H., 1993. Arthroscopic multiple osteochondral transplantation to the chondral defect in the knee associated with anterior cruciate ligament disruption. *Arthroscopy*, 9(3), pp.318–321. Available at: https://doi.org/10.1016/S0749-8063(05)80428-1.

Mente, P.L. & Lewis, J.L., 1989. Experimental method for the measurement of the elastic modulus of trabecular bone tissue. *Journal of orthopaedic research.*, 7(3), pp.456–461.

Mesallati, T., Buckley, C.T. & Kelly, D.J., 2017. Engineering cartilaginous grafts using chondrocyte-laden hydrogels supported by a superficial layer of stem cells. *Journal of Tissue Engineering and Regenerative Medicine*, 11(5), pp.1343–1353.

Mescher, A.L., 2016. Junqueira ' s Basic Histology Text & Atlas (14th ed .). , (January), pp.295–304.

Minas, T., 2001. Autologous chondrocyte implantation for focal chondral defects of the knee. *Clinical Orthopaedics and Related Research®*, 391, pp.S349–S361.

Mine, K. et al., 2017. The effectiveness of braces and orthoses for patients with knee osteoarthritis: A systematic review of Japanese-language randomised controlled trials. *Prosthetics and Orthotics International*, 41(2), pp.115–126.

Mirahmadi, F. et al., 2013. Enhanced mechanical properties of thermosensitive chitosan hydrogel by silk fibers for cartilage tissue engineering. *Materials Science & Engineering C*, 33(8), pp.4786–4794.

Mitchell, M.J. & King, M.R., 2014. Engineering Cartilage Tissue. *Adv Drug Deliv Rev*, 60(1), pp.1–23.

Mobasheri, A. et al., 2014. Chondrocyte and mesenchymal stem cell-based therapies for cartilage repair in osteoarthritis and related orthopaedic conditions. *Maturitas*, 78(3), pp.188–198. Available at: http://dx.doi.org/10.1016/j.maturitas.2014.04.017.

Mohabatpour, F., Karkhaneh, A. & Sharifi, A.M., 2016. A hydrogel/fiber composite scaffold for chondrocyte encapsulation in cartilage tissue regeneration. *RSC Advances*, 6(86), pp.83135–83145.

Montalbano, G. et al., 2018. Synthesis of bioinspired collagen/alginate/fibrin based hydrogels for soft tissue engineering. *Materials Science and Engineering C*, 91(March), pp.236–246. Available at: https://doi.org/10.1016/j.msec.2018.04.101.

Mouser, V.H.M. et al., 2017. Three-Dimensional Bioprinting and Its Potential in the Field of Articular Cartilage Regeneration.

Cartilage, 8(4), pp.327–340.

Mow, V.C., 1998. Structure and function of articular cartilage and meniscus. In *Basic Orthopaedic Biomechanics*. pp. 181–258. Available at: http://content.wkhealth.com/linkback/openurl?sid=WKPTLP:landingpage&an=00005768-199804000-00025.

Mow, V.C., 2009. Temperature-Dependent viscoelastic properties of the human Supraspinatus tendon. *Journal of Biomechanics*, 42(4), pp.546–549.

Mow, V.C., Ratcliffe, A. & Robin Poole, A., 1992. Cartilage and diarthrodial joints as paradigms for hierarchical materials and structures. *Biomaterials*, 13(2), pp.67–97.

Mow, V.C., Wang, C.C. & Hung, C.T., 1999. The extracellular matrix, interstitial fluid and ions as a mechanical signal transducer in articular cartilage. *Osteoarthritis and Cartilage*, 7(1), pp.41–58.

Mutlu, L., Hufnagel, D. & Taylor, H.S., 2015. The endometrium as a source of mesenchymal stem cells for regenerative medicine. *Biology of Reproduction*, 92(6).

Nafee, N., Zewail, M. & Boraie, N., 2017a. Alendronate-loaded, biodegradable smart hydrogel: a promising injectable depot formulation for osteoporosis. *Journal of Drug Targeting*, pp.1–13.

Nafee, N., Zewail, M. & Boraie, N., 2017b. Alendronate-loaded, biodegradable smart hydrogel: a promising injectable depot formulation for osteoporosis. *Journal of Drug Targeting*, 0(0), pp.1–13. Available at: https://doi.org/10.1080/1061186X.2017.1390670.

Nagamura-Inoue, T., 2014. Umbilical cord-derived mesenchymal stem cells: Their advantages and potential clinical utility. *World Journal of Stem Cells*, 6(2), p.195. Available at: http://www.wjgnet.com/1948-0210/full/v6/i2/195.htm.

Nazempour, A. & Van Wie, B.J., 2016. Chondrocytes, Mesenchymal Stem Cells, and Their Combination in Articular Cartilage Regenerative Medicine. *Annals of Biomedical Engineering*, 44(5), pp.1325–1354.

Nelson, A.E. et al., 2014. A systematic review of recommendations and guidelines for the management of osteoarthritis: The Chronic Osteoarthritis Management Initiative of the U.S. Bone and Joint Initiative. *Seminars in Arthritis and Rheumatism*, 43(6), pp.701–712. Available at: https://www.sciencedirect.com/science/article/pii/S0049017213002588?via%3Dihub [Accessed August 8, 2018].

Ng, H.Y., Lee, K.A. & Shen, Y., 2017. Articular Cartilage : Structure , Composition , Injuries and Repair. *JSM Bone and Joint Diseases*, 1(2), pp.1–6.

Nguyen, Q.T. et al., 2012. Cartilage-like mechanical properties of poly (ethylene glycol)-diacrylate hydrogels. *Biomaterials*, 33(28), pp.6682–6690. Available at: http://dx.doi.org/10.1016/j.biomaterials.2012.06.005.

NICE, 2017. Autologous chondrocyte implantation for treating symptomatic articular cartilage defects of the knee | Guidance and guidelines | NICE. , (October 2017), pp.1–6. Available at: https://www.nice.org.uk/guidance/TA477/chapter/1-Recommendations.

Nisbet, D.R. et al., 2006. Morphology and gelation of thermosensitive xyloglucan hydrogels. *Biophysical Chemistry*, 121(1), pp.14–20.

Papadopoulos, A. et al., 2011. Injectable and Photopolymerizable Tissue-Engineered Auricular Cartilage Using Poly(Ethylene Glycol) Dimethacrylate Copolymer Hydrogels. *Tissue Engineering Part A*, 17(1–2), pp.161–169. Available at: http://www.liebertonline.com/doi/abs/10.1089/ten.tea.2010.0253.

Park, H., Woo, E.K. & Lee, K.Y., 2014. Ionically cross-linkable hyaluronate-based hydrogels for injectable cell delivery. *Journal of Controlled Release*, 196, pp.146–153. Available at: http://dx.doi.org/10.1016/j.jconrel.2014.10.008.

Patrulea, V. et al., 2015. Chitosan as a starting material for wound healing applications. *European Journal of Pharmaceutics and Biopharmaceutics*, 97, pp.417–426. Available at: http://www.sciencedirect.com/science/article/pii/S0939641115003367.

Peng, Q. et al., 2013. Injectable and biodegradable thermosensitive hydrogels loaded with PHBHHx nanoparticles for the sustained and controlled release of insulin. *Acta Biomaterialia*, 9(2), pp.5063–5069. Available at: http://www.sciencedirect.com/science/article/pii/S1742706112004710.

Peng, Y. et al., 2013. Optimization of thermosensitive chitosan hydrogels for the sustained delivery of venlafaxine hydrochloride. *International Journal of Pharmaceutics*, 441(1), pp.482–490. Available at: http://www.sciencedirect.com/science/article/pii/S0378517312010125.

Pontikoglou, C. et al., 2011. Bone Marrow Mesenchymal Stem Cells: Biological Properties and Their Role in Hematopoiesis and Hematopoietic Stem Cell Transplantation. *Stem Cell Reviews and Reports*, 7(3), pp.569–589.

Pridie, K.H., 1959. A Method of resurfacing osteoarthric knee joints. *J Bone and Joint Surg41-B*, 3, pp.618–619.

Pritchard, C.D. et al., 2011. An injectable thiol-acrylate poly (ethylene glycol) hydrogel for sustained release of methylprednisolone sodium succinate. *Biomaterials*, 32(2), pp.587–597.

Qi, Y. et al., 2012. The restoration of full-thickness cartilage defects with mesenchymal stem cells (MSCs) loaded and cross-linked bilayer collagen scaffolds on rabbit model. *Molecular Biology Reports*, 39(2), pp.1231–1237.

Revell, C.M. & Athanasiou, K., 2009. Success Rates and Immunologic Responses of Autogenic, Allogenic, and Xenogenic Treatments to Repair Articular Cartilage Defects. *Tissue Engineering Part B-Reviews*, 15(1), pp.1–15.

Ribeiro, R.D.C. et al., 2017. Temporary Single-Cell Coating for Bioprocessing with a Cationic Polymer. *ACS Applied Materials and Interfaces*, 9(15), pp.12967–12974.

Richardson, S.M. et al., 2008. Human mesenchymal stem cell differentiation to NP-like cells in chitosan-glycerophosphate hydrogels. *Biomaterials*, 29(1), pp.85–93.

Richardson, S.M. et al., 2015. Mesenchymal stem cells in regenerative medicine: Focus on articular cartilage and intervertebral disc regeneration. *Methods*, 99, pp.69–80. Available at: http://dx.doi.org/10.1016/j.ymeth.2015.09.015.

Rieppo, J. et al., 2003. Structure-function relationships in enzymatically modified articular cartilage. *Cells Tissues Organs*,

175(3), pp.121–132.

Rodrigo, J.J., 1994. Improvement of full-thickness chondral defect healing in the human knee after debridement and microfracture using continuous passive motion. *Am J Knee Surg*, 7, pp.109–116.

Roughley, P.J., 2001. Articular cartilage and changes in arthritis noncollagenous proteins and proteoglycans in the extracellular matrix of cartilage. *Arthritis Research*, 3(6), pp.342–347.

Roughley, P.J., 2016. The structure and function of cartilage proteoglycans. *European cells & materials*, 12(SUPPL.1).

Ruel-Gariépy, E. et al., 2004. A thermosensitive chitosan-based hydrogel for the local delivery of paclitaxel. *European Journal of Pharmaceutics and Biopharmaceutics*, 57(1), pp.53–63. Available at: http://www.sciencedirect.com/science/article/pii/S093964110300095X.

Ruel-Gariépy, E. et al., 2000. Characterization of thermosensitive chitosan gels for the sustained delivery of drugs. *International Journal of Pharmaceutics*, 203(1), pp.89–98. Available at: http://www.sciencedirect.com/science/article/pii/S0378517300004282.

Ruel-Gariépy, E. & Leroux, J.C., 2004. In situ-forming hydrogels - Review of temperature-sensitive systems. *European Journal of Pharmaceutics and Biopharmaceutics*, 58(2), pp.409–426.

Sánchez-Téllez, D.A., Téllez-Jurado, L. & Rodríguez-Lorenzo, L.M., 2017. Hydrogels for cartilage regeneration, from polysaccharides to hybrids. *Polymers*, 9(12), pp.1–32.

Sarkar, N. & Walker, L.C., 1995. Hydration—dehydration properties of methylcellulose and hydroxypropylmethylcellulose. *Carbohydrate Polymers*, 27(3), pp.177–185. Available at: http://www.sciencedirect.com/science/article/pii/014486179500061B.

Schliephake, H., Neukam, F.W. & Klosa, D., 1991. Influence of pore dimensions on bone ingrowth into porous hydroxylapatite blocks used as bone graft substitutes: A histometric study. *International Journal of Oral and Maxillofacial Surgery*, 20(1), pp.53–58. Available at: http://www.sciencedirect.com/science/article/pii/S0901502705806988.

Schon, B.S., Hooper, G.J. & Woodfield, T.B.F., 2017. Modular Tissue Assembly Strategies for Biofabrication of Engineered Cartilage. *Annals of Biomedical Engineering*, 45(1), pp.100–114.

Shariatinia, Z. & Jalali, A.M., 2018. Chitosan-based hydrogels: Preparation, properties and applications. *International Journal of Biological Macromolecules*, 115, pp.194–220. Available at: https://doi.org/10.1016/j.ijbiomac.2018.04.034.

Shim, W.S. et al., 2006. Biodegradability and biocompatibility of a pH- and thermo-sensitive hydrogel formed from a sulfonamide-modified poly(ε-caprolactone-co-lactide)-poly(ethylene glycol)-poly(ε-caprolactone-co-lactide) block copolymer. *Biomaterials*, 27(30), pp.5178–5185.

Simon, T.M. & Jackson, D.W., 2018. Articular Cartilage: Injury Pathways and Treatment Options. *Sports Medicine and Arthroscopy Review*, 26(1), pp.31–39.

Skwarczynska, A. et al., 2018. The structural (FTIR, XRD, and XPS) and biological studies of thermosensitive chitosan chloride gels with β-glycerophosphate disodium. *Journal of Applied Polymer Science*, 135(27), pp.1–8.

Soltz, M.A., 2000. Functional Tissue Engineering of Articular Cartilage Through Dynamic Loading of Chondrocyte-Seeded Agarose Gels. *Journal of biomechanical engineering.*, 122(3), pp.252–260.

Sophia Fox, A.J., Bedi, A. & Rodeo, S.A., 2009. The basic science of articular cartilage: Structure, composition, and function. *Sports Health*, 1(6), pp.461–468.

Spoliti, M. et al., 2012. In vitro release and expansion of mesenchymal stem cells by a hyaluronic acid scaffold used in combination with bone marrow. *Muscles, ligaments and tendons journal*, 2(4), pp.289–94. Available at: http://www.ncbi.nlm.nih.gov/pubmed/23738312%5Cnhttp://www.pubmedcentral.nih.gov/articlerender.fcgi?artid=PMC3666531.

Stoop, R., 2008. Smart biomaterials for tissue engineering of cartilage. *Injury*, 39(1), pp.77–87. Available at: https://doi.org/10.1016/j.injury.2008.01.036.

Supper, S. et al., 2013. Rheological Study of Chitosan/Polyol-phosphate Systems: Influence of the Polyol Part on the Thermo-Induced Gelation Mechanism. *Langmuir*, 29(32), pp.10229–10237. Available at: https://doi.org/10.1021/la401993q.

Supper, S. et al., 2014. Thermosensitive chitosan/glycerophosphate-based hydrogel and its derivatives in pharmaceutical and biomedical applications. *Expert Opinion on Drug Delivery*, 11(2), pp.249–267. Available at: http://www.tandfonline.com/doi/full/10.1517/17425247.2014.867326.

van Susante, J.L.C. et al., 1999. Resurfacing potential of heterologous chondrocytes suspended in fibrin glue in large full-thickness defects of femoral articular cartilage: an experimental study in the goat. *Biomaterials*, 20(13), pp.1167–1175.

Suzawa, Y. et al., 2015. Biomineral/agarose composite gels enhance proliferation of mesenchymal stem cells with osteogenic capability. *International Journal of Molecular Sciences*, 16(6), pp.14245–14258.

Szymańska, E. et al., 2014. Influence of unmodified and β-glycerophosphate cross-linked chitosan on anti-candida activity of clotrimazole in semi-solid delivery systems. *International Journal of Molecular Sciences*, 15(10), pp.17765–17777.

Szymańska, E. et al., 2015. The effect of β-glycerophosphate crosslinking on chitosan cytotoxicity and properties of hydrogels for vaginal application. *Polymers*, 7(11), pp.2223–2244.

Tao, H., Lodge, T.P. & Von Meerwall, E.D., 2000. Diffusivity and viscosity of concentrated hydrogenated polybutadiene solutions. *Macromolecules*, 33(5), pp.1747–1758.

Thompson, Y., Piez, K.A. & Seyedin, S.M., 1985. in Agarose Gel Culture differentiation [I-3]. In studies on cartilage induction and differentiation , intra- shown to evoke the formation of hyaline cartilage and bone [4 , 51 . Extraction of ate and form cartilage and bone has been the subject of inte. *Experimental Cell Research*, 157, pp.483–494.

Toh, W.S. & Loh, X.J., 2015. Advances in hydrogel delivery systems for tissue regeneration. *Materials Science and*

Engineering C, 45, pp.690–697. Available at: http://dx.doi.org/10.1016/j.msec.2014.04.026.

Tsuchiya, K. et al., 2004. The effect of coculture of chondrocytes with mesenchymal stem cells on their cartilaginous phenotype in vitro. *Materials Science & Engineering C-Biomimetic And Supramolecular Systems*, 24(3), pp.391–396.

Uliniuc, A. et al., 2012. New Approaches in Hydrogel Synthesis - Click Chemistry: A Review. *Cellulose Chemistry and Technology*, 46(1–2), pp.1–11. Available at: http://www.cellulosechemtechnol.ro/pdf/CCT1-2(2012)/p.1-11.pdf.

Ullah, I., Subbarao, R.B. & Rho, G.J., 2015. Human mesenchymal stem cells - current trends and future prospective. *Bioscience Reports*, 35(2), pp.1–18. Available at: http://bioscirep.org/cgi/doi/10.1042/BSR20150025.

Vårum, K.M., Ottøy, M.H. & Smidsrød, O., 1994. Water-solubility of partially N-acetylated chitosans as a function of pH: effect of chemical composition and depolymerisation. *Carbohydrate Polymers*, 25(2), pp.65–70. Available at: http://www.sciencedirect.com/science/article/pii/0144861794901406.

Vemuri, M.C., Chase, L.G. & Rao, M.S., 2011. *Mesenchymal stem cell assays and applications.*,

Verhaar, G., 2009. *Mathematical Modeling of Uniaxial Mechanical Testing of Biological Tissue*,

Wagenseil, J.E. et al., 2003. One-Dimensional Viscoelastic Behavior of Fibroblast Populated Collagen Matrices. *Journal of Biomechanical Engineering*, 125(5), p.719. Available at: http://biomechanical.asmedigitalcollection.asme.org/article.aspx?articleid=1410815.

Wang, L. & Stegemann, J.P., 2010. Thermogelling chitosan and collagen composite hydrogels initiated with β-glycerophosphate for bone tissue engineering. *Biomaterials*, 31(14), pp.3976–3985. Available at: http://www.sciencedirect.com/science/article/pii/S0142961210001791.

Watt, F.M., 1988. Effect of seeding density on stability of the differentiated phenotype of pig articular chondrocytes in culture. *J Cell Sci*, 89 (Pt 3)(April 1988), pp.373–378. Available at: http://www.ncbi.nlm.nih.gov/pubmed/3058725%5Cnhttp://www.ncbi.nlm.nih.gov/entrez/query.fcgi?cmd=Retrieve&db=PubMed&dopt=Citation&list_uids=3058725.

Westendorf, J.J. & Van Wijnen, A.J., 2014. Osteoporosis and osteoarthritis. *Osteoporosis and Osteoarthritis*, 1226, pp.1–211.

Wouters, G. et al., 2007. Isolation of amniotic fluid-derived mesenchymal stem cells. *Journal of prenatal medicine*, 1(3), pp.39–40. Available at: http://www.ncbi.nlm.nih.gov/pubmed/22470826%5Cnhttp://www.pubmedcentral.nih.gov/articlerender.fcgi?artid=PMC3309337.

Wu, J. et al., 2007. A thermosensitive hydrogel based on quaternized chitosan and poly(ethylene glycol) for nasal drug delivery system. *Biomaterials*, 28(13), pp.2220–2232.

Wu, L. et al., 2011. Trophic Effects of Mesenchymal Stem Cells Increase Chondrocyte Proliferation and Matrix Formation. *Tissue Engineering Part A*, 17(9–10), pp.1425–1436. Available at: http://search.proquest.com/docview/862860106/.

Wylie, J.D. et al., 2016. Failures and Reoperations after Matrix-Assisted Cartilage Repair of the Knee: A Systematic Review. *Arthroscopy - Journal of Arthroscopic and Related Surgery*, 32(2), pp.386–392. Available at: http://dx.doi.org/10.1016/j.arthro.2015.07.025.

Yan, C. & Pochan, D., 2010. Rheological properties of peptide-based hydrogels for biomedical and other applications. *Chemical Society Reviews*, 39(9), pp.3528–3540. Available at: http://pubs.rsc.org/en/content/articlehtml/2010/cs/b919449p.

Yan, L.P. et al., 2010. Genipin-cross-linked collagen/chitosan biomimetic scaffolds for articular cartilage tissue engineering applications. *Journal of Biomedical Materials Research - Part A*, 95 A(2), pp.465–475.

Yang, Q. et al., 2011. Evaluation of an extracellular matrix-derived acellular biphasic scaffold/cell construct in the repair of a large articular high-load-bearing osteochondral defect in a canine model. *Chinese medical journal*, 124(23).

Yang, Y.-H., Lee, A.J. & Barabino, G.A., 2012. Coculture-Driven Mesenchymal Stem Cell-Differentiated Articular Chondrocyte-Like Cells Support Neocartilage Development. *STEM CELLS Translational Medicine*, 1(11), pp.843–854. Available at: http://doi.wiley.com/10.5966/sctm.2012-0083.

Yu, L., 2004. Regulation of an ATG7-beclin 1 Program of Autophagic Cell Death by Caspase-8. *Science*, 304(5676), pp.1500–1502. Available at: http://www.sciencemag.org/cgi/doi/10.1126/science.1096645.

Zhang, D. et al., 2013. A magnetic chitosan hydrogel for sustained and prolonged delivery of Bacillus Calmette–Guérin in the treatment of bladder cancer. *Biomaterials*, 34(38), pp.10258–10266. Available at: http://www.sciencedirect.com/science/article/pii/S0142961213011101.

Zhang, W. et al., 2016. Current research on pharmacologic and regenerative therapies for osteoarthritis. *Bone Research*, 4(December 2015).

Zhang, Y. et al., 2018. Co-culture systems-based strategies for articular cartilage tissue engineering. *Journal of Cellular Physiology*, 233(3), pp.1940–1951.

Zhang, Y.S. et al., 2017. 3D Bioprinting for Tissue and Organ Fabrication. *Annals of Biomedical Engineering*, 45(1), pp.148–163.

Zhang Y and Jordan M, 2010. Epidemiology of Osteoarthritis. *Clin Geriatr Med.*, 26(154), pp.355–369.

Zhao, Z. et al., 2018. Co-implantation of bone marrow mesenchymal stem cells and chondrocytes increase the viability of chondrocytes in rat osteo-chondral defects. *Oncology Letters*, 15(5), pp.7021–7027.

Zhou, H.Y. et al., 2008. Effect of molecular weight and degree of chitosan deacetylation on the preparation and characteristics of chitosan thermosensitive hydrogel as a delivery system. *Carbohydrate Polymers*, 73(2), pp.265–273.

Zhou, H.Y. et al., 2015. Glycerophosphate-based chitosan thermosensitive hydrogels and their biomedical applications. *Carbohydrate Polymers*, 117, pp.524–536.

Zhu, J. & Marchant, R.E., 2011. Design properties of hydrogel tissue-engineering scaffolds. *Expert Review of Medical Devices*, 8(5), pp.607–626.

Zhu, Y. et al., 2014. Manufacture of layered collagen/chitosan-polycaprolactone scaffolds with biomimetic

microarchitecture. *Colloids and Surfaces B: Biointerfaces*, 113, pp.352–360. Available at: http://dx.doi.org/10.1016/j.colsurfb.2013.09.028.